ADVANCED FUNCTIONAL MATERIALS
www.afm-journal.de

Strategic Advances in Spatiotemporal Control of Bioinspired Phenolic Chemistries in Materials Science

*Zhaojun Jia, Min Wen, Yan Cheng, and Yufeng Zheng**

Nature-inspired phenolic chemistries have substantially nourished the engineering of advanced materials for widespread applications in energy, catalysis, and biomedicine, among others. To achieve predictable yet adaptable material structures and properties, the spatial and/or temporal control over the phenolic chemistries per se is increasingly demanded. In this review, a systematic overview of recent strategical advances in the spatiotemporal control of phenolic chemistries in materials science is given. The chemical diversity and reactivity of catechols and polyphenols are first introduced as phenolic building blocks. With a main focus on catechols (especially dopamine), renewed insights into their mechanisms of polymerization/assembly, adhesion, and cohesion are provided. The conditions for tuning phenolic polymerization/assembly are also outlined. This paper focuses on the latest strategies for imparting controlled manipulation of phenolic chemistries in terms of many aspects: growth kinetics, chemical compositions and structures, dimensions and architectures, spatial patterns, and surface functionality. Finally, critical issues facing this field with perspectives delivered on future research are discussed. As envisaged, this review will provide helpful guidance to orchestrate state-of-the-art phenolic chemistries and materials science for producing materials with intended, application-oriented properties and functions.

1. Introduction

Nature's abundance of phenolic compounds or residues has inspired a myriad of materials with unparalleled properties for numerous applications.[1] One group is catechol-containing molecules, which are essential for the substrate adhesion and/or structural reinforcement of living organisms, including mussels, geckos, sandcastle worms, insects, and squids.[2–6] As a noticeable example, marine mussels secrete catecholic amino acid-consisting proteins to form sticky byssus threads for spectacular wet adhesion. This portion of mussel powder has motivated the development of poly(catecholamine) coatings, showing universal robust substrate adherence and the versatility for secondary functionalization. The coating procedure is facile, involving pH-triggered oxidative polymerization of catecholamines, such as 3,4-dihydroxyphenylalanine (DOPA),[7] dopamine (DA),[2] and norepinephrine.[8] On the other hand, pyrogallol (PG)-derived polyphenolic compounds, such as gallic acid (GA), tannic acid (TA), and epicatechin gallate (ECG), are found omnipresent in the plant kingdom (e.g., barnacle, green tea, grapes, chocolate beans), where they play multiple biological roles as pigments, flavonoids, and antioxidants.[9–11] These dietary phenolics represent a new research spotlight owing to their low cost, high availability, and great structural diversity. In particular, metal–phenolic networks (MPNs) have recently spurred interest as dynamic materials for drug delivery and beyond.[12] Aside from these natural building blocks, the intentional incorporation of phenolic moieties into synthetic polymers derives a near-infinite library of artificial polymeric materials (particles, elastomers, gels, adhesives, etc.), whose chemical functionality can be designed to be sophisticated.[13]

Over the past decade, phenolic chemistries have been extensively pursued in biomedicine, and energy and environmental science, among others (for comprehensive reviews see refs. [1,14–17]). This field is fast-growing, with an exponential number of publications, yet seems far from being fully exploited. In the meantime, the community's expectation for what phenolics can further offer is on the rise. As our knowledge on phenolic chemistries deepens,[18–20] the paradigm that drives current research is shifting from simply "where to apply" to a more critical one, regarding "how to apply well." Controlled

Dr. Z. Jia, Prof. Y. Zheng
Beijing Advanced Innovation Center for Materials Genome Engineering and Department of Materials Science and Engineering
College of Engineering
Peking University
Beijing 100871, China
E-mail: yfzheng@pku.edu.cn
Dr. Z. Jia
Department of Chemistry and Chemical Biology
Rutgers University
Piscataway, NJ 08854, USA
Dr. M. Wen
Shenzhen Engineering Center for the Fabrication of Two-Dimensional Atomic Crystals
Shenzhen Institutes of Advanced Technology
Chinese Academy of Sciences
Shenzhen 518055, China
Prof. Y. Cheng
Academy for Advanced Interdisciplinary Studies
Peking University
Beijing 100871, China
The ORCID identification number(s) for the author(s) of this article can be found under https://doi.org/10.1002/adfm.202008821.

DOI: 10.1002/adfm.202008821

manipulation of phenolic chemistries and related materials, in a spatiotemporally defined manner, has recently received priority. Next-generation phenolic materials, as more and more scientists come to agree, should be custom designed to incorporate spatiotemporal precision in chemistry, processing, mechanics, and architectures to render predictable yet adaptable application-oriented properties.[10,13,17,21]

A major target is to impart control over the reversibility of phenolic chemistries, which is key to developing intelligent materials with durable dynamic self-healing or elastotic deformation capacities. Strategies to this end include switchable catechol/quinone transformation, metal–phenolic complexion, and the protection/deprotection of catechol. First and foremost, it is central to tune the catechol/quinone ratios to effectively surmount the dilemma between adhesion and cohesion in adhesive science.[22–23] Nanospace confined polymerization has value for this by counteracting the oxidation of catechol.[24] In addition, substantial endeavors have been devoted to tailor the growth kinetics (including the onset and termination) of phenolic oxidization/assembly. The kinetics of catechol polymerization is reported to be adaptable across hour-to-second time scales. By addition of oxidants (e.g., Cu^{2+}),[25] and radical species,[26] and the use of ultraviolet (UV) irradiation,[27] microwave,[28] and atmospheric pressure plasma,[29] the deposition time for polydopamine (PDA) coatings can be reduced by several orders of magnitudes (e.g., ≈500 nm thickness in 60 s by plasma[29] vs ≈50 nm thickness in 24 h traditionally). Some of these conditions can even induce catechol polymerization in an otherwise oxidization-inhibiting acidic environment.[30] On the contrary, metal–polyphenol assembly chemistry by its nature has ultrafast kinetics (ceasing in seconds), which imposes a problem to obtain thick and continuous films with exquisite structures. In light of better temporal control, investigators have recently adopted stepwise oxidization strategies including Fe^{2+} as the precursor metal, which can effectively slow down the kinetics while increasing film thickness.[31–32]

Controlled synthesis of phenolic nanomaterials with regard to size and morphology represents another imperative need. Nanoparticles with defined sizes and monodispersed characters are desirable for fluorescence imaging[33] and structural color displaying.[34] They can be obtained by using unique polymerization conditions or emerging techniques such as microfluidic-assisted polymerization.[35] Based on a palette of controlled polymerization strategies, current syntheses can cover low-dimensional and higher-order architectures of PDA, to name just a few, nanofibers,[36] nanosheets,[37] hollow nanospheres,[38] capsules,[39] nanotubes,[40] and hierarchical flowers.[41] Implausibly, chiral and twisted nanoribbons have been created leveraging chiral amphiphiles as modulators.[42] Moreover, the preferential growth of PDA has been well exemplified recently to potentiate Janus nano-sheets/particles with anisotropic surface properties,[43–44] as well as to control the folding of reprogrammable DNA origami.[45]

Aided by cutting-edge microfabrication technologies, such as photolithography,[46] microcontact printing,[47] and 3D printing,[48] spatially and/or temporally controlled phenolic polymerization/assembly has also become a reality, enabling functional phenolic micropatterns/nanocoatings that are indispensable to fabricate microelectronics, photonics, microdevices,

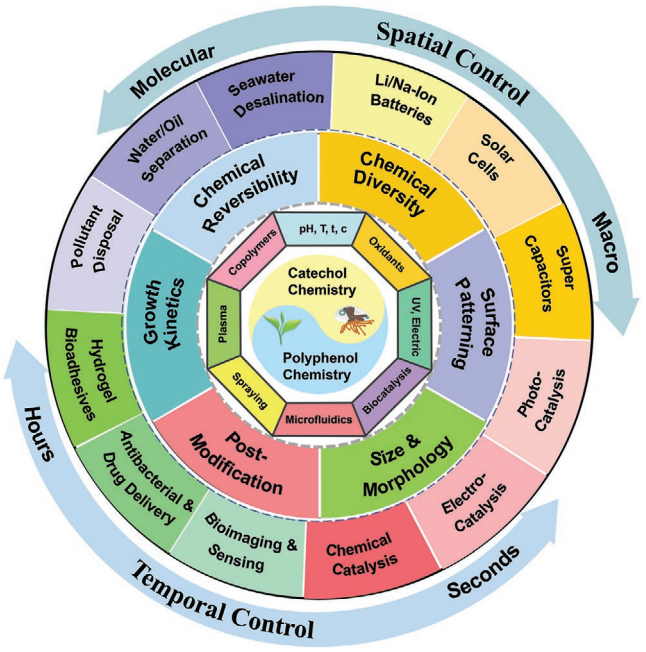

Figure 1. Outline of the review. The spatiotemporal control of phenolic chemistries (i.e., mussel-/plant-inspired catechol/polyphenol chemistries), spanning across molecular-to-macro and second-to-hour scales, can lead to advanced phenolic materials with controlled structures, properties, and functionalities for a wide range of applications in energy, environmental, and biomedical fields. The fundamentals of phenolic chemistries, including PDA formation pathways, adhesion and cohesion mechanisms of catechols, and conditions to tailor catechol/polyphenol polymerization/assembly, are summarized in Section 2. The contexts of spatial and temporal control are arbitrarily allocated into subsequent sections: 1) control of the dynamic redox structures and chemical reversibility of phenolics (Section 3); 2) control of coating kinetics of PDA (Section 4); 3) size and morphology control for catechol-based nanomaterials (Sections 5 and 6); 4) surface patterning of catechols and polyphenolics (Section 7); and 5) postmodifications of catechol/polyphenolics-based coatings and nanomaterials (Section 8).

and tissue niches with extensive utilities. Finally, the postpolymerization control of phenolic chemistries offers a second opportunity for tailoring material properties.[49] The surface moieties or bulk properties of catechol-based materials can be post-modified by grafting,[2] doping,[49] etching,[50] carbonization,[51] etc. to satisfy a particular function demand, including roughness, hydrophilia, and catalytic and biological properties, etc. Alternatively, the post-control of phenolic chemistries allows for material recycling. For instance, the often-useless PDA aggregates in solution can be degraded and reassembled to form new coatings.[52]

The above constitutes key aspects of our latest efforts in controlled manipulation of phenolic chemistries in contemporary materials science. However, to the best of our knowledge, there lacks a systematic review on these topics. Herein, we highlight recent strategical innovations in the spatiotemporal control of phenolic chemistries and provide a timely update on research in various fields (**Figure 1**). The focus is on strategies, design principles, and characteristics rather than comprehensiveness in gathering field-specific examples. We begin by giving an overview of phenolic chemistries (Section 2), briefly encompassing mechanisms of DA polymerization, the reversibility of phenolic

chemistries, the catechol–amine synergism, and the reactivity of quinones for crosslinking and functionalization. Additionally, canonical and noncanonical conditions that are potent to steer phenolic chemistries are outlined. In Section 3, we dedicate a lot of space to elaborate the manifold reversibility in catechol for production of smart dynamic materials. In Section 4, we outline possible routes to controlling the kinetics of PDA coating. In Sections 5 and 6, we enumerate PDA-based materials with dimensional and morphological diversity, while discussing methodologies for their controlled synthesis. In Section 7, we describe the current state-of-the-art techniques to install phenolic chemistries with spatial precision for micropatterning and substrate engineering. Furthermore, in Section 8, we survey established and emerging approaches in the postpolymerization control of catechol/polyphenol chemistries via surface engineering. Finally, in Section 9, we assess existing limitations and propose opportunities ahead for future innovations.

2. Fundamentals of Phenolic Chemistries

Before moving on, we organize this section to shed light on the state-of-the-art phenolic chemistries, which are the key to developing strategies for imparting spatiotemporal control over the relevant materials. We will discuss pathways for catechol polymerization, versatility of catechol/polyphenol chemistry, conditions for polymerization/assembly of catechol/polyphenol compounds and the properties of catechol/polyphenol derived materials.

2.1. Formation Pathways of PDA

Catecholamine compounds, such as DA, undergo self-polymerization under mild conditions to produce a polymeric structure of PDA.[2] Albeit for the widespread use of PDA, the mechanism behind PDA formation remains elusive.[53–55] Lee et al. suggested that the polymerization process begins with oxidation of DA to DA quinone, followed by cyclization, further oxidation, and rearrangement to 3,4-dihydroxyindole (DHI) (**Figure 2**A).[2] Although the oxidation conversion of DA to DHI is widely acknowledged, it is controversial regarding the subsequent processes. In particular, Hong et al. identified that noncovalent self-assembly of trimeric complexes of $(DA)_2$/DHI should constitute a complementary pathway for DHI oligomerization (Figure 2B).[56]

Noteworthily, however, DHI alone was found insufficient to initiate a coating under standard conditions.[57] Copolymerization studies using DA and DHI (with controls using either DA or DHI) had suggested that both molecules serve as a building block of PDA (Figure 2C). Researchers have become gradually aware of the structural diversity of PDA since the identification of pyrrolecarboxylic acid (PCA) moiety (Figure 2D), based on which a mechanism of partial degradation of catechol rings was proposed.[58] There is a growing recognition that noncovalent interactions play a pivotal role at a later stage. Ding et al. surmised that PDA is a supramolecular aggregate of $(DHI)_2$/PCA trimer complexes.[59] Recently, Hong et al. have pointed out that cation–π interaction is crucial for the intermolecular assembly in PDA.[20] Observations from a set of computational studies also supported that PDA is composed of small oligomers that appear to be stacked together via π–π interaction.[60]

Other possible mechanisms have been proposed in parallel to the above studies supporting the synergetic oligomerization and supramolecular aggregation. For example, Dreyer et al. believe that PDA is a supramolecular aggregate of DHI and its dione derivative, which are held together through multiple interactions, including charge transfer, π–π stacking, and hydrogen bonds (Figure 2E).[61] By contrast, Liebscher et al. demonstrated an alternative structure of PDA (Figure 2F). In this model, DHI and indoledione units, with differing degrees of (un)saturation, are covalently connected by C—C bonds between their benzene rings.[62] All these reports underline the importance of DHI. However, a recent study postulated that quinone-amine conjugation should be a major driving force for PDA formation rather than the DHI-based oligomerization.[63] The dispute might arise partly from the variations in experimental conditions. The formation of PDA can be affected by a couple of factors, including monomer concentration, buffer and pH, and the existence of an oxidant.[58] Nonetheless, the mainstream opinion is that both covalent and noncovalent interactions are involved in PDA formation. This has been recently validated by Messersmith group using single-molecule force spectroscopy. As the authors believe, PDA films are a polymer in essence, since they are composed of high-molecular-weight polymeric chains with covalently linked subunits, while simultaneously showing weak, reversible, noncovalent intramolecular interactions.[64]

2.2. Phenolic Chemistry

Mussel-inspired PDA and its derivatives are abundant in catechol and o-quinone groups. These two kinds of chemical groups are interconvertible through a semiquinone structure,[65–66] a property that, when combined with the versatile chemical reactivity of catechol and quinone, endows PDA with a variety of capacities, including strong and substrate-independent adhesion and the ease for secondary material functionalization, etc.[1,67–68]

2.2.1. Versatility and Chemical Reactivity of Catechols

PDA and its derivatives have exhibited impressive adhesiveness toward a diverse range of material substrates, regardless of their surface properties, sizes, and shapes. Numerous studies have been performed to disclose the precise mechanism of this behavior, with catechol found to have played a critical role.[69] The diverse reactivity of catechol groups is illustrated in **Figure 3**. On the one hand, the aromaticity allows for the interplay with aromatic compounds and many cations (sodium, ammonium, etc.) via π–π stacking and cation–π effect, respectively.[70–71] On the other, the OH groups of catechols form hydrogen bonds with a multitude of inorganic and organic materials, or alternatively, bind to metals and metal oxides via coordination.[65,67] The effectiveness of the latter mechanism is highly dependent on pH.[14,72] Catechols form relatively strong and long-lasting bidentate hydrogen bonds with diverse hydrophilic surfaces at lower pH conditions. According to Bell theory,

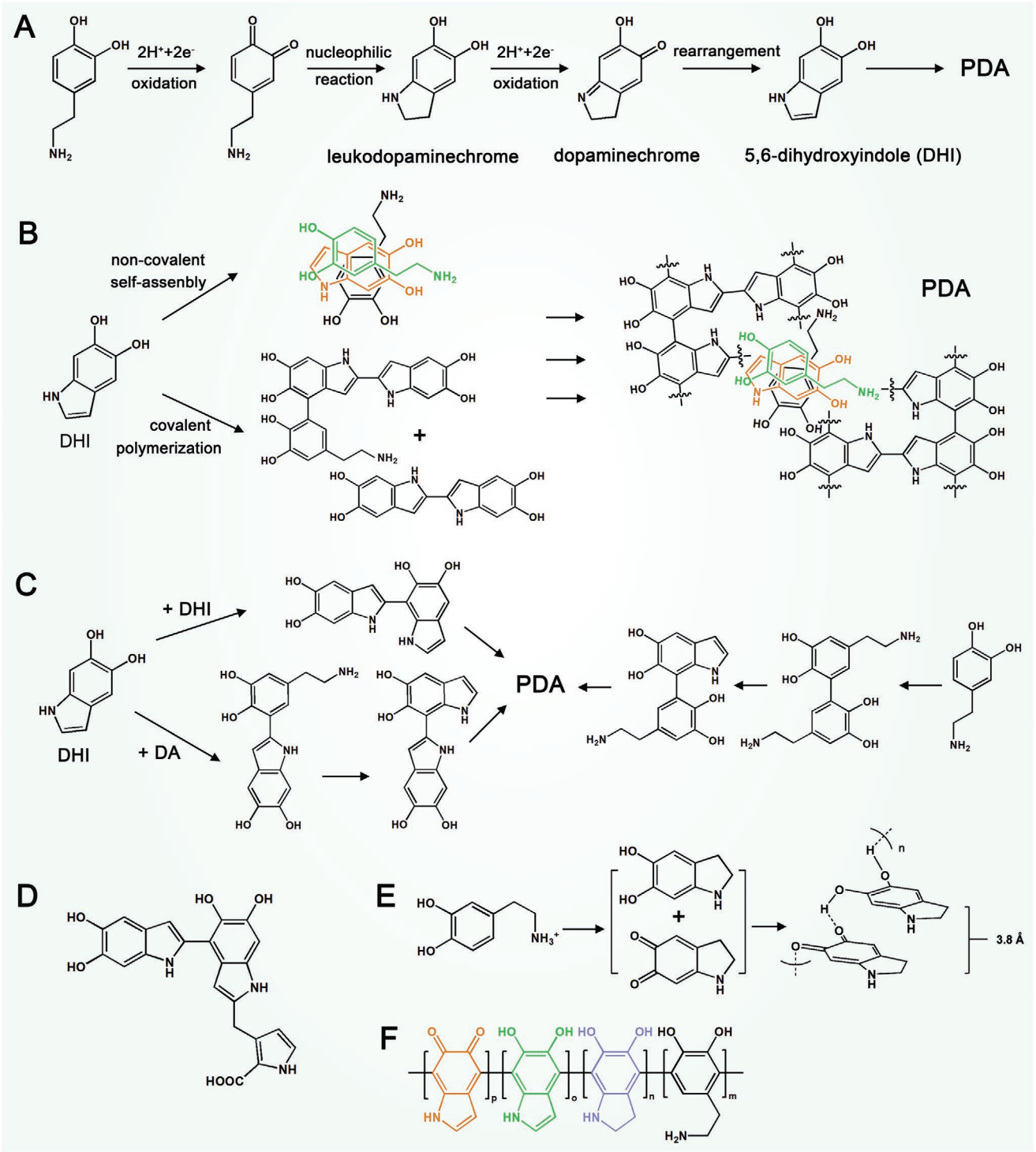

Figure 2. Plausible mechanisms involved in PDA formation.

the lifetime of bidentate hydrogen bonds is predicted to be 10^6 folds greater than that of the monodentate.[21,73] This interaction is disrupted at higher pHs as the aryl OH groups deprotonate. Nonetheless, it does not necessarily cause declines in substrate adhesion, because the loss of hydrogen bonds could be compensated by much stronger coordinate crosslinks. For instance, it was found that the adhesion strength of Mfp-3f, a catechol-rich adhesive protein of mussel adhesive plaque, to titanium oxides decreased significantly as the pH was changed from 3 to 5.5, but it was gradually restored when the pH was elevated to >7.0.[74] It is noteworthy however that such alkali-mediated curing effect contributes only when catechols have been preabsorbed to a

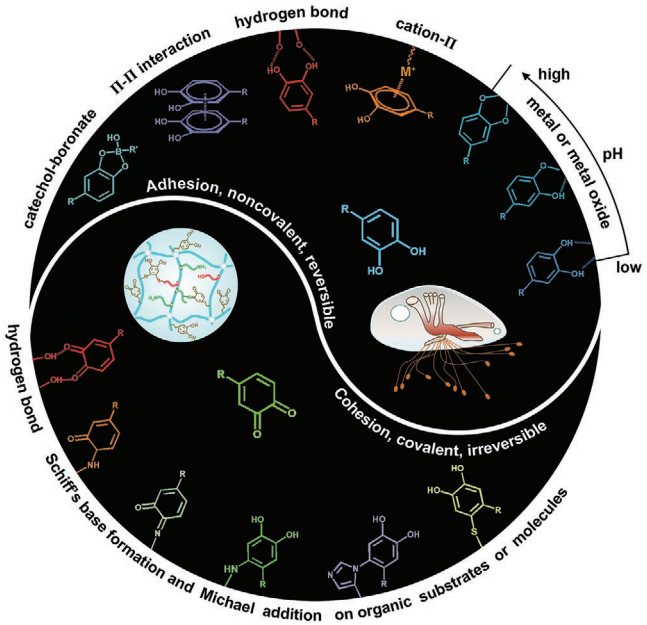

Figure 3. The versatility and reactivity of catechol and quinone groups. The diverse reactivity of catechol groups includes the pH-dependent coordination to metal or metal oxides, the cation–π effect with special cations, the hydrogen bonding to molecules or surfaces as catechol/donor, the π–π stacking with other aromatic moieties, and the reversible complexation to boronate. The reactivity of quinone groups includes the hydrogen bonding to molecules or surfaces as quinone/acceptor, and the covalent bonding to organic molecules or substrates via Schiff base reaction, and Michael addition with amines and thiols.

surface. In other words, catecholic molecules must adhere to a substrate prior to the occurrence of oxidative or coordination-mediated curing, as induced by an increasing pH.[21] Similarly, catechols can assume mono-, bis-, and tris-chelation to metal ions as the pH decreases.[75–78] In this sense, the interactions between PDA and substrate material could be easily regulated by pH-triggered protonation and deprotonation of catechols.

Furthermore, catechols interact with boron acids and silyl species in a reversible way (despite some degree of covalent bonding),[79–81] which could be readily leveraged for synthesizing various advanced dynamic materials (see details in Section 3.2). Another attractive merit of catechols is their redox activity, which is sufficient to reduce some noble metal ions such as Ag^{+}, Pt^{3+}, Pd^{2+}, and Au^{3+}.[49,82–84] This character, along with the mentioned metal-chelating ability, has found use in in situ synthesis of diverse functional materials, such as the hydroxyapatites, metal oxides, metal nanoparticles, and metal-doped materials, which hold great promise in practical fields, ranging from biomaterials and nanomedicine to energy storage and conversion.[49,85–88]

2.2.2. Synergy between Phenolics and Amines in Mussel Adhesion

Importantly, noncovalent interactions alone are insufficient to explain the strong, robust, yet material-independent adhesiveness of PDA, especially considering that amine-deficient catechol monomers lack equivalent adhesion behaviors. To give insights into the precise adhesion mechanism, control studies utilizing different catechol analogues have proven helpful. For instance, when DA and its analog hydroxytyrosol were employed for coating, only the former led to a visually detectable coating.[58] In a work from Lee group, poly(catecholamine) coatings demonstrated adhesive strength 30 times greater than that of poly(catechol) coatings.[89] These studies suggest a synergistic action between catechols and amine groups in mussel-mimetic adhesion. Further work revealed an adaptive synergy between catechol and vicinal lysine (a cationic amino acid residue in Mfps) under seawater through salt displacement.[18,76] Specifically, the amine groups in lysine can act as a molecular vanguard to evict surface hydration layers, which would otherwise disable efficient catechol bidentate binding. While being well demonstrated, a controversy persists as to the role of the adjacency of catecholic and cationic moieties on the synergistic effects. A very recent work from Messersmith group aims to address this question.[19] The authors compared the adhesion strength of separate monomers with decoupled amino and catechol moieties to that of catecholamines, where catechols and amines are coupled in the same monomer side chain. Importantly, optimal cooperative effects were observed only in the latter case, as indicated by the significantly improved macroscopic adhesion performance. In addition, amine groups can amplify the cation–π interplays of DOPA, serving as a contributor to cohesion.[70] Intriguingly, the mentioned synergistic effect seems to also hold true for polyphenol systems, where the presence of amine groups significantly enhanced the coating formation ability and stability of PG coatings.[90] Yet, it is worthy to note that some amine-free catechols and polyphenol analogues can still adhere to substrates and form coatings under tailored conditions, for example, with a proper pH value or by addition of salts or transition metal ions. These shall be detailed below.

2.2.3. "Polymerization" of Amine-Free Phenolics

Some amine-free catechols, polyphenols and analogues also possess the ability to develop multifunctional coatings. However, the substrate adhesion and coating stability are closely correlated to experimental factors, including pH, precursors, salts, UV irradiation, and additional chemicals.[11,91] For example, coating using extracts of cacao bean proved much more effective in buffered saline (0.6 M NaCl, pH 7.8) in comparison to pure water.[11] When PG and TA were employed as the precursor to coat Au and titanium dioxide, the former resulted in an inferior coating in regard to thickness (20 nm for PG vs 65 nm for TA in 8 h).[11] Additionally, a slight increase of pH from 7.8 to 8.0 would largely eliminate the adhesion of both TA and PG coatings.[91] In contrast to PG, GA, bearing a carboxyl on phenyl ring, failed to develop coatings. The failure could be ascribed to the altered electronic structure and elimination of the potential reaction site on phenyl ring.[91] This issue can be bypassed by assistance of UV irradiation. Accumulating evidence showed the capability of UV light to trigger rapid deposition of GA, as well as another carboxyl-containing phenolic compound caffeic acid.[46,92] It is interesting to note that UV not only accelerates the polymerization kinetics but also imparts exceptional spatiotemporal control over coating deposition. In a very recent

report, $CuSO_4/H_2O_2$ was also employed to promote poly(caffeic acid) formation.[93] To attain increased cohesion in coating, it is fruitful to copolymerize catechols/polyphenols with amine-rich compounds.[94–95] For instance, hexamethylenediamine has been recently added to caffeic acid to allow a more stable poly(caffeic acid) coating to form.[94]

Owing to the versatile chelation ability, phenolic monomers such as TA can coordinate with a variety of metal ions, providing a new material-independent surface modification strategy referred to as MPNs.[10] A prominent advantage of MPNs surface chemistry is its rapid kinetics, which allows coating/film formation in seconds. Recently, spatiotemporally tailorable formation of MPNs has also been accomplished, which will be described in Section 3.5.

2.2.4. Versatility and Chemical Reactivity of Quinone

The oxidation of catechol to o-quinone is an essential step in mussel-inspired polymerization. As catechol is oxidized to quinone, the intermolecular interfacial hydrogen bonding would switch from the mode of catechol/donor to quinone/acceptor.[65] The quinone moieties endow catecholic polymers with great chemical reactivity. Quinones can react with amine- or thiol-molecules via Michael-type addition and/or Schiff base reaction, affording covalent linkages to various organic substrates/molecules (Figure 3).[96–97] This property, coupled with the operational simplicity and mildness in reaction, has made PDA and derivatives widely useful in surface grafting. For example, Sheng et al. demonstrated that the polymerization of DA on self-assembled octadecylamine bilayers can lead to the formation of well-defined asymmetric Janus nanosheets (named after the two-faced Roman God) with hydrophilic PDA and hydrophobic alkylchains on opposing sides.[43] From another point of view, the intermolecular Michael addition (or Schiff base reaction) between quinones and monomer DA should have also contributed to the strong cohesion of PDA materials. Considering their cooperative roles, it is critical to seek a balanced point in the ratio of catechol/quinone so as to accomplish desirable adhesion, cohesion, and material functionality.

2.2.5. Reversibility for Development of Dynamic Materials

The catechol chemistry features several dynamic processes, briefly encompassing: i) pH-dependent catechol–metal complexes; ii) pH-dependent catechol–boronate complexation; iii) reversible catechol–silyl reaction; and iv) interconvertible catechol and quinone moieties. Precise control of these processes is nontrivial to the development of smart dynamic materials, as shall be detailed further in Section 3.

2.3. Conditions for Phenolic Polymerization/Assembly

2.3.1. Classical Conditions for Catechol Polymerization

Typically, the polymerization of DA is implemented under weak alkaline conditions involving oxygen as the oxidant. This would result in simultaneous deposition of both PDA coating (on a substrate) and nanoparticles (in solution) in ≈24 h (**Figure 4**A). The rate-determining step is the abstraction of a hydrogen atom from the deprotonated hydroxyl by oxygen, which can be affected by pH, temperature, DA concentration, and the abundance of oxygen.[98] In a nutshell, PDA develops more rapidly in an mild alkaline condition in contrast to a neutral-to-acidic one. Increasing DA concentrations expedites PDA coating, and verse visa. Higher concentration of O_2 leads to highly uniform, ultrasmooth PDA coating via accelerated reaction kinetics.[99] In addition, the thickness of a PDA coating increases over time before it starts to level off, but the kinetics is dependent on other factors (see details in Section 4). The constituent of buffer affects the way how PDA forms as well. For example, Tris buffer has been reported to be more or less incorporated into the final products.[58]

2.3.2. Special Conditions for Catechol Polymerization

The canonical DA polymerization has encountered some limitations. It is incompatible with alkali-sensitive materials, and its slow kinetics adds cost to large-scale production. Modified polymerization strategies on the basis of special conditions have been increasingly researched and implemented to address these issues. For example, UV-irradiation, microwave, and microplasma electrochemistry are employed to accelerate DA polymerization through the generation of free radicals (Figure 4B, a–c).[27,28,100,101] Alternatively, the electrochemical polymerization of PDA has been reported, which utilizes electrons from electrodes to drive DA-to-DHI oxidization and subsequent oxidative coupling, boding well for rapid surface functionalization of conductive materials (Figure 4B, d).[102,103] Moreover, the introduction of a hydrothermal condition was able to potentiate DA polymerization at even pH = 1 (Figure 4B, e).[30]

Innovations have also been made as to how to apply the coating to a surface. Unlike the common dip coating process, Lee group[104] found that, by spray coating, it took only 1 min to obtain a 20 nm thick PDA film. Given the ultrafast kinetics and minimal monomer dosages required, this method is advantageous for large-scale surface modification of bulk substrates (Figure 4B, f). Very recently, microfluidic technology has received attention for controlled polymerization of DA.[35,105] For example, the flow of DA solution through a double-crossing step gradient led to a covalently conjugated gradient of PDA.[105] Particularly, superfast preparation of PDA nanoparticles with tunable sizes and monodispersity has been enabled by an innovative yet relatively simple microfluidic device.[35] As shown in Figure 4B, g, the device is composed of three sequentially aligned glass capillaries. DA solution flew within the inter capillary and was then mixed with the outer one containing NaOH fluid to initiate the polymerization. At a certain distance, the polymerization was terminated by HCl. The high-precision control of the distance enabled easy tuning of the size of PDA nanoparticles. In addition to the solution per se, the mist of DA solution has the ability to form membrane. As a prominent example, Mun et al. reported that, by using the atmospheric pressure plasma and DA mist, a ≈536 nm thick polymer film could be deposited in 60 s.[29]

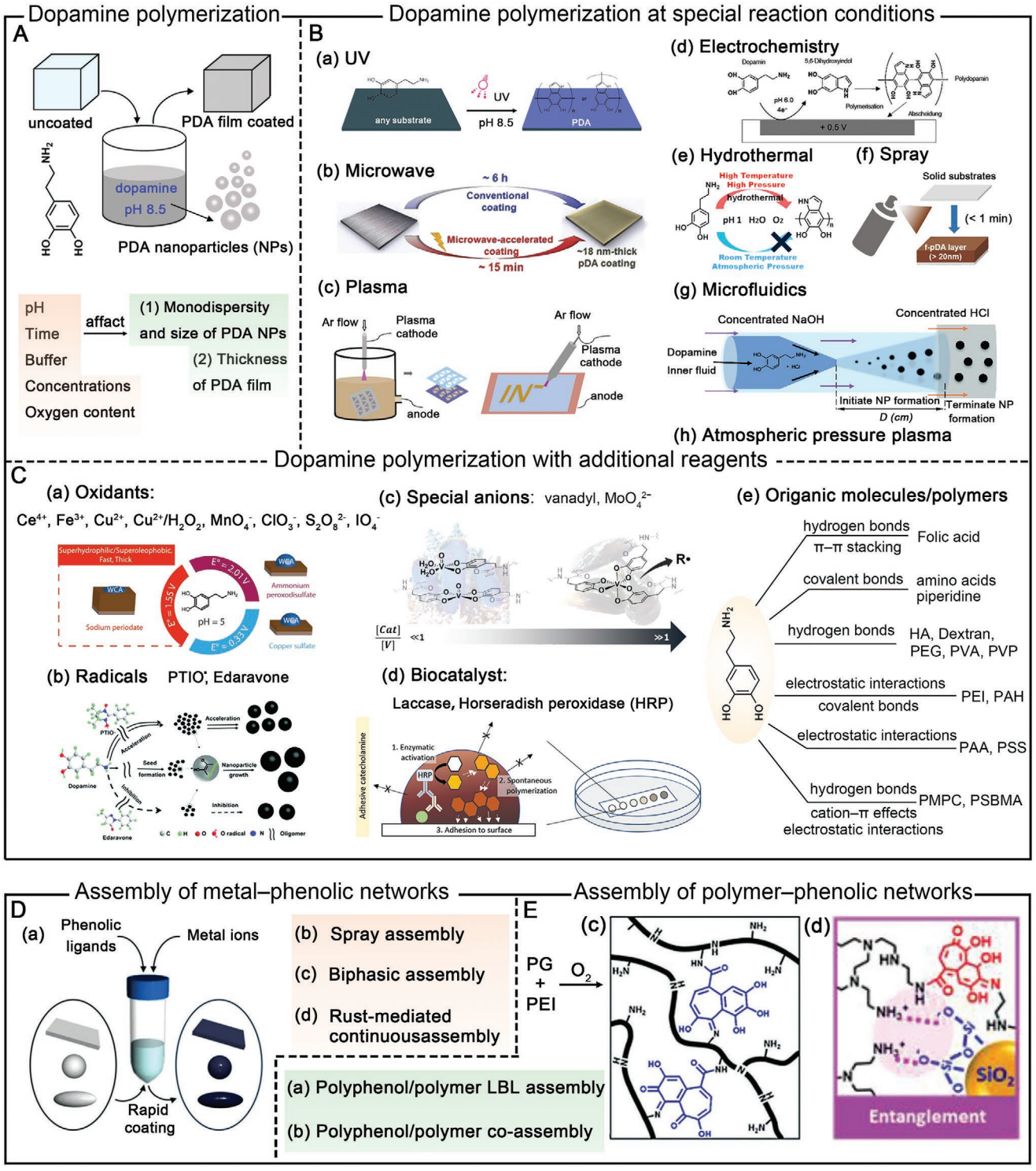

Figure 4. A–C) Polymerization of DA at different conditions. (A) Classical polymerization.[2] (B) Modified polymerization under special conditions. a) UV irradiation. Reproduced with permission.[100] Copyright 2015, The Royal Society of Chemistry. b) Microwave irradiation. Reproduced with permission.[28] Copyright 2017, Wiley. c) Plasma treatment. Reproduced with permission.[101] Copyright 2017, The Royal Society of Chemistry. d) Electrochemical stimulation. Reproduced with permission.[103] Copyright 2012, Wiley. e) Hydrothermal treatment.[30] f) Spray coating. Reproduced with permission.[104] Copyright 2016, Wiley. g) Microfluidics. Reproduced under the terms of the Creative Commons Attribution-Non Commercial 3.0 Unported Licence.[35] Copyright 2020, The Royal Society of Chemistry. h) Atmospheric pressure plasma.[29] (C) Modified polymerization with additional reagents. a) Oxidants. Reproduced with permission.[25] Copyright 2016, American Chemical Society. b) Radicals. Reproduced with permission.[26] Copyright 2019, The Royal Society of Chemistry. c) Special anions. Reproduced with permission.[113] Copyright 2014, American Chemical Society. d) Biocatalysts. Reproduced with permission.[116] Copyright 2020, Wiley. e) Organic molecules or polymers (hyaluronic acid (HA), poly(ethylene glycol) (PEG), poly(vinyl alcohol) (PVA),

2.3.3. Catechol Polymerization Assisted with Additives

The inclusion of unique reagents is also a valuable approach to regulate the polymerization of DA, aimed at altered deposition dynamics and tailored structures and properties of PDA.[25,106–111] On the one hand, many oxidants, such as Cu^{2+}, ClO_3^-, $S_2O_8^{2-}$, and IO_4^-, have shown an impact on PDA deposition (Figure 4C, a).[25,111] Especially, Cu^{2+} not only helps oxidize DA to DA quinone and trigger subsequent polymerization,[107] it also favors the selective formation of 2,2′ dimers of DHI.[112] Ball et. al. found that the PDA materials obtained by oxidization of DA in air and by Cu^{2+} had distinct optical and colloidal properties.[107] Likewise, reactive oxygen species can also accelerate the polymerization. It is worth noting that, besides the in situ generated free radicals, the introduction of either stable free radicals (e.g., PTIO•) or free radical scavengers (e.g., edaravone) can tune the polymerization process for size-controllable synthesis of monodispersed PDA nanoparticles (Figure 4C, b).[26] The former accelerated the seed formation process, whilst the latter inhibited the seeding and subsequent growth of PDA, both leading to decreased particle sizes.

On the other hand, anions such as vanadyl and MoO_4^{2-}, have been adopted to modify the polymerization of DA.[37,113] The chelation between MoO_4^{2-} and catechol enables morphology control of PDA (see Section 6). As for vanadyl, its effect is related to the ratio of [vanadyl]/[catechol] (Figure 4C, c).[113] An excess of catechol can trigger more organic radicals to allow a greater degree of chemical crosslinking. Contrarily, excessive vanadium confines catechols in the chelates, inhibiting the polymerization. Biocatalysis is able to accelerate the oxidation and polymerization of DA.[114] For example, Li et al. found that horseradish peroxidase could expedite the polymerization of DA by 300 times.[115] More importantly, the ultrafast and localized deposition of PDA at the target catalytic sites can lead to biosensors with enhanced sensitivity in biological detection and highly concentrated colorimetric signal for spatial biomarker labeling (Figure 4C, d).[115–116] Furthermore, organic molecules, including folic acid,[36] amino acids,[117] pyridine,[118] hexamethylenediamine,[119,120] and polymers[121] (e.g., polycations, polyanions, nonionic polymers, polysaccharides) are all potent additives to tailor the structures and properties of PDA for desired utilities (Figure 4C, e).

All these approaches could provoke the polymerization of DA, but each has its pros and cons. In cases where special conditions are employed, the resultant PDA materials usually feature a similar chemical structure and property as compared to those fabricated in a standard condition. The same might not be true in approaches that include an additional reagent, which would likely interact with the building blocks via oxidative degradation, chelation, or nucleophilic addition. The generated PDA-based coatings or nanoparticles, however, could find new utilities in biomedicine, catalysis, energy storage, and other fields.[117,122–126]

2.3.4. Assembly of Polyphenols

The introduction of polyphenols with a polymerization or assembly character akin to DA-based compounds has significantly expanded the family of phenolic materials. Besides their self-assembly ability, as already discussed in Section 2.2.3, multidentate phenolic ligands can coordinate strongly with metal ions to rapidly form an MPN coating on variety of substrates (Figure 4D). Besides the dip-coating approach, other techniques, including spray assembly, biphasic assembly, and rust-mediated continuous assembly, have been pioneered for the engineering of MPNs. These have been recently well documented[10] and will not be discussed further here. In addition, some polyphenols (e.g., TA) can form hydrogen and/or electrostatic bonds with biomolecules and synthetic polymers (e.g., chitosan), allowing for layer-by-layer construction of functional films. Specially, copolymerization of polyphenols with polymers that bear amines is possible, given the reactivity of polyphenol–quinones toward amino groups (Figure 4E). For example, hexamethylenediamine was efficient to crosslink GA and form coatings on different substrates.[95] Recently, Lee and co-workers demonstrated that atmospheric oxygen is effective to trigger a rapid oxidative crosslinking between PG and polyethylenimine (PEI), leading to the formation of robust adhesive self-sealing PG/PEI films (Figure 4E, c).[51] By further inclusion of oxygen-delivering silica agglomerates into a polyphenol–PEI copolymerization system, the same group prepared superglues with impressive mechanical properties and versatile adhesive properties.[127] The synergy of polyphenol with amine-rich polymer resulted in strong mechanical properties and versatile adhesive properties, showing new prospects in the development of gels and carbon materials.

2.4. Properties of Catechol/Polyphenol Derived Materials

As a typical poly(catecholamine) polymer, PDA exhibits many important properties, including, among others, robust adhesion, high reactivity, photothermal effect, biocompatibility, and biodegradation (in detail reviewed in refs. [1,98]). These physicochemical properties are closely related to their chemical structure and composition, and most of them will be further discussed in later sections with regard to how they can be tailored. In this section, we highlight the antioxidant properties of phenol-based, melanin-like polymers.

PDA resembles melanins in structure and property. Melanins are distributed throughout the human body, such as hair, eyes, epidermis, muscles, and viscera.[128] The most remarkable aspect of melanins is their ability to scavenge radical species.[129] And the degree of activity is largely determined by the structure of as-formed polymers. In a pioneering study, the structure–property relationship of DHI and 5,6-dihydroxyindole-2-carboxylic acid (DHICA) melanins was well elucidated.[130]

poly(*N*-vinyl pyrrolidone) (PVP), polyethyleneimine (PEI), poly(allylamine hydrochloride) (PAH), poly(acrylic acid) (PAA), poly(styrene sulfonate) (PSS), poly(sulfobetaine methacrylate) (PSBMA), poly(methacryloyloxyethyl phosphorylcholine) (PMPC), pyrogallol (PG)). D) Methods for assembly of MPNs. Reproduced with permission.[10] Copyright 2019, Wiley. E) Assembly of polymer-phenolic networks via a) layer-by-layer (LBL) assembly and b) coassembly methods. c) Schematic reactions for crosslinking in PG/PEI copolymer. Reproduced with permission.[51] Copyright 2020, Wiley. d) Polymeric entanglement of PG/PEI network on surfaces of silica particles. Reproduced with permission.[127] Copyright 2020, Wiley.

DHICA melanin was found to be a far more efficient scavenger than DHI and DOPA melanin. This superiority is attributed to hindered interunit conjugation and weak aggregating interactions derived from the twist inter-ring oligomeric angles. This microstructure accounts for strong accessibility of free radicals in comparison with the compact π-stacked DHI melanin. This discovery shed light on a promising approach to improve the ROS scavenging activity of PDA materials. Recently, Yang et al. reported that introduction of amino acid can destroy the compact microstructures of PDA, leading to formation of weak aggregate structures with super antioxidant effects.[117] It should also be noted that, unlike PDA with strong substrate adherence, poly(DOPA) usually experiences difficulty in forming adherent films by spontaneous autoxidation of DOPA. However, in a report from Messersmith group, adherent poly(DOPA) films were formed on a variety of substrates at high ionic strengths.[131]

The ability to scavenge free radicals is one of the most celebrated features of plant polyphenols, which is associated with their abundant hydroxyl groups on the benzene ring.[132] Kim et al. found that GA functionalized poly(2-hydroxyethyl methacrylate) hydrogel had greater antioxidant activity compared to DA-functionalized counterpart.[133] Importantly, the antioxidant activity of polyphenols can also be inherited by their coating forms. The coating and ROS-scavenging abilities of plant polyphenols were fully leveraged by Messersmith group.[11] Impressively, they demonstrated that TA-modified culture plates could assist NIH 3T3 fibroblasts that grew on them to combat intracellular radical stress. Such intracellular protective effect was attributed to the liberation of dissolved polyphenols into media.

3. Control of Phenolic Chemistry

Organisms in Nature, such as marine mussels and sandcastle worms, can actively secrete unique catechol-containing adhesive proteins to help implement two underwater activities: i) to bind or absorb to a substrate via interfacial adhesion, and ii) to bond or glue materials together via cohesion.[23] This brings up the necessity of optimizing catechol contents, e.g., by tuning the catechol/quinone conversion, to achieve an ideal adhesive–cohesive balance. Given that catechols can be easily oxidized to quinones, it is of ultimate importance to prevent their exposure to hostile oxidants, especially in the synthesis and application of catechol-containing polymers. Protecting chemistry and confined polymerization are useful strategies to counteract such a liability. On the other hand, the abundant catechol groups can reversibly chelate metal ions, boding bell for the development of dynamic materials. This section is dedicated to deal with the above issues.

3.1. Tunable Catechol/Quinone Transformation

The diverse reactivity of catechol and quinone moieties is the foundation for the development of materials with dynamic adhesion, robust cohesion, and versatile surface functionality (**Figure 5**A, a). Catechol/quinone conversion can be realized by using various strategies, which are illustrated in Figure 5A, b. Redox reactions and annealing have been applied to promote the oxidization of catechol to quinone. Reversible switching of catechol and quinone moieties has been achieved with the aid of charged nanospace, external electrical field and plasmon effects. Michael-type addition enables the conversion of quinone to catechol, while facilitating the curing of catechol-based materials via covalent crosslinking. Examples of recent advances in catechol/quinone conversion and the corresponding applications will be highlighted in this section.

3.1.1. Catechol-to-Quinone Oxidization

Catechol is convertible to quinone through three general pathways: auto-oxidation, enzymatic oxidation, and chemical oxidation (Figure 5B, a).[96,134] Auto-oxidation here refers to spontaneous oxidation by air O_2. By contrast, enzymatic oxidation using tyrosinase and horseradish peroxidase/H_2O_2 can help circumvent the huge energy barrier encountered in auto-oxidation. Noticeably, not only catechol but also monophenol could be converted to o-quinone by using tyrosinase. Chemical oxidants, such as $NaIO_4$, $(NH_4)_2S_2O_8$, and $FeCl_3$, are also frequently adopted to drive the oxidation of catechol toward quinone. In addition, the conversion can be promoted by thermal annealing. Sun et al. found that quinone-rich PDA could be obtained when they treated the polymerization system simultaneously with heat and $(NH_4)_2S_2O_8$, both of which had a role on catechol-to-quinone oxidation (Figure 5B, b).[135] Considering that the oxygen atom in o-quinone can effectively coordinate with lithium or sodium ions, quinone-rich PDA promises efficient electrode material in the fabrication of lithium- or sodium-ion batteries for energy storage (Figure 5B, c).[135,136] Impressively, as contrasted to counterpart electrodes using classic PDA, superior capacities of 1818 mA h g^{-1} (lithium-ion batteries) and 500 mA h g^{-1} (sodium-ion batteries) were afforded by using quinone-rich PDA annealed at 180 °C (Figure 5B, d). Notwithstanding, the following deserves attention: although a higher capacity is favored by abundant quinone species, excessive oxidation would presumably counteract the conductivity, thus deteriorating device performance.

The conversion of catechol to quinone was also achieved by mild post-annealing of PDA at 130 °C.[137] The elevated quinone amounts facilitated the attachment of nucleophiles to PDA coatings. Simultaneously, annealing was found to enhance the intermolecular and cohesive interactions in PDA. In consequence, it led to enhanced mechanical robustness and the chemical stability against alkalinity (Figure 5B, e).

3.1.2. Dynamic Catechol/Quinone Conversion

The dynamic catechol/quinone conversion greatly affects the performances of catechol-based dynamic materials, including adhesives and glues. In fact, mussel retains its long-term adhesiveness by a reductive footprint protein with a dynamic catechol/quinone balance.[23] Mimicking this, Lu group devised a tough and reusable hydrogel composed of Ag–lignin

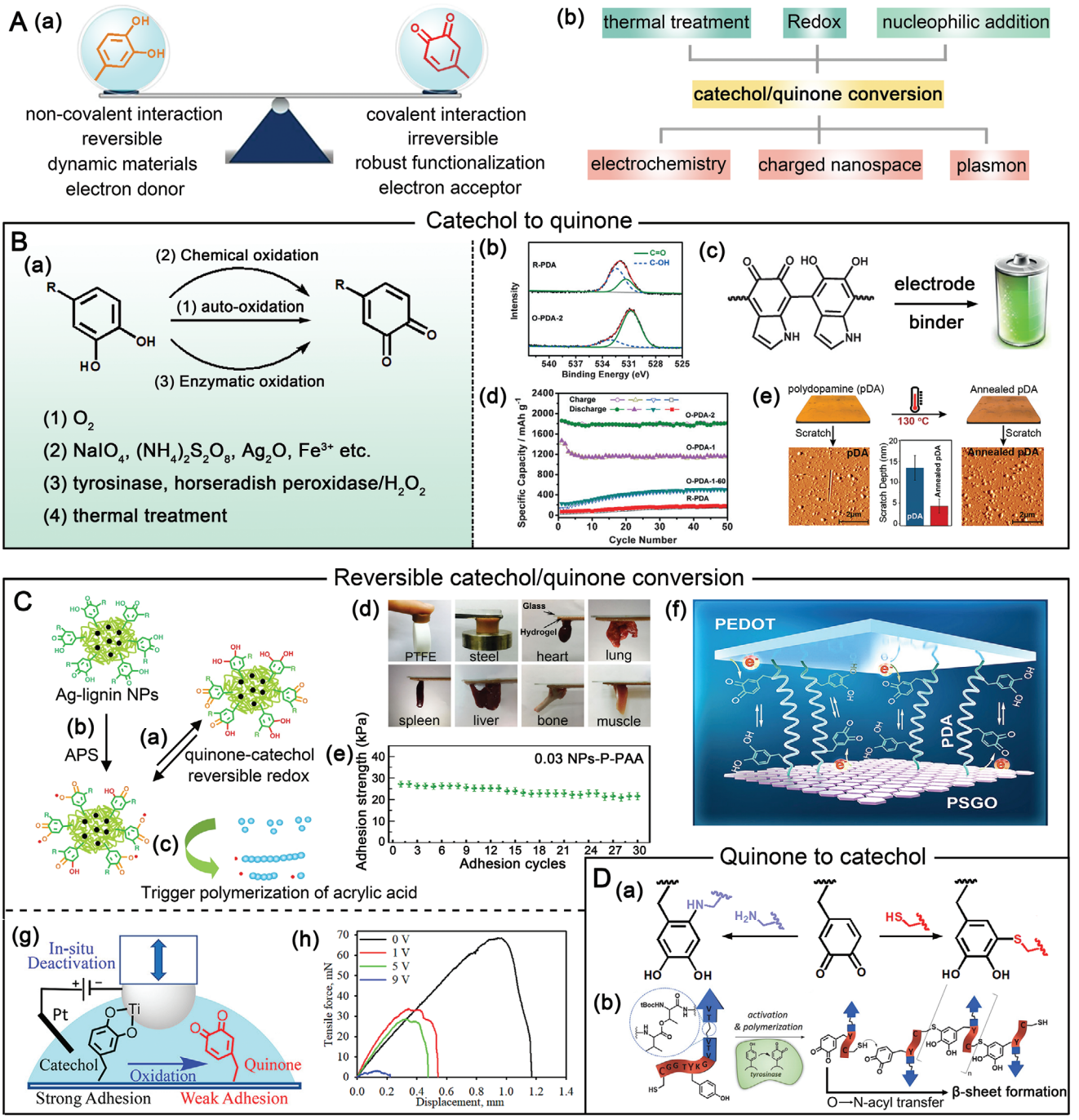

Figure 5. A) a) Characteristics of catechol and quinone, and b) strategies for catechol/quinone conversion. B) Catechol-to-quinone oxidization. a) Overview of strategies. b) Comparison of the O 1s XPS spectra of PDA obtained at different conditions. c,d) PDA samples used as the electrode and binder materials for lithium-ion batteries with different performances. Reproduced with permission.[135] Copyright 2016, Wiley. e) Comparison of the mechanical property of PDA before and after annealing. Reproduced with permission.[137] Copyright 2019, American Chemical Society. C) Reversible catechol/quinone conversion. a) Reversible catechol-quinone redox by plasmon effect. b) Radicals generated by the redox between Ag–lignin NPs and ammonium persulfate (APS) for c) triggering the gelation of the hydrogel. d) Hydrogels adhered to various substrates. e) Repeated adhesion behaviors to porcine skin. Reproduced under the terms of the CC-BY license.[138] Copyright 2019, The Author(s), Published by Springer Nature. f) Reversible switching of quinone–catechol in charged nanospace between PEDOT and PSGO. Reproduced with permission.[139] Copyright 2019, Wiley. g) Scheme of the in situ deactivation of catechol-containing adhesive using electrochemistry. Reproduced with permission.[142] Copyright 2020, American Chemical Society. h) Typical JKR contact curve testing performed with in situ applied voltages for 1 min. D) Conversion from quinone to catechol via a) Michael-type addition and b)Thiol-Michael-addition inspired crosslinking. Reproduced under the terms of the CC-BY license.[144] Copyright 2020 The Authors. Published by Wiley-VCH.

nanoparticles (Figure 5C, a–e).[138] The phenolic groups in lignin reduced Ag^+ to Ag nanoparticles (AgNPs), while themselves were oxidized to quinones. As AgNPs are typical plasmonic metal NPs, the surface plasmon resonance of Ag–lignin NPs allowed free electrons to be relayed to quinone and reduce the latter to phenolic groups. In this way, a dynamic redox environment can be established inside the hydrogel network. In addition, radicals generated by the redox reaction between Ag–lignin NPs and ammonium persulfate can trigger self-gelation of the hydrogel under ambient environment. Thanks to the coexistence of covalent and noncovalent interactions, this hydrogel exhibited adhesiveness to a variety of substrates (Figure 5C, d). The inner dynamic redox balance was recognized to account for the repeatable and long-term adhesiveness (Figure 5C, e). Gaining insights from this study, dynamic catechol/quinone redox chemistry is achievable through a designer electron transfer process.

Very recently, a confined nanospace-charged layer has also been constructed to tune the content of catechol/quinone by control of electron transfer (Figure 5C, f).[139] Specifically, PDA and sulfonate cofunctionalized graphene oxide (PSGO) was used as template to direct poly(3,4-ethylenedioxythiophene) (PEDOT) assembly, which resulted in sandwich-like PSGO–PEDOT nanosheets. Importantly, the nanosheets formed a confined space-charge layer between the electron-enriched PSGO and electron-depleted PEDOT, permitting a dynamic switching in-between the "quinone" and "catechol" statuses.

In addition, the catechol/quinone redox could be manipulated by applying a sufficiently positive or negative potential.[140–141] Harnessing the electrochemically dynamic switching, Daboss et al. recently prepared a PDA-modified colloidal atomic force-scanning electrochemical microscopy probe, which could provide instrumental insights into the adhesion properties of bacteria, cells, and tissues.[141] In addition, the electrochemical catechol/quinone switching can be a facile way to in situ tailor the adhesiveness of catechol-based materials. Recently, Akram Bhuiyan et al. evaluated the effect of electrical field on the adhesive property of catechol using a Johnson–Kendall–Roberts (JKR) contact mechanics test setup (Figure 5C, g).[142] They found that an in situ electrical stimulation was efficient to deactivate the adhesive property of catechol-containing adhesive through oxidization of catechol. More elaborate control of the adhesive properties was exerted by fine-tuning the applied voltage, the exposure time to the applied electricity, and the salt concentration of the interfacial buffer (Figure 5C, h). This represents a new dimension in the design of synthetic mimics of mussel adhesive proteins. One inadequacy is that the accumulated hydroxyl ions near the cathode would facilitate irreversible cross-linking of catechol near the interface, thus compromising the reversibility of inactivated catechol.

3.1.3. Nucleophilic Addition-Mediated Quinone/Catechol Conversion

In addition to the foregoing dynamic conversion, quinone can also be transformed to catechol by its reaction with nucleophiles. Electrophilic quinone can undergo Michael addition with nucleophilic amine and thiols, while getting reduced to catechol groups (Figure 5D, a). Noteworthily, Michael addition is nonspecific and often competes with Schiff-base reaction, in which catechol is not anticipated as a product. Additionally, these reactions can be varied by a specific pH condition or the types of nucleophiles and substituents in use. Details could be found in this review.[96] In fact, the quinone-mediated Michael addition with thiols is a natural mechanism that affords the meticulous combination of adhesion and cohesion in mussel glue apparatus. Nonetheless, replicating this property is anything but easy, mainly due to the oversimplified biomimetic system of catechol/quinone. To impart better control over the adhesion/cohesion behaviors of artificial mussel-glue proteins, tyrosinase-activated polymerization has recently gained interest (Figure 5D, b).[143,144] Briefly, peptides containing cysteine (Cys) and tyrosine (Tyr) residues are synthesized. With the aid of tyrosinase, the Tyr residues can be oxidized to quinones, which then react with Cys residues in adjacent molecules via Michael addition to give crosslinked adhesive polymers.

3.2. Protection and Deprotection of Catechols

For both natural adhesive proteins and synthetic catechol-containing materials, the oxidation of catechol to quinone can sacrifice their reversible adhesion ability, thus hindering applications in high-performance adhesives and smart self-healing materials.[145,146] In light of the oxygen-susceptibility of catechol, measures for combating the oxidization have become a rising demand in the application of catechol-based adhesives. In this section, we summarize strategies for protection and deprotection of catechol groups and illustrate some of the derived applications. Generally, it is possible to temporarily mask the catechol functionalities by protecting groups, which can be removed at a specified time by an unmasking treatment. Because the removal of the mask is somehow traumatic to the structure of catecholic polymers, it is desirable to select protecting groups with a facile cleavage mechanism (i.e., under conditions as mild as possible). Some candidates include boronate, silyl, and nitrobenzyl moieties, as described below.

3.2.1. Reversible Catechol–Boronate Complexation

The fact that seawater is composed of 0.45×10^{-3} M[147] of borate provides a new clue to recapitulate the robust yet reversible mussel adhesion. Under basic conditions, boron acids form 1:1 complexes (via boronate ester linkage) with catechols, while the complexion could be reversed by decreasing the pH to the acid range.[148] This catechol–boronate chemistry has emerged as a valuable tool to engineer smart adhesives that can switch between their adhesive/nonadhesive statuses on demand.[149] Narkar et al. recently developed such an adhesive by copolymerization of catechols and boronic acid based precursors (**Figure 6**A, a).[79] Strong adhesion was secured in an acidic pH that favors catechol/borate–substrate binding. Nevertheless, the opposite is true at a basic pH as

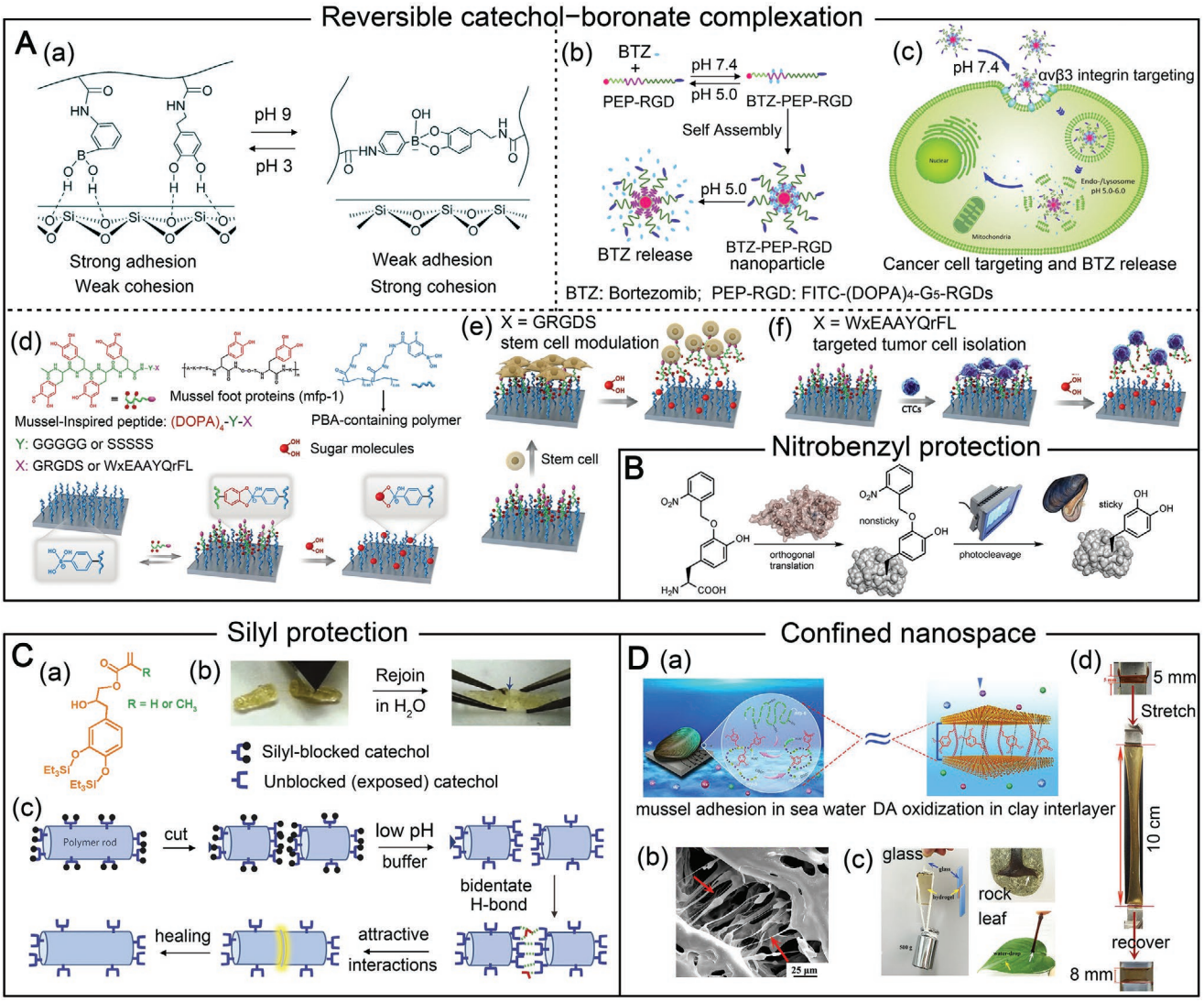

Figure 6. Protection and deprotection of catechol. A) Dynamic catechol–boronate complexation. a) Catechol–boronate complexation at basic condition reduced adhesion, while decreasing the pH to the acidic range led to strong adhesives. Reproduced with permission.[79] Copyright 2016, American Chemical Society. b,c) The pH-sensitive prodrug nanocarrier based on catechol–boronate chemistry for cancer cell targeting and drug release. Reproduced with permission.[151] Copyright 2019, American Chemical Society. d) Formation of catechol–boronate inspired dynamic biointerface and its sugar-responsiveness for applications in e) modulation of cell adhesion and f) cancer-cell isolation.[156] B) Nitrobenzyl protection of catechol for production of light-controllable biomimetic glues. Reproduced with permission.[158] Copyright 2017, Wiley. C) Silyl protection of catechol. a) Silane-protected eugenol acrylates or methacrylates serve as precursors for the preparation of b,c) self-healing polymers. Reproduced with permission.[146] Copyright 2014, Nature Publishing Group. D) Preserving catechol functionality in confined nanospace. a) The confined nanospace of mussel's plaque inspires the strategy of DA polymerization in interlayer of clay nanosheets. b) The layered architecture and interconnected networks in PDA–clay–PAM hydrogel. c) The adhesion behavior to various surfaces, and d) the stretching and recovery of PDA–clay–PAM hydrogel. Reproduced with permission.[24] Copyright 2017, American Chemical Society.

catechol–boronate complexes can be formed instead. Additionally, this chemistry has been widely exploited to prepare pH-responsive capsules,[150] assemblies,[151] and coatings,[152] which have utilities in bioimaging, cancer cell targeting, and drug delivery (Figure 6A, b,c). It has also ignited great interest in the development of self-healing materials that work under ambient humidity conditions.[153–155]

The reversibility of catechol–boronate complexation can also be established via ligand exchange that substitutes catechol. Liu et al. developed a biointerface capable of dynamic presentation of cell-binding motifs, through exploring a sugar-responsive catechol–boronate chemistry (Figure 6A, d).[156] Specifically, a mussel-inspired biomimetic peptide was synthesized, showing a catechol end and a bioactive-sequence-displaying end. The former can anchor to a phenylboronic acid (PBA)-modified substrate, making the latter available for cell recognition. Further, by addition of cis-diol group containing sugars, catechol groups were disassociated with PBA by sugar-induced molecular exchange, liberating surface-bound peptides. Through using designer bioactive peptide sequences, the resulting

biointerface exhibited activities in dynamic modulation of stem cell adhesion and selective isolation of targeted tumor cells (Figure 6A, e,f).

3.2.2. Nitrobenzyl Protection

Photoremovable protecting groups (PPGs) hold promise in eliciting spatiotemporal control over catechol chemistry.[81,157] Nitrobenzyl compounds, one of the most established PPGs, have recently been explored for producing biomimetic catechol-containing glues with light-controlled wet adhesion power in vivo (Figure 6B).[158] Specially, nitrobenzyl was applied to temporarily mask the catechol functionality, which can be recovered in response to precise light triggers. This approach surmounts the reliance on external chemicals for deprotection. However, it is faced with other issues. For example, the cleavage of protecting groups might generate hostile reactive intermediates, such as nitrosobenzaldehydes, which might induce unfavorable modifications at deprotected sites.

3.2.3. Silyl Protection

Silyl protection, classically employed to reserve oxidization-liable catechol moieties during chemical synthesis, can provide an alternative approach to tuning the reactivity of catechol-derived smart materials. The silation of catechol can be catalyzed by tris(pentafluorophenyl)borane, whereas the silyl-protecting groups could be eliminated in a moderate acid environment to restore catechol functionality.[159] With silane-protected eugenol acrylates or methacrylates as monomer, Ahn et al. synthesized catecholic polymers that were able to self-heal in water (Figure 6C).[146] Immersing the half-cut materials in a low-pH buffer rapidly regenerated catechol moieties by initiating hydrogen bonding to bridge the scission, culminating in complete wet self-mending.

3.3. Catechol Polymerization in Confined Nanospace

In the above, we have discussed various chemical approaches to mask/unmask catechols for on-demand catechol reactivity. Since catechol is oxidized by dissolved oxygen, catechol polymerization can also be tailored by means of oxygen content. Actually, mussels "perform" catechol polymerization in nanoconfined plaques, seemingly a Nature's strategy to reduce premature or excessive oxidation. Emulating this, nanoconfined polymerization of catechols has recently prompted intrigue. The core idea is to use hollow nanomaterials (e.g., nanoclays) to physically isolate DA molecules from dissolved oxygen underwater. As a notable example, Han et al. intercalated DA into the oxygen-deficient interlayer nanospace of layered double hydroxides clays (Figure 6D, a).[24] In this way, the very limited free-oxygen in the nanoclays allowed DA to be only partially polymerized. The resulting catechol-enriched PDA-intercalated nanoclay sheets were then mixed with acrylamide, the monomer for polyacrylamide (PAM) formation, to form PDA–clay–PAM double-network hydrogels with durable and repeatable adhesiveness (Figure 6D, b–d). Other nanolayered or nanospaced materials are deemed to have a similar property.

3.4. Reversible Catechol–Metal Complexes

Robust yet reversible crosslinking can be rendered via catechol–metal complexion. It has been widely documented that catechol–Fe^{3+} complexes constitute an important crosslinking mechanism of mussel glue proteins. Depending on the pH, three catechol–Fe^{3+} complexes are accessible: mono, bis, and tris (**Figure 7**A).[77,160] Specially, the noncovalent coordination bonds provide the uniqueness of being dynamic and spatially reconfigurable, as is highly desired in dynamic materials, such as toughening elastomers, batteries, and self-healing hydrogels. Generally, three approaches can allow for reversible conversion of catechol–Fe complexes: elastic deformation, pH, and redox. These have increasingly become a toolkit for constructing dynamic functional materials, as will be detailed below.

3.4.1. Catechol–Metal Mediated Dynamic Elastic Deformation

The spatial reconfigurability of catechol–Fe^{3+} chemistry has been taken advantage of to induce elastic deformation of elastomers, conferring simultaneously high stiffness and extensibility.[77,161] For example, by incorporating the reversible catechol–Fe^{3+} crosslinks into a dry and loosely crosslinked epoxy network, Filippidi and co-workers obtained a self-toughening elastomer (Figure 7B, a). The Fe^{3+}-treated networks were found to exhibit pronounced stiffness, tensile strength, and tensile toughness, which were 2–3 orders of magnitude of those of Fe^{3+}-free counterparts (Figure 7B, b). Such toughing effects arise from the high dissociation energy of catechol–Fe^{3+} coordination bonds, which is comparable to covalent bonds, while the strain recovery is attributed to the dynamic catechol chemistry. It is worth noting that the recovery is also dependent on the strains applied. Upon small strains ($\varepsilon < 30\%$) that fell within the shape-memory capacity, the network can be fully restored to the unstretched state. However, with strains greater than 50%, residual strain was observed as coordinate bonds broke and deformed at newly accessible sites (Figure 7B, c).

Such self-healing capability of catechol–Fe^{3+} complexes is useful in designing batteries that can undergo large-volume changes. Specifically, the lithiation/delithiation is usually accompanied with large volume expansion that is detrimental to battery performance. The dynamic and robust catechol–Fe^{3+} coordination can withstand large strain and thus the volume change. Recently, Jeong and Choi developed a copolymer binder with catechol–Fe^{3+} crosslinks, which contributed to the self-healing effects of silicon anodes (Figure 7B, d).[162] The high strength of the coordination bonds prompted the recovery of dissociated bonds during lithiation/delithiation processes, profiting the development of sustainable batteries (Figure 7B, e). Furthermore, the recoverable nature of catechol–metal ions could be extended to other metallopolymers to customize the physicochemical properties of self-healing polymers.

In addition to the reversible bonding with free ferric ions, the catechol chemistry can also work to afford dynamic interfacial

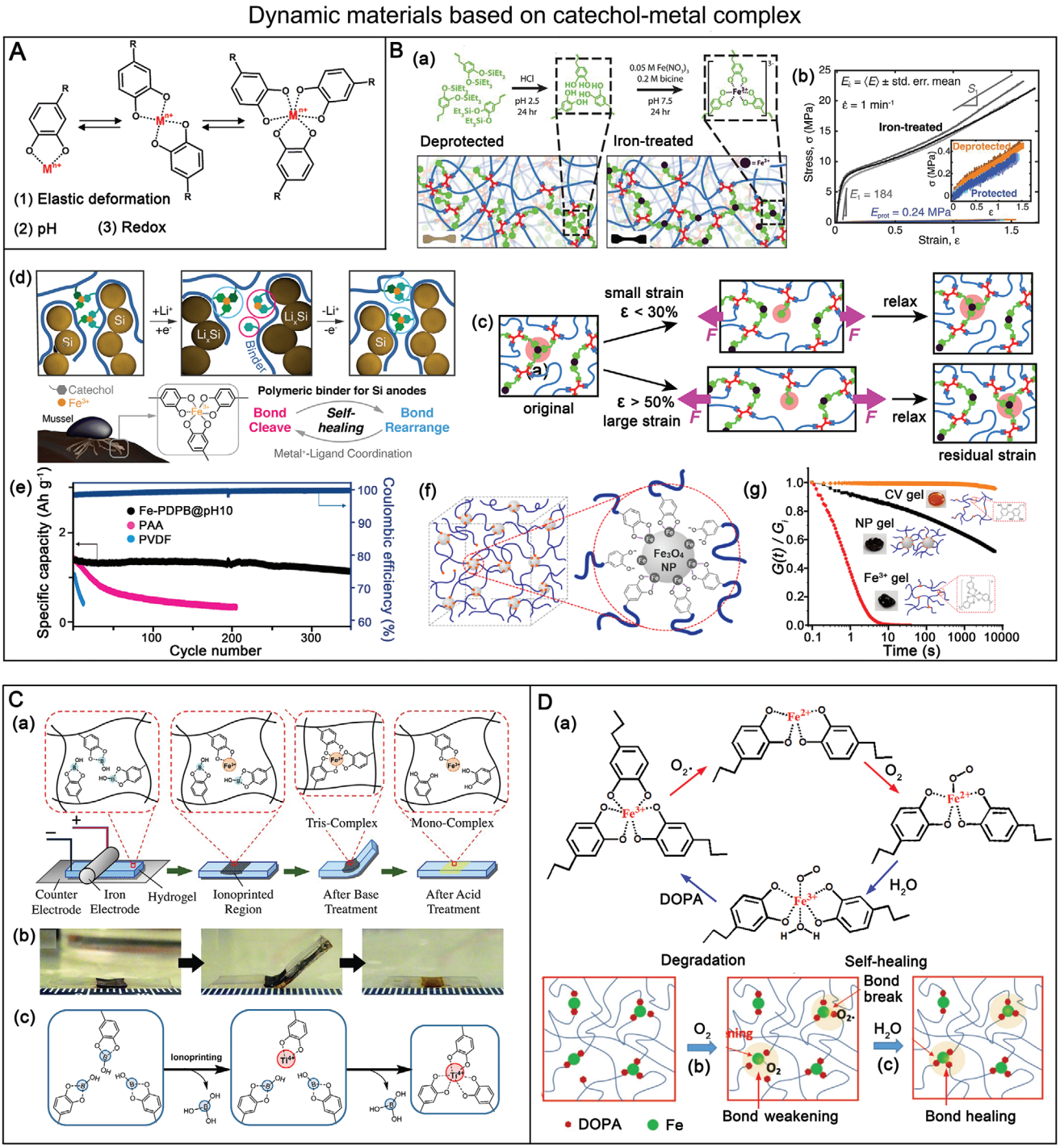

Figure 7. Reversible catechol–metal chelation and the derived dynamic materials for various applications. A) Strategies for dynamic catechol–metal chelation. B) Dynamic catechol–metal chelation induced by elastic deformation. Reproduced with permission.[161] Copyright 2017, The American Association for the Advancement of Science. a) Cleavage of silyl protecting groups and catechol–iron complex formation in the elastomers. b) Engineering stress as a function of strain of protected, deprotected, and iron-treated samples. c) Strain recovery with respect to small and large strains. d) Self-healing metallopolymers for Si anodes and the network configuration during cycling.[162] e) Performances of Si electrodes based on Fe–PDBP@pH10, PAA, and PVDF. Reproduced with permission.[162] Copyright 2019, American Chemical Society. f) Structure of Fe_3O_4 nanoparticle-crosslinked hydrogel.[163] g) Step strain relaxation curves of the NP gel, Fe^{3+} gel, and CV gel. Reproduced with permission.[163] Copyright 2016, American Chemical Society. C) The pH dependent catechol-metal coordination. a–c) Ionoprinting of Fe^{3+} or Ti^{4+} in hydrogel and the pH-dependent bending and restoration. Reproduced with permission.[164] Copyright 2014, Wiley. Reproduced with permission.[165] Copyright 2016, Elsevier. D) Dynamic catechol-metal chelation from redox. a) Changes of catechol–Fe coordination in the degradation and self-healing processes of cuticle. b,c) Adsorption of O_2 led to bond weakening and breaking while H_2O adsorption resulted in bond healing. Reproduced under the terms of the CC-BY license.[168] Copyright 2019. The Authors. Published by Wiley-VCH.

coordination with solid materials. Li et al. has reported such a dynamics in a catechol-modified polymer network that had Fe_3O_4 nanoparticles as crosslinking motifs (Figure 7B, f).[163] The resulting composite hydrogels, compared to their (intercatechol) covalently crosslinked and fluid-like ionic counterparts, showed dramatically distinct mechanical properties, featuring solid-like yet reversible hydrogel mechanics (Figure 7B, g).

3.4.2. Dynamic Catechol–Metal Complex from pH

The three pH-dependent coordination states of catechol–Fe^{3+} complexes are mono at pH < 5.6, bis at 5.6 < pH < 9.1, and tris at pH > 9.1. Self-healing materials can be prepared by leveraging the pH-responsiveness of catechol–Fe^{3+} complexes.[77] By synergizing this chemistry with an ionoprinted technique, Lee and Konst successfully created a hydrogel actuator (Figure 7C, a,b).[164] In their study, electrochemical oxidation of iron electrode led to local deposition of Fe^{3+} into catechol-based hydrogel. The catechol groups formed a tris-complex with the deposited Fe^{3+} at a basic pH to afford a higher crosslinking density. The variations in crosslinking density between the ionoprinted site and the bulk counterpart actuated the hydrogel. Benefitted from the dynamics of multiple catechol–Fe crosslinks, the bending status of hydrogel can be restored by simple treatment with acid. In addition to Fe^{3+}, other metal ions (copper, zinc, aluminum, and titanium) can also induce the movements of such catechol–metal hydrogel actuators.[165]

3.4.3. Dynamic Catechol–Metal Complex from Redox

Cuticles of mussel byssal threads, primarily containing DOPA and ferric ions, exhibit remarkable hardness, extensibility, and self-healing capability.[166] The metal-coordination in the crosslinks can self-adapt in response to a changing environment.[77,166,167] Apart from the well-known Fe^{3+}, Xu et al. provided direct evidence of Fe^{2+} inside the cuticle recently.[168] The interconversion of different catechol–Fe species, plays a crucial role in maintaining the self-healing capacity of the cuticle (Figure 7D, a). With the adsorption of oxygen, the tris-catechol–Fe^{3+} crosslinks are weakened and even converted to the bis- catechol–Fe^{2+} form, leading to decreased strength and extensibility of the mussel byssus cuticle (Figure 7D, b). However, spraying water can restore the catechol–Fe^{3+} complexes (Figure 7D, c). The gradient distribution of Fe^{2+} and Fe^{3+} across the cuticle thickness may contribute to the overall properties of the threads. These findings provide a theoretical basis in the design of robust, extensible, and self-healing bioinspired materials.

3.5. Reversible Polyphenol–Metal Complexes

3.5.1. Classical Assembly of MPNs

MPNs, originally constructed as the coordination complexes of natural polyphenols (e.g., TA) and metal ions (e.g., Fe^{3+}), are emerging self-adherent nanomaterials.[10] Like PDA, they can be applied as a coating to various material substrates (**Figure 8**A, a). On the other hand, distinct from PDA, the MPN coatings and capsules exhibit pH-triggered disassembly behaviors owing to the pH-dependent metal/polyphenol coordination.[169] In addition, the MPN assembly features a much faster kinetics, giving rise to films and capsules within seconds. It should be also noted that MPNs can be preferentially assembled onto one material over another, potentiating site-specific patterning. Recently, Caruso group has demonstrated patterned MPN films by site-specific deposition of TA–Fe^{3+} onto templated patterns of natural biomolecules (e.g., lipids, proteins, polysaccharides, and nucleic acids) (Figure 8A, b). Subsequent deposition of AgNPs can confer enhanced optical properties to visualize biological patterns, such as latent fingerprints (Figure 8A, c,d).[170]

The diversity of MPNs is well dictated by the palette of phenolic ligands and metal ions (Figure 8A, e). The identity of both metals and phenolics can significantly affect the assembly and properties of MPNs. At least one vicinal diol group in the phenolic structure is needed to induce MPN assembly into films.[171,172] The assembly/disassembly characteristics, film thickness, and fluorescence properties vary when different metal ions come to mate the same phenolic ligand.[173] For example, Al^{3+}-based MPNs can disassemble at physiologically-relevant pHs (5 ≈ 7.4), boding well for drug-delivery applications.[174]

Attractively, MPNs can also form in situ on living matters (e.g., yeasts, bacteria, mammalian cells), producing cell-in-shell structures (a.k.a. "artificial spores") (Figure 8B, a).[175,176] The coating procedure is facile, requiring simply bathing the targeted cells with polyphenols and metal ions for a timeframe of seconds. The resultant shell layers are mechanically durable and widely protective against harsh conditions, while providing the versatility to manipulate cell metabolism and division, amongst other functions.[177] In particular, the pH sensitivity of MPNs (e.g., TA–Fe^{3+} MPN) can install the semiartificial system with on-demand degradability and reconfgurability that is promising in biocatalysis and cell-based sensors and therapies.[178] Aside from the co-incubation strategy, a "feeding/assembly" approach has also proven success. In one representative example, yeast cells were continuously fed with Fe^{3+} ions and then subjected to TA solution, leading to interfacial assembly of TA–Fe^{3+} MPN (Figure 8B, b). In addition, the resultant MPN allowed good cell survival and secondary surface functionalization of serum proteins (Figure 8B, c).

3.5.2. Emerging Methods for Control of MPN Assembly

It remains a demanding challenge in the field of MPNs to engineer thick, continuous films. Owing to the coordination-driven interfacial assembly, conventional MPNs feature discrete film growth that would typically cease in 1 min. Rahim et al. have recently developed a solid-state etching/interfacial assembly strategy aimed at continuous growth of MPN films. Specifically, GA was employed to etch iron rust, during which GA–Fe^{3+} complexes were continuously assembled at the substrate/solution interface.[179] More recently, Kang et al. found that thick MPN films can be prepared in a solvent-free manner

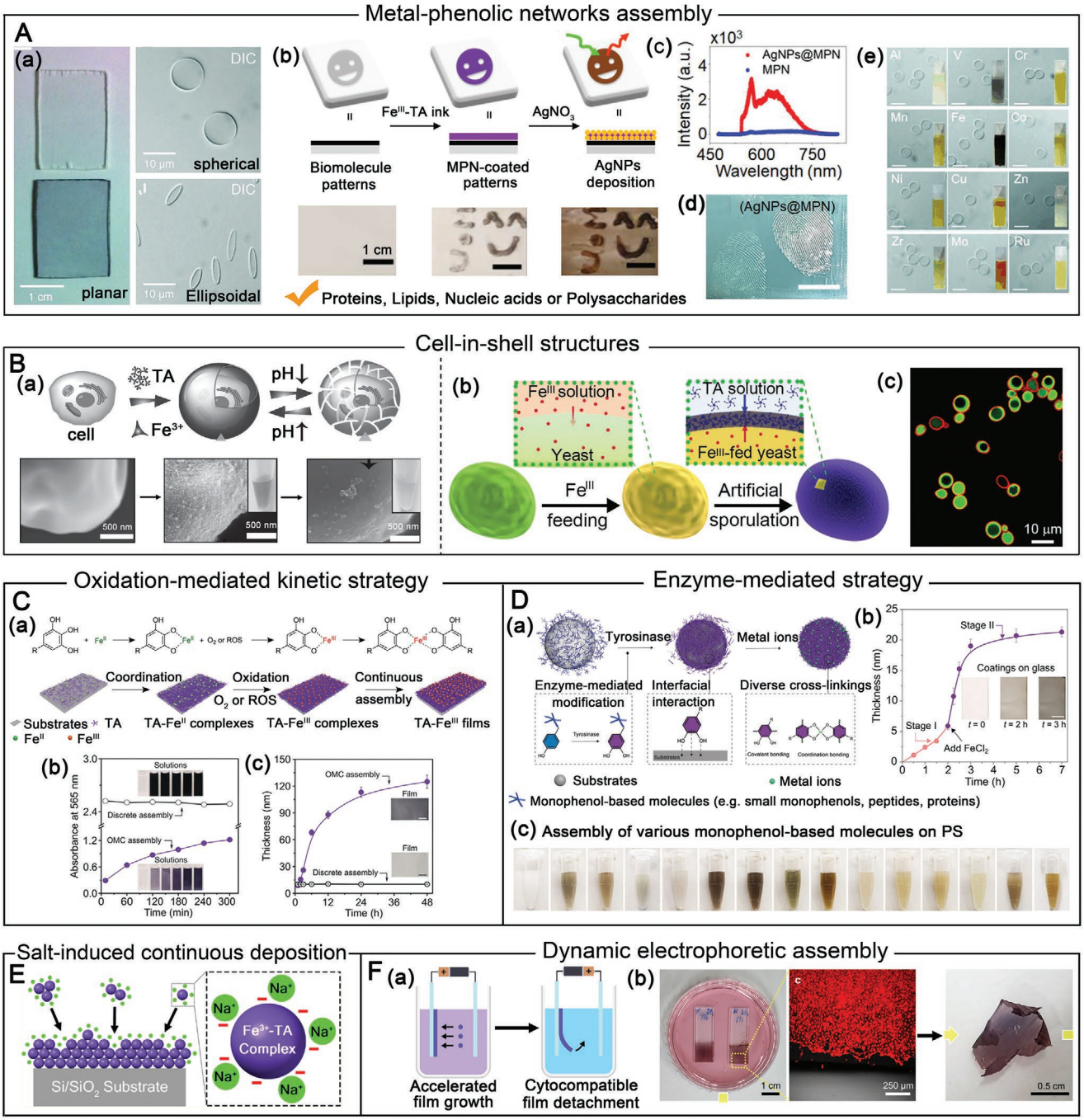

Figure 8. Assembly of polyphenols and metal ions to form MPNs. A) MPN assembly on various substrates. a) Fe^{3+}–TA films/capsules on planar, spherical and ellipsoidal substrates. Reproduced with permission.[169] Copyright 2013, The American Association for the Advancement of Science. b) Preferential deposition of Fe^{3+}–TA on biomolecules and the enhanced visualization by Ag deposition. c,d) Fluorescence emission spectra of Fe^{3+}–TA networks before and after Ag deposition and its application in visualizing fingerprint patterns. Reproduced with permission.[170] Copyright 2019, Wiley. e) Capsules prepared from different TA/metal systems. Reproduced with permission.[173] Copyright 2014, Wiley. B) Cell-in-shell structure. a) Reversible assembly and removal of Fe^{3+}–TA on yeast cells. Reproduced with permission.[175] Copyright 2015, Wiley. b) Biphasic film formation of Fe^{3+}–TA on *S. cerevisiae*. c) CLSM image of yeast-in-shell hybrids after visualization of shells (red rings). Reproduced with permission.[176] Copyright 2017, Wiley. C) Oxidation-mediated kinetic strategy for MPN engineering. a) Possible reactions of TA with Fe^{2+} and Fe^{3+} for the assembly of MPNs. b,c) Comparison of the MPN formation in solution and on the film by using discrete and oxidation-mediated coordination assembly. Reproduced with permission.[31] Copyright 2019, Wiley. D) Enzyme-mediated assembly of MPNs. a) Tyrosinase mediated monophenol-based MPN assembly. b) Film growth over time. c) Photographs show the assembly of various monophenol-based molecules, peptides, and proteins. Reproduced with permission.[181] Copyright 2020, Wiley. E) Salt-induced continuous deposition of Fe^{3+}–TA. Reproduced with permission.[182] Copyright 2018, American Chemical Society. F) Dynamical electrophoretic approach. a) Growth and detachment of MPN coatings. b) Fabrication of freestanding cell sheets. Reproduced with permission.[183] Copyright 2020, American Chemical Society.

via tribochemistry to promise mechanosynthesis.[180] The film thickness was tailorable from 1.5 nm to 2.2 μm by simply varying the friction parameters and reaction time. Further investigations showed that these films harbored a gradient bilayer structure. The bottom layer was formed as a result of the chelation of TA and metal ions, while the top layer was dominant by hydrogen bonding or π–π stacking among oligomers of phenolic moieties.

Besides the utilization of solid-state reactants, oxidation-mediated kinetic strategy has shown effectiveness to impart spatial and temporal control over MPN growth by Caruso group.[31] Instead of Fe^{3+} ions, Fe^{2+} ions acted as the precursors to be oxidized to Fe^{3+}, thereafter mediating coordination assembly of polyphenols (Figure 8C). This strategy has two latent benefits. On the one hand, the inferior reactivity of Fe^{2+} toward polyphenol inhibits instantaneous coordination. On the other hand, the gradual oxidation of TA–Fe^{2+} into TA–Fe^{3+} allows for conformational rearrangement and self-correction. Overall, the initial coordination and subsequent oxidation process are dependent on time and concentration, signifying spatiotemporal control over the thickness and microstructure of MPN films. In addition, by using reactive oxygen species, the oxidation of TA–Fe^{2+} into TA–Fe^{3+} could be significantly accelerated, showing ≈30 times' increase in film growth. Furthermore, the same group has newly combined the oxidation-mediated assembly with an enzymatic strategy for controlled MPN assembly (Figure 8D, a,b).[181] This time, they demonstrated in situ conversion of monophenols to catechols via tyrosinase, which substantially expands the toolbox of MPNs, by including various small molecules, peptides, and proteins (Figure 8D, c).

In fact, continuous MPN growth can also be realized by salt-induced assembly (Figure 8E).[182] Through addition of salts, Park et al. turned the one-off coating kinetics of Fe^{3+}–TA complex to a continuous one. Systematic investigations identified cations as the key factor. Salts with higher-valence and larger-size cations can minimize the concentrations of salts required to plateau the coating growth. A charge screening mechanism was postulated, wherein the negative surface charges of Fe^{3+}–TA complexes can be screened by positively-charged salt cations, resulting in coagulation and continuous film deposition.

Despite those efforts in controlled film growth, the robust adhesion of MPNs hinders the acquisition of freestanding films. Recently, Yun et al. developed a dynamical electrophoretic approach to regulate the cohesion and adhesion behaviors of MPNs (Figure 8F).[183] The electrophoretic movement and locally concentrated metal–phenolic species increased film growth rates by 2–3 orders of magnitude (Figure 8F, a). Promisingly, simple positive-to-negative current switching can detach the films, even those cultured with living cells, suiting utilities in tissue engineering and nanomedicine (Figure 8F, b). Furthermore, freestanding films with tunable thickness can be obtained.

4. Control of PDA Coating Kinetics

Surface coating using DA occurs normally slow, but the kinetics is tailorable, for example, by external additives. The kinetic curves of DA polymerization under various conditions are summarized in **Table 1**. Classically, the thickness of PDA film increases as a function of reaction time, plateauing at about 50 nm after 24 h (curve 1).[2] However, a near-linear kinetics is possible if fresh DA is regularly introduced to repeatedly coat the surface (curve 2).[106] Ponzio et al. investigated the effects of three oxidants, namely $NaIO_4$, $(NH_4)_2S_2O_8$, and $CuSO_4$, on the coating kinetics (curve 3).[25] The presence of $NaIO_4$ speeded up the formation of a PDA film; however, it was encountered with a plateau in 2 h. By contrast, when $(NH_4)_2S_2O_8$ was used as the oxidant, the film thickness increased gradually to overtake that of the $NaIO_4$ oxidized film in 5 h. The addition of $CuSO_4$ can significantly expedite DA polymerization, especially in the presence of O_2 or H_2O_2. For example, the $CuSO_4/H_2O_2$ couple triggered a ≈30 nm thick PDA coating in 40 min (curve 4), a process that is attributed to in situ generated reactive oxygen species.[109] In the deoxygenated atmosphere, Cu^{2+}-assisted PDA deposition clearly showed a slower but linear growth (curve 5), resulting in a thickness greater than 70 nm in 80 h.[106] More interestingly, the deposition kinetics can be elevated with chloride ions (Cl^-) that have the ability to enhance the oxidizing power of Cu^{2+}. It was reported that the formal potential of the Cu^{2+}/Cu^+ could be positively shifted to +0.53 V in the presence of 0.1 M Cl^-.[108,184]

Likewise, reactive oxygen species generated from UV irradiation can accelerate PDA deposition (curve 6).[27,100] Du et al. investigated the polymerization of DA under pH 7.0 and 8.5, with/without UV irradiation.[27] For substrates immersed in a neutral solution (pH 7.0), a 4 nm thick PDA coating was obtained in 2 h under UV irradiation, which was comparable to that obtained in an alkaline condition (pH 8.5). While, no PDA layer was formed for the counterparts without illumination. Additionally, the UV-induced polymerization is controllable via the ON/OFF flexibility, as well as by varying the light intensity applied. In another report, the thickness of PDA films climbed to ≈80 nm in 10 h under UV irradiation.[100] Plasma is another approach for radical generation. Wang et al. found that the microplasma cathode could dramatically accelerate the polymerization kinetics, leading to a 35.3 nm thick PDA coating in 40 min (curve 7).[101] The kinetics could be easily regulated by the input current.

Microwave irradiation is also well suited for rapid PDA coating, which produces free radicals while raising the reaction temperature.[28] As studied by Lee and co-workers, the thickness of PDA coating was increased to ≈18 nm under 1000 W microwave irradiation for 15 min (curve 8). Two contributors were proposed: i) the O_2-involved oxidation at the early stage, and ii) the microwave-based, radical/heat-assisted oxidation throughout the coating process. As discussed in Section 2.3, organic radical species generated in the presence of DA and vanadium can facilitate PDA coating. Surface coating was observed only in solutions with a higher portion of DA. For example, a [catechol]/[V] ratio of 4.0 led to PDA coating (58.1 nm) nearly six times thicker than a pure PDA coating (8.6 nm) that lacked vanadium (curve 9).[113] Electrochemical polymerization of DA at 0.5 V produced an ≈10 nm PDA film (curve 10). Although the thickness increased drastically in the first 25 min, its growth was slowed down later on.[103] Apart from the aforementioned, ionic strength is another important factor affecting the coating kinetics.[131]

Table 1. Kinetics of DA polymerization at different conditions. Curve 1: Reproduced with permission.[2] Copyright 2007, The American Association for the Advancement of Science. Curves 2 and 5: Reproduced with permission.[106] Copyright 2011, American Chemical Society. Curve 3: Reproduced with permission.[25] Copyright 2016, American Chemical Society. Curve 4: Reproduced with permission.[109] Copyright 2016, Wiley. Curve 6: Reproduced with open access permission from ref. [100]. Curve 7: Reproduced with permission.[101] Copyright 2017, The Royal Society of Chemistry. Curve 8: Reproduced with permission.[28] Copyright 2017, Wiley. Curve 9: Reproduced with permission.[113] Copyright 2014, American Chemical Society. Curve 10: Reproduced with permission.[103] Copyright 2012, Wiley.

Conditions	Kinetics	Conditions	Kinetics
DA: 2 mg mL^{-1} pH: 8.5 buffer: Tris substrate: Si[2]	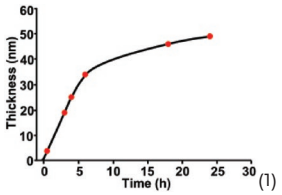 (1)	DA: 2 mg mL^{-1} pH: 8.5 buffer: Tris substrate: Si inject fresh DA[106]	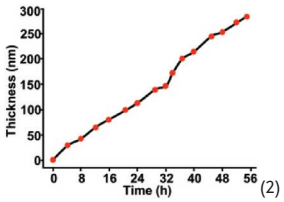 (2)
DA: 2 mg mL^{-1} pH: 5.0 buffer: sodium acetate oxidants: 20×10^{-3} M substrate: Si[25]	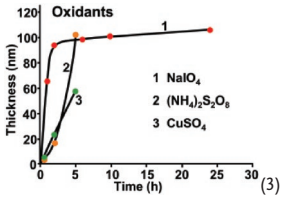 (3)	DA: 2 mg mL^{-1} pH: 8.5 buffer: Tris $CuSO_4/H_2O_2$ ($5 \times 10^{-3}/19.6 \times 10^{-3}$ M) substrate: Si [109]	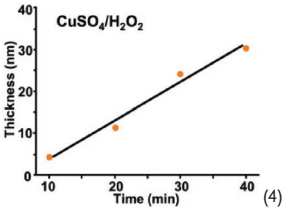 (4)
DA: 2 mg mL^{-1} pH: 4.5 buffer: Tris $CuSO_4$: 30×10^{-3} M deoxygenated substrate: Si[106]	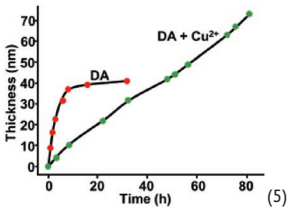 (5)	DA: 2 mg mL^{-1} pH: 8.5 buffer: Tris UV: 36 W lamp substrate: Si[100]	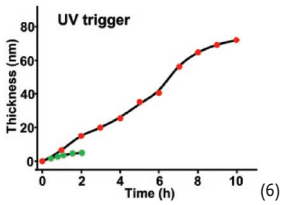 (6)
DA: 2 mg mL^{-1} pH: 5.0, buffer: PBS Plasma cathode substrate: Si[101]	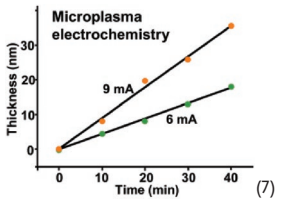 (7)	DA: 2 mg mL^{-1} pH: 8.5 buffer: Tris Microwave substrate: Au[28]	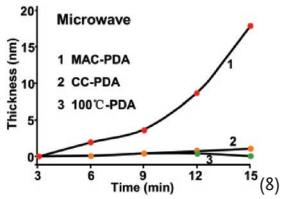 (8)
DA: 2 mg mL^{-1} pH: 7.4 buffer: PBS Vanadyl substrate: Ti[113]	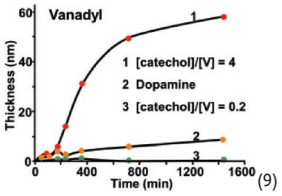 (9)	DA: 10×10^{-3} M pH: 6.0 buffer: PBS 0.5 V substrate: Au[103]	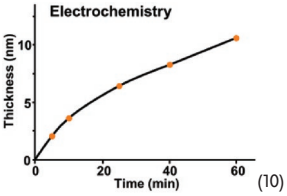 (10)

5. Size Control for PDA Nanomaterials

Defined sizes are desirable for practical applications of PDA nanoparticles, especially in the fields of biomaterials, structural color materials, and pollutant disposal. For example, the optical property of nanoparticles is related to the particle size.[185] Nanoparticles smaller than 200 nm are preferred for drug delivery so as to avoid rapid biorecognition and thus clearance by host immune. And the enlarged specific surface areas provided by smaller nanoparticles will benefit the adsorption and degradation of pollutants.[186] However, it is difficult to obtain size-tailored monodisperse PDA nanoparticles by a classic polymerization condition (Tris buffer, pH 8.5), mainly concerning the diverse covalent and noncovalent interactions that foster particle aggregation. In this section, we will describe methods for the preparation of size-tunable PDA nanoparticles for demonstrated applications.

5.1. Classical Methods for Size Control

The size of PDA nanomaterials is highly dependent on parameters that can influence the rate constant of DA oxidation, briefly including pH, temperature, and DA concentration (**Figure 9**A). Size-defined nanoparticles of PDA could be obtained through neutralizing DA hydrochloride with NaOH, followed by spontaneous oxidation of DA.[34,187,188] The resulting size can range from dozens to hundreds of nanometers,

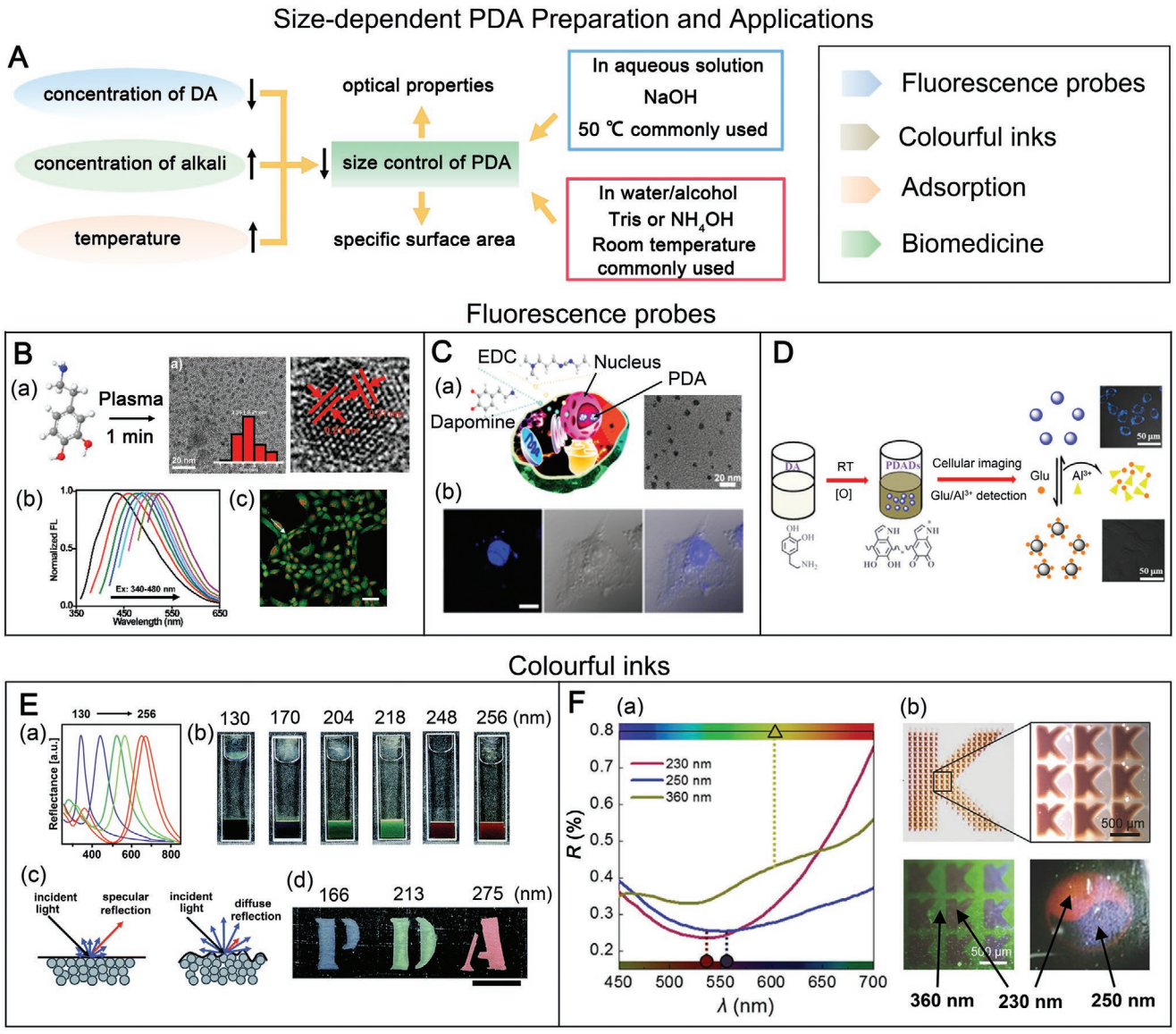

Figure 9. A) Size control of PDA nanoparticles for various applications. B) Fluorescent PDA nanodots for cell imaging. a) Synthesis and characterization of PDA dots. Reproduced with permission.[196] Copyright 2019, American Chemical Society. b) Fluorescence emission spectra of PDA dots under different excitation wavelengths. c) Imaging live cells using PDA dots. C) Fluorescent PDA nanoparticles for nucleus labeling. a) In situ synthesis of PDA within live cell nucleus. b) Confocal images of live A549 cells with nuclei labeled by PDA. Reproduced with permission.[197] Copyright 2017, American Chemical Society. D) PDA dots for reversible detection of glutamic acid and Al^{3+}. Reproduced with permission.[198] Copyright 2018, American Chemical Society. E) Noniridescent structural color materials based on monodispersed PDA nanoparticles. a) Reflection spectra, and b) digital camera images of PDA at different sizes. c) Influence of nanoparticle arrangement on the structural colors of PDA. d) Photographs of structural color films from PDA black particles. Reproduced with permission.[185] Copyright 2015, The Royal Society of Chemistry. F) PDA inks for creating micropatterns. a) Reflectance spectra of PEGDA films containing PDA nanospheres with different diameters, and b) photographs of micropatterns under spot light. Reproduced with permission.[34] Copyright 2017, Wiley.

depending on the reaction temperature, the amount of DA, and the ratio of DA to NaOH. In specific, it decreased as reaction temperature rose, whilst increased as DA concentration increased. By contrast, a greater amount of NaOH led to smaller PDA nanoparticles until the molar ratio of NaOH/DA reached 1.0. When the amount of NaOH exceeded that of DA, an amorphous structure instead of particles was obtained.

The introduction of alcohols, such as methanol and ethanol, represents another versatile strategy for size control of PDA nanoparticles.[185,186,189–191] The presence of alcohols was found to significantly retard DA polymerization, implying a more controllable kinetics than that in water-phase.[192] Ammonia has been adopted as a new source of alkali ions alternative to Tris to buffer the polymerization system. It was found that the particle sizes decreased with an increase in ammonia input.[186] On the basis of this, monodisperse PDA nanospheres of diameters ranging from 2 to 900 nm can be easily attained. Additionally, the microfluidic technology has arisen as an emerging tool to control the size of PDA nanoparticles, as discussed in Section 2.3.

5.2. Controllable Preparation of PDA Nanodots

Like natural melanins, PDA shows extremely low radiative quantum yields, as the majority of absorbed energy is subjected to ultrafast nonradiative relaxation.[193] It was also observed that the intermolecular or intramolecular stacking of PDA backbones is unfavorable for fluorescence emission. Rather, the oligomers of DA, with a lower degree of π–π interaction, are the main source of fluorescence.[194] It could be envisioned that the PDA nanodots could serve as fluorescent probes.[191,195–198] Liu et al. demonstrated a route for ultrafast synthesis of PDA nanodots for fluorescent imaging (Figure 9B).[196] Specifically, ultrasmall PDA nanodots, with an average size of 3 nm, were obtained in 1 min by nonthermal plasma treatment (Figure 9B, a). These PDA nanodots exhibited excitation-dependent emission property and size-dependent nucleus-targeting capability, promising live cell imaging (Figure 9B, b,c). In a recent report,[197] through coincubating DA and EDC (an oxidant) with cells, fluorescent PDA nanodots were synthesized in situ within live-cell nucleus (Figure 9C). The resultant nanodots displayed minimal cytotoxicity and superior quantum yield (≈35.8%), allowing for label-free and prolonged tracking of nucleus. Ci et al. developed a PDA dot-based fluorescent nanoswitch assay that was able to reversibly detect glutamate (Glu) and Al^{3+} in serum/cells at a limit of 0.12×10^{-6} and 0.2×10^{-6} M, respectively.[198] The working principle is that the fluorescence of PDA dots could be quenched by Glu and resumed by addition of Al^{3+} (Figure 9D).

5.3. Size-Dependent Structural Colors

The light reflection of PDA nanoparticles has motivated the development of structural colors. In nature, amorphous arrays of melanin granules produce beautiful structural colors.[185] Small changes in the granule size can significantly alter the color reflected.[199] Given their biomimicry to eumelanin, PDA particles are potential structural color materials.[34,185,200] The structural colors and resultant textures capitalize on the size and monodispersity of PDA particles. For example, Kohri et al. prepared a series of monodispersed PDA black nanoparticles, which showed noniridescent size-dependent structural colors (Figure 9E).[185] Such structural color is also related to the topography of substrates on which PDA nanoparticles are deposited. Flat surfaces increased the specular reflectance and thus produced a metallic texture, whereas rough surfaces featuring diffuse reflection led to a matte texture (Figure 9E, c). Using these PDA nanoparticles as inks, structurally colored patterns could be sketched easily (Figure 9E, d). Specifically, Cho et al. investigated the coloration of PDA nanospheres under strong white light. They found that the high absorbance of PDA would suppress multiple scattering, making resonant Mie scattering a predominant pattern (Figure 9F, a).[34] Apart from the size effect, the resonant colors were found dependent on dispersion medium. Therefore, the prepared PDA inks can be utilized to encrypt and selectively disclose multicolor micropatterns (Figure 9F, b).

6. Morphology Control for PDA Nanomaterials

It is well recognized that the properties of PDA materials are highly dependent on their morphologies. For one example, hollow structures hold promise as nanoreactors/reservoirs for drug delivery and energy storage. For another, 3D hierarchical nanostructures built from 2D nanosheets can provide synergistic catalytic performances. In this section, we summarize methods that impart morphology control in the preparation of PDA-based materials of different dimensions (**Figure 10**A).

6.1. Overview of Morphologies

Although the oxidative polymerization of DA normally produces solid nanoparticles, various morphologies, including hollow nanospheres, nanotubes, capsules, nanofibers, nanosheets, hierarchical flowers, bowl-like nanoparticles, chiral and spiral nanoribbons, and so on, can be strategically prepared under noncanonical conditions.

6.2. Methods for Morphology Control

6.2.1. Templating Methods

Hollow PDA nanostructures with controlled shape, size, composition, and porosity are typically prepared via templating approaches. A wide range of materials, including SiO_2, $CaCO_3$, ZnO, CdS, organic polymers, emulsions, curcumin, and sodium citrate, etc., have shown success to template the synthesis of hollow-structured PDA (Figure 10A, a–c).[38–40,201–203] These sacrificial materials are often categorized into hard, soft, and salts templates. Compared to the hard ones, the soft and salt templating methods permit easier removal of the template. For example, Caruso group prepared PDA capsules on the soft template of dimethyldiethoxysilane emulsion droplets, which can be removed with ethanol (Figure 10A, a).[39] Additionally, by virtue of emulsion preloading, such a template allows for facile encapsulation of functional substances, such as magnetic nanoparticles, quantum dots, and hydrophobic drugs. Recently, Li et al. presented a green route for fast synthesis of PDA nanospheres. Simply by washing with water, the authors were able to remove the sodium citrate template (Figure 10A, c).[38] Noticeably, the mentioned templating approaches can be integrated with a further annealing step to produce functionalized carbonaceous materials. For example, the direct pyrolysis of CdS-PDA nanospheres generated S-doped carbon with hierarchically porous structures owing to the evaporation of Cd.[203]

Self-etching of templates offers an in situ mild approach to prepare PDA nanocapsules.[204] Ye et al. found that the catechol chelation of metal nodes would automatically etch the metal–organic framework (MOF) templates during PDA coating, giving rise to nonspherical PDA capsules (Figure 10B, a). In addition, the MOF@PDA hybrids, with a biocompatible PDA shell and a metastable MOF core, could be internalized by cancer cells. The self-etching of the MOF core resulted in continuous releasing of metal ions that killed HeLa cells. In

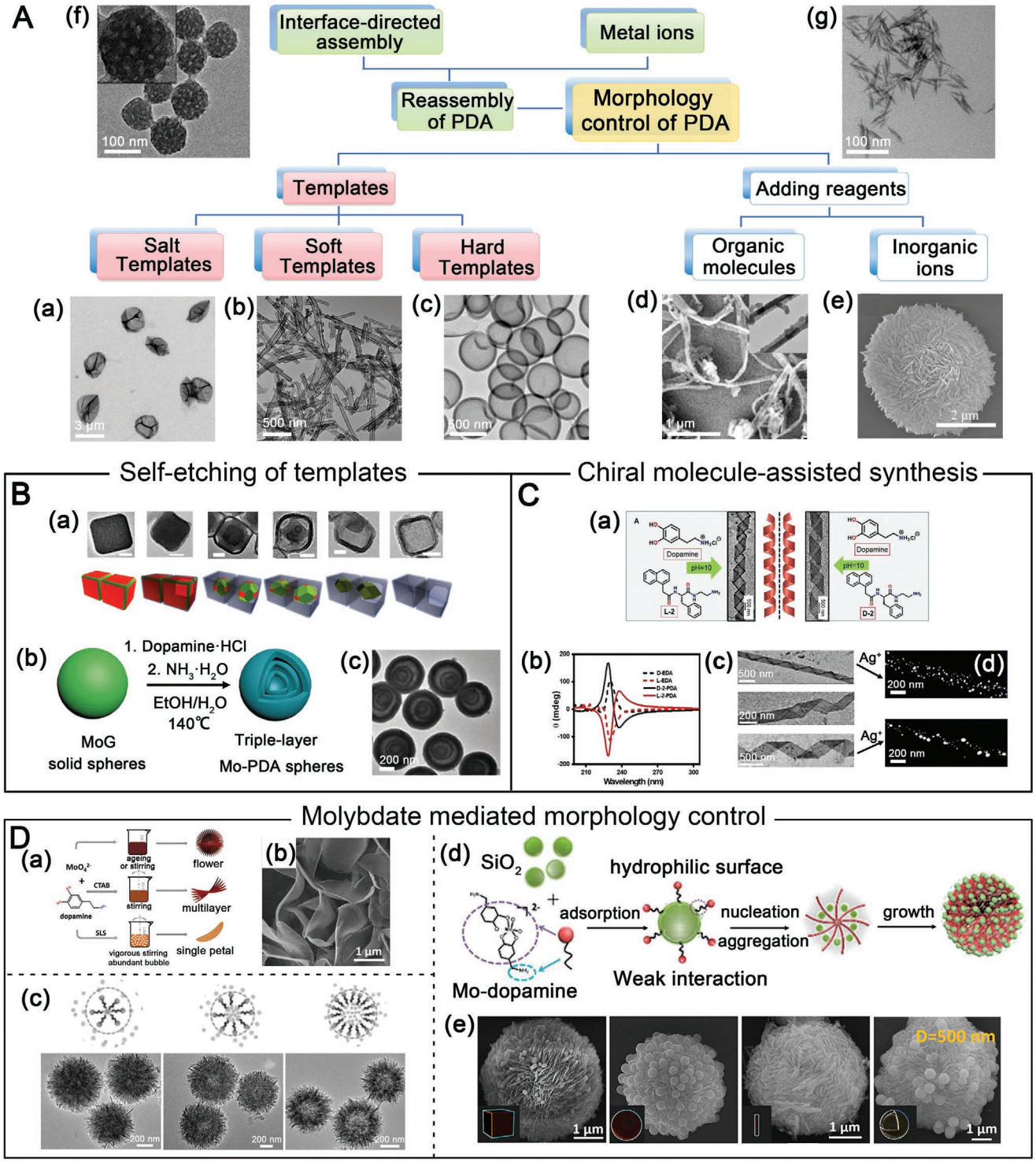

Figure 10. Classical strategies for morphological control of PDA-based nanostructures. A) Classic methods for preparation of various PDA nanostructures. a) capsules, Reproduced with permission.[39] Copyright 2010, Wiley. b) nanotubes, Reproduced with permission.[202] Copyright 2016, American Chemical Society. c) hollow nanospheres, Reproduced with permission.[38] Copyright 2019, The Royal Society of Chemistry. d) nanofibers, Reproduced with permission.[36] Copyright 2014, Wiley. e) flowerlike PDA–phosphotungstic acid, Reproduced with permission.[206] Copyright 2014, Wiley. f) mesoporous nanoparticles, Reproduced with permission.[211] Copyright 2016, American Chemical Society. g) willow-leaf-like PDA. Reproduced with permission.[212] Copyright 2017, Elsevier. B) Self-etching template assisted morphological control. a) Self-etching of MOF templates for preparation of PDA capsules. Reproduced with permission.[204] Copyright 2017, American Chemical Society. b,c) Formation of multishelled Mo–PDA hollow structures through a sequential self-templating mechanism. Reproduced with permission.[205] Copyright 2016, Wiley. C) Chiral molecule-assisted synthesis of chiral PDA nanoribbons. a) Control of twist chirality of PDA nanoribbons. b) Circular dichroism profiles of the obtained nanoribbons. c) pH-induced

another report, Lou group prepared multishelled Mo–PDA hollow structures using Mo-glycerate (MoG) as the template (Figure 10B, b).[205] Under alkaline condition, DA polymerized at the surface of MoG spheres while simultaneously etching the spheres, forming multishelled Mo–PDA hollow structures (Figure 10B, c). Furthermore, the number of shells can be tuned by the size of MoG template and the amount of ammonia used. Owing to the increasing amounts of active species and enhanced structure stability of multishells, these hollow spheres have great potential in energy storage.

6.2.2. Additive-Mediated Synthesis

The introduction of certain additives can have a dramatic effect on the morphologies of PDA.[37,205–207] One class of such additives are organic molecules that can exert supramolecular interactions to modulate the initial internal interactions.[36,42,208,209] Yu et al. introduced folic acid to modulate the formation of PDA nanobelts and nanofibers (Figure 10A, d).[36] The underlying mechanism was deemed to involve the folic acid-assisted stacking of protomolecules of PDA via π–π effects and hydrogen bonds. Using chiral phenylalanine-based amphiphiles as modulators, Awasthi et al. fabricated chirally twisted ultrathin PDA nanoarchitectures, e.g., helical nanoribbons and nanotubes. Intriguingly, the resulting structures allowed spontaneous assembly of AgNPs along their edges (Figure 10C).[42] This study verifies that nucleophilic functional groups such as amines and thiols are useful for controlled synthesis of PDA.

Certain inorganic modulators, e.g., phosphotungstic acid (PTA) and molybdate, have been utilized to fabricate novel PDA-like nanostructures. The strong hydrogen bonding and electrostatic interaction between DA and PTA can trigger their coassembly, leading to 3D flowerlike hierarchical nanostructures.[206] MoO_4^{2-} anions can chelate DA molecules to form Mo–DA precursors.[37,41] In water, the Mo–DA precursors would self-assemble into hierarchical flowers with Mo–PDA nanopetals. Notably, when the surfactant sodium lauryl sulfate was added to inhibit the nanopetals assembled process, uniform 2D single nanopetals of Mo–PDA were obtained instead (Figure 10D, a,b).[37] Under a water-in-oil environment, the Mo–DA precursors would self-assemble at the water/oil interface. And this self-assembly could be controlled by altering the amounts of DA, giving rise to hollow spheres with tunable cavities (Figure 10D, c).[41] These works signify the promise of using DA for controllable synthesis of organic–inorganic hybrid materials.

Owing to the universal adhesion of catechol groups, the 3D Mo–PDA complex can act as a binder and curing agent to control the assembly of superstructures at the microscale (Figure 10D, d).[210] This system was shown compatible with various particle building blocks, such as nanospheres, nanocubes, nanorods, and hollow spheres, etc. (Figure 10D, e). The resultant materials after thermal and etching treatments qualified multifunctional carriers for energy storage.

6.2.3. Reassembly and Transformation of PDA Nanostructures

Either templates or additives control the morphologies of PDA by regulating particle nucleation and growth during synthesis. Differently, the postsynthesis assembly of PDA nanoparticles can also lead to innovative PDA-based nanostructures. For example, Chen et al. reported a novel interface-directed coassembly approach to fabricate mesoporous PDA hollow spheres (Figure 10A, f).[211] They prepared primary solid PDA nanoparticles and coassembled them with Pluronic F127 stabilized emulsion droplets at the interfaces of water/1,3,5-trimethylbenzene (TMB), in which the π–π interactions between PDA and TMB played a key role. In addition to reassembly, the morphology transformation of PDA nanostructures is also feasible. In a recent study by Qi et al., PDA dots with an aggregated platelike morphology were transformed to a uniform willow-leaf-like morphology by addition of Fe^{3+} (Figure 10A, g).[212] Interestingly, this morphology transformation was associated with fluorescence quenching, which allowed for easy detection of Fe^{3+}.

6.2.4. Gas Diffusion-Assisted Synthesis

Other innovative approaches have also been exploited to impart precise control over PDA's morphologies. For example, Liu group reported a simple gas diffusion procedure to prepare $CaCO_3$–PDA hollow spheres (**Figure 11**A).[207] In their method, a solution of Ca^{2+} ions and DA was placed in an enclosed chamber along with a metastable solid compound of NH_4HCO_3. The growth of hollow $CaCO_3$–PDA nanoparticles followed an inside-out ripening mechanism (Figure 11A, a). First, the oxidatively generated PDA would coordinate with Ca^{2+} to form Ca–PDA seeds. Then, the CO_2 by natural decomposition of NH_4HCO_3 would continuously diffuse into the solution and interact with Ca^{2+}, depositing $CaCO_3$ on surface of the Ca–PDA core. Since Ca^{2+} ions compared to PDA have greater affinity with CO_3^{2-}, they would gradually diffuse out from the core to bind to surface CO_3^{2-}, eventually forming $CaCO_3$–PDA hollow spheres (Figure 11A, b,c). With their acid-sensitive decomposition property, these hollow nanoparticles can find utility in pH-triggered on-demand delivery of theranostic drugs (Figure 11A, d).

6.2.5. Seed-Mediated Anisotropic Growth

Anisotropic growth can provide new options for synthesizing spatially defined PDA-based materials. However, its realization is technically challenging. The inherent adhesive/cohesive ability of

unfolding of the nanotubes. d) Helical arrangement of AgNPs on the nanoribbons. Reproduced with permission.[42] Copyright 2019, Wiley. D) Molybdate mediated morphological control of Mo–PDA. a) Synthesis of Mo–PDA whose morphologies were changed from 2D single nanopetal to hierarchical microflowers. b) SEM image of nanopetals in (a). Reproduced with permission.[37] Copyright 2018, Wiley. c) Synthesis of hollow spheres with tunable cavities via self-assembly of Mo–DA. Reproduced with permission.[41] Copyright 2017, Wiley. d) Assembly process of SiO_2 nanospheres and Mo–PDA for superstructure fabrication. e) Superstructures constructed using Mo–PDA and different building blocks. Reproduced with permission.[210] Copyright 2018, American Chemical Society.

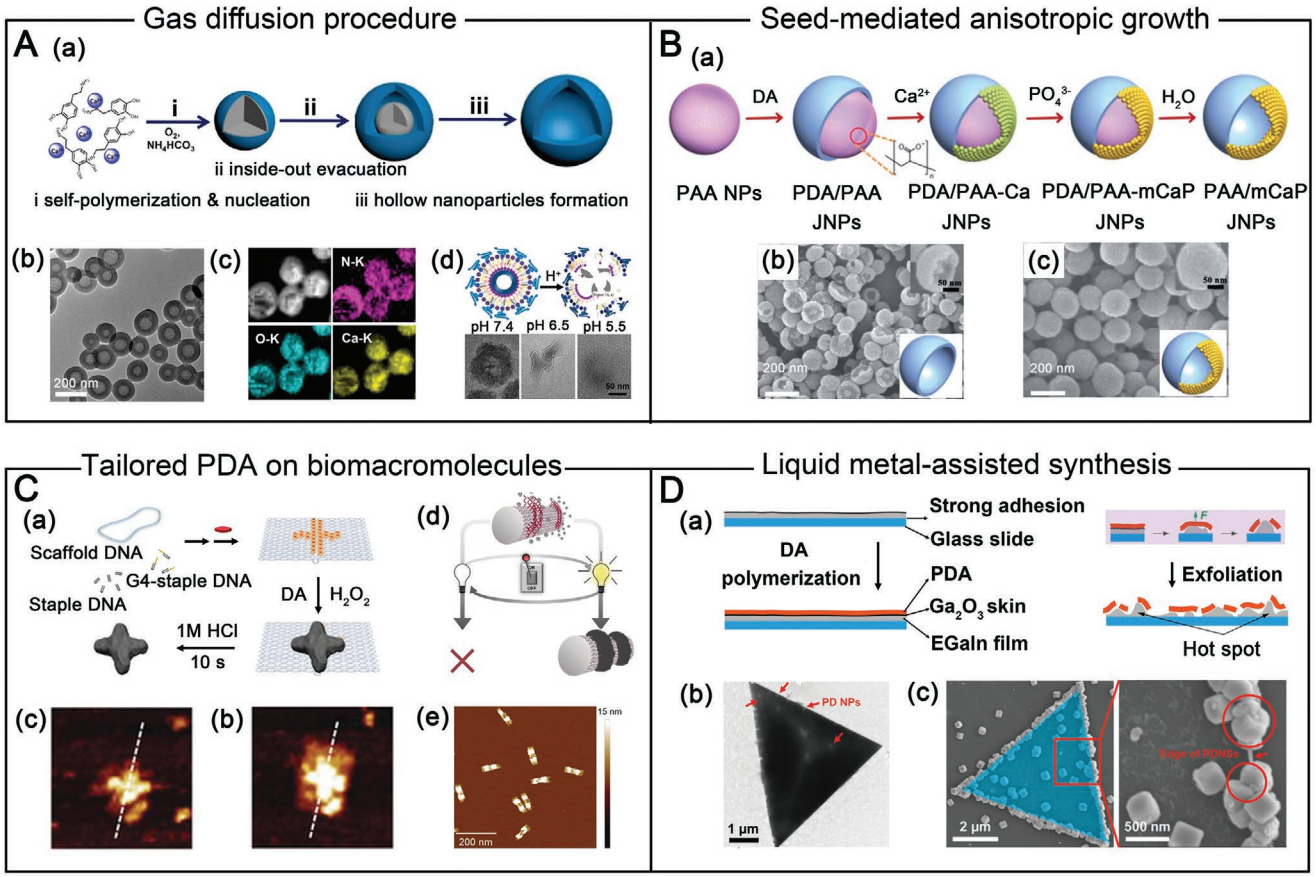

Figure 11. Emerging methods for morphology control of PDA-based nanostructures. A) Gas diffusion-assisted preparation of hollow biomineralized $CaCO_3$–PDA nanoparticles. a) Inside-out ripening process of the hollow nanoparticles. b,c) TEM image and STEM mapping analysis of $CaCO_3$–PDA hollow nanoparticles. d) pH-responsibility of $CaCO_3$–PDA–PEG hollow nanoparticles. Reproduced with permission.[207] Copyright 2018, American Chemical Society. B) Controllable seed-mediated anisotropic growth of PDA and synthesis of PDA/mCaP hollow Janus nanoparticles (PDA/mCaP H-JNPs). a) The controlled synthesis process. b) SEM images of bowl-like PDA NPs and c) PDA/mCaP H-JNPs. Reproduced with permission.[44] Copyright 2017, The Royal Society of Chemistry. C) Tailored PDA ultrastructure on biomacromolecules. a–c) Growth of defined PDA nanostructures on DNA nanotile carrying G4/hemin DNAzyme domain and the extraction of PDA via HCl treatment. Reproduced with permission.[45] Copyright 2018, Wiley. d,e) Light-triggered zonal growth of PDA on DNA origami. Reproduced with open access permission from ref. [214]. D) a) Liquid metal-assisted synthesis process of b) freestanding quasi-2D PDA nanosheets and c) subsequent templated assembly of silver nanocubes. Reproduced with permission.[215] Copyright 2020, Wiley.

PDA accounts for indiscriminate molecule adsorption and particle aggregation, which prevents a zonal coating to be formed. Recently, Zhang and co-workers found that the PDA can be deposited onto only one side of polyacrylic acid (PAA) nanoparticles (Figure 11B).[44] The mechanism involves a Volmer–Weber-like growth mode. As envisaged, a portion of PDA molecules selectively nucleated on PAA to form primary islands that served as seeds for further anisotropic growth of PDA. The morphology of PDA can be progressively steered by the reaction time: from a plate-like one to a bowl-like one, followed by a single-hole morphology, and finally to intact PDA NPs without openings (Figure 11B, a). These are useful to fabricate polymer–inorganic Janus nanoparticles, which promise multipurpose applications in drug delivery, bioimaging, and biosensing.[213]

6.2.6. Tailored PDA on Biomacromolecules

PDA architectures with distinct shapes could also be generated in situ on DNA origami (Figure 11C).[45] Weil group found that a G-quadruplex/hemin-based DNA enzyme can be employed as a redox catalyst to accelerate the polymerization of DA. The DNA enzyme had reaction centers at distinct nanodomains on the DNA origami, which provided a catalytic microenvironment for triggering site-specific PDA deposition (Figure 11C, a).[45] In return, the precisely positioned, bioadhesive PDA served as a local nanoglue to induce and control DNA origami folding. Importantly, the unique PDA nanostructures preserved their initial geometry after removal of the origami. Very recently, the same group accomplished another way of topical PDA coating on DNA origami. This time, they installed DNA origami with a photosensitive polymerization system, whose ON/OFF switching allowed facile spatiotemporal control of DA polymerization at the nanoscale (Figure 11C, b).[214] As an added merit, the deposition of PDA could enhance the stability of DNA origami, so that it can withstand even pure water conditions (typically DNA is vulnerable to unbuffered water), thus broadening the scope of application.

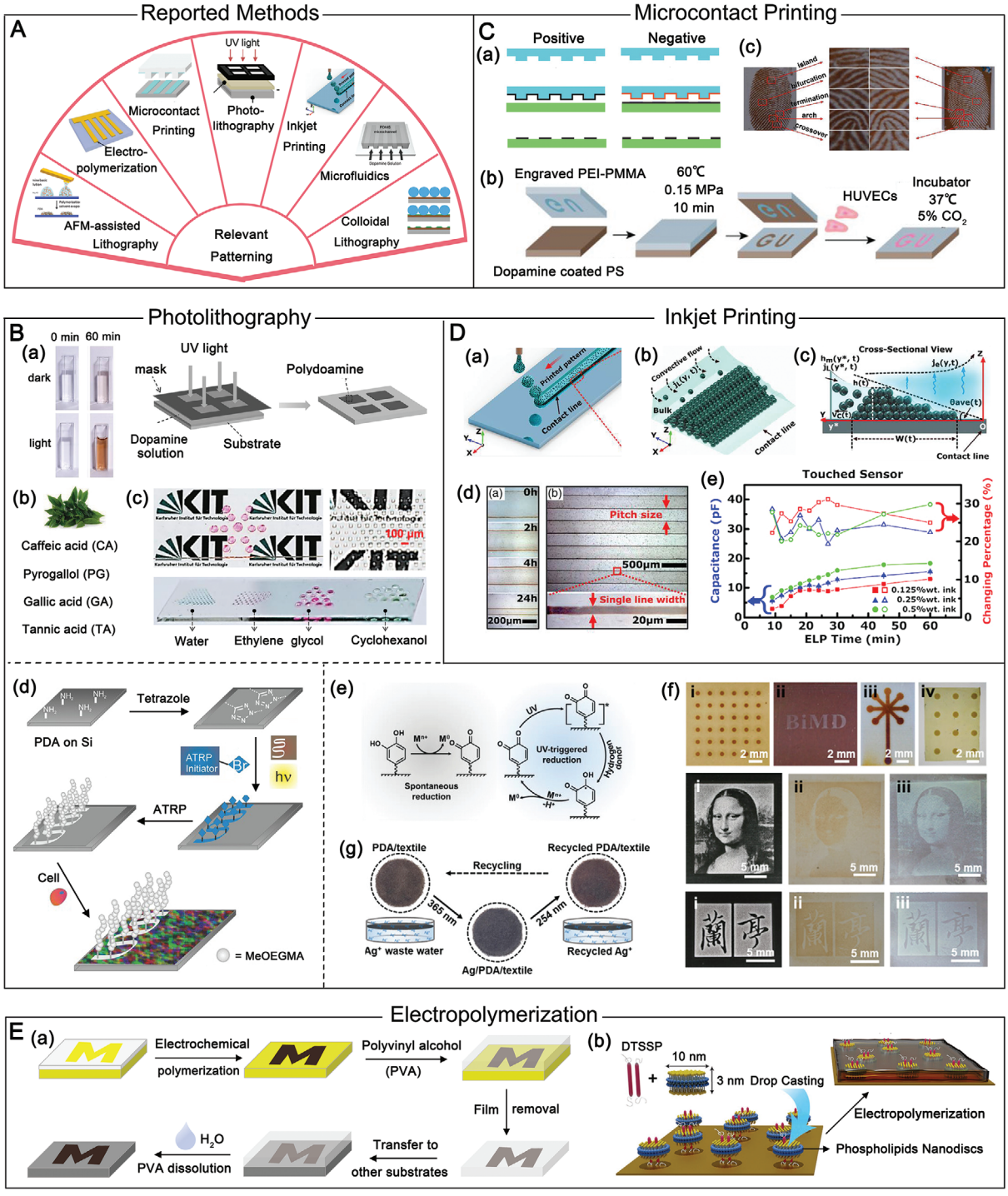

Figure 12. A) Reported methods for PDA patterning. Reproduced with permission.[229] Copyright 2014, Wiley. Reproduced with permission.[221] Copyright 2012, American Chemical Society. Reproduced with permission.[225] Copyright 2013, American Chemical Society. Reproduced with permission.[227] Copyright 2010, American Chemical Society. Reproduced with permission.[228] Copyright 2012, American Chemical Society. Reproduced with permission.[46] Copyright 2017, Wiley. Reproduced with permission.[48] Copyright 2020, Wiley. B) Photolithography. a) Comparison of DA polymerization with/without UV light, and schematic of photolithography-assisted patterning of PDA. Reproduced with permission.[27] Copyright 2014, Wiley. b) Plant-derived polyphenols that are suitable for photopatterning. Reproduced with permission.[46] Copyright 2017, Wiley. c) Droplet microarray of dyed water, ethylene glycol, and cyclohexanol on surfaces micropatterned/grafted with hydrophilic/hydrophobic entities. Reproduced with permission.[230] Copyright 2018, American Chemical Society. d) Photopatterning of silicon wafers and SI-ATRP-induced grafting of poly(MeOEGMA) to impart antifouling property. Reproduced with permission.[219] Copyright 2013, Wiley. e) Mechanisms of spontaneous reduction and UV-triggered reduction of metal ions on PDA surface. f) Various metallic patterns fabricated on PDA-coated substrates. g) Recyclable PDA-coated textile for wastewater treatment. Reproduced with permission.[232] Copyright 2019, Wiley. C) Microcontact printing. a) Illustration of the modes of positive and negative microcontact

6.2.7. Liquid Metal Assisted Synthesis

A liquid metal-assisted polymerization-exfoliation strategy has been recently demonstrated capable to fabricate quasi-2D nanosheets of PDA (Figure 11D, a,b).[215] Succinctly, liquid EGaIn (a liquid metal) was printed onto a glass slide to form a continuous film, onto which PDA was deposited. Subsequently, the Ga_2O_3 skin between the liquid metal and PDA was removed, and the interface between EGaIn and glass was disrupted by acid. The rupturing and fusing of the EGaIn film, as induced by surface tension effects, led to the formation of "hot spots" that broke apart the PDA coating. The resulting nanosheets inherited the versatile chemical reactivity of PDA, suggesting a potent platform for fabricating tailored 2D composite materials. For example, the quasi-2D nanosheets could be used as both a reductant and template to help assemble silver nanocubes. Interestingly, the obtained silver nanocubes preferentially adhered to the edges and precisely sketched the boundaries of the nanosheets (Figure 11D, c). It should be noted that this is distinct from the classic PDA-assisted silver deposition that is incapable of obtaining nanocubes.

7. Spatially Controlled Polymerization: Patterning and Beyond

Micropatterning and substrate engineering are indispensable tools in the development of microelectronics, photonics, microdevices, tissue engineering constructs, and so on.[216,217] Recently, the tying of micropatterning and mussel-inspired chemistries has attracted much attention, permitting versatility in creating spatially defined chemical compositions and/or topographic features. Adding to this, PDA micropatterns further allow for site-specific immobilization of metal particles, chemical molecules, proteins, and cells, thus advancing applications, including but not limited to, biochips and biosensors. In this section, we summarize the repertoire of micro-/nanofabrication technologies for spatially controlled mussel-inspired patterning (**Figure 12**A), including photolithography,[27,46,100,218–220] microcontact printing,[47,221–223] inkjet printing,[48,224] electropolymerization,[225,226] microfluidics,[105,227] colloidal lithography,[228] and atomic force microscopy (AFM)-assisted lithography.[229]

7.1. Photolithography

In 2007, Lee et al. reported photopatterning of PDA by coupling DA polymerization with photolithography, which may represent the first-ever attempt for patterning PDA layers.[2] Audaciously, in 2014, Levkin group utilized UV irradiation as a spatiotemporal trigger (with ON/OFF possibility) to initiate and terminate the process of DA polymerization while allowing photopatterning. The authors realized tailor-made PDA patterns in short time (Figure 12B, a).[27] This research team in 2017 ascertained that, in addition to DA, polyphenolic compounds, including PG, GA, TA, and caffeic acid, can also form spatially defined patterns and gradients via the photolithographic approach, extending the scope of potential applications (Figure 12B, b).[46] Critically, though being interesting, these micropatterns have limited practical value. In a follow-up work, they developed micropatterns with defined wettability (Figure 12B, c).[230] To this end, hydrophilic/hydrophobic molecules were grafted onto photopatterns of an alkenyl-terminal derivative of macrocyclic polyphenols via thiol–ene photoclick reaction.

The above methods grossly fall into the category of "grafting to" photopatterning strategy. By contrast, it is also feasible to implement photolithographic patterning in a "grafting from" fashion leveraging catechol precursor coatings. Instead of directly patterning PDA, Rodriguez-Emmenegger et al. grew PDA film on a Si substrate and functionalized it with a photoactive tetrazole, onto which they photopatterned maleimide-atom transfer radical polymerization (ATRP) initiators via nitrile imine-mediated tetrazole–ene cycloaddition. Assisted by the ATRP initiators, they easily grew poly(MeOEGMA) brushes on the patterned areas, which showed site-selective cell-repellent property (Figure 12B, d).[219,220] In theory, it is also viable to directly synthesize catechol-ATRP precursors and use them for the photoassisted spatially controlled growth of antifouling brushes. The reported strategy, with tailorable property and functionality in the resultant patterns, can find applications in membrane science, tissue engineering, biosensing, and regenerative medicine.[231]

Very recently, rapidly formed, dynamic, erasable micropatterns have been achieved, through wavelength-selective UV-triggered secondary modification of PDA.[232] The authors demonstrated that 365 nm UV irradiation remarkably increased the kinetics of Michael-addition (or Schiff base reaction) by 12 folds. In addition, the metallization kinetics was accelerated by more than 550 times (Figure 12B, e). Sophisticated metal patterns can be generated at intended locations by spatially manipulating the metallization (Figure 12B, f). More importantly, the deposited metallic patterns could be erased by UV irradiation at 254 nm, affording a dynamic, controllable, yet reversible patterning process (Figure 12B, g). This metallization/erasure mechanism can find use in the recyclable extraction of noble metal.

In short, taken together the temporal and spatial controllability of light and the substrate-independent adhesiveness of catechols/polyphenols, mussel-inspired photolithographic patterning should bode well for fabricating functional patterns

printing. b) Preparation of a spatially defined PDA coating for guided growth of HUVECs. Reproduced with permission.[47] Copyright 2019, Wiley. c) Images of latent fingerprint on glass slide (positive image, left) and PDMS flake (negative image, right). Reproduced with permission.[223] Copyright 2016, American Chemical Society. D) Inkjet printing. Reproduced with open access permission from ref. [226]. a–c) Schematic of the evaporation-driven convective particle self-assembly at the liquid contact line of printed pattern. d) Optical micrographs of "twin lines" formed on PET substrates and the as-printed line arrays of PDA nanoparticles. e) Capacitance variation for a touched sensor. Reproduced with permission.[48] Copyright 2020, Wiley. E) Electropolymerization. a) Procedures for the preparation, removal, and transfer of freestanding, patterned films of PDA, and b) the embedding of phospholipid nanodiscs with an integrated transmembrane domain of glycophorin A into the PDA film. Reproduced with open access permission from ref. [226].

for applications in various fields. Despite its attractive features, constraints of photopatterning, such as the required specifications for costly specialized equipment, clean room facilities, and multistep exquisite operations, have prevented interested researchers from stepping into this field. By contrast, some alternative technologies, as discussed below, could offer greater accessibility, simplicity, and cost-effectiveness.

7.2. Microcontact Printing

Microcontact printing ranks amongst the most popular microfabrication techniques. Positive and negative microcontact printing constitute the two common working modes, as schematically illustrated in Figure 12C, a. Generally, this technique is based on the contact transfer of a material of interest from a "stamp" to the target substrate, a process reminiscent of imprinting. PDA patterns have been imprinted onto a broad variety of substrates via the positive microcontact printing using soft poly(dimethylsiloxane) (PDMS) stamps.[221] With additional preactivation by oxygen plasma, PDMS stamps can also be used to create PDA patterns via a negative microcontact manner.[222] Besides soft lithography, patterned PDA layers can be selectively transferred from one "hard" substrate to another via the so-called "subtractive thermal transfer printing" (Figure 12C, b).[47] The imprinted PDA patterns retained the capability for secondary functionalization, which further led to spatially defined patterns of proteins, cells, and bacteria.[47,221,222,233–235] Additionally and interestingly, the process of interfacial transfer of PDA and subsequent selective silver deposition was shown potent to render direct visualization of latent fingerprints for personal identification (Figure 12C, c).[223] In addition, synthetic analogues of DA have also been adopted for microcontact printing to generate functional catechol-based patterns. For example, using a 4-dibenzocyclooctynol containing, catechol-derived molecule, Zheng et al. successfully fabricated organic dye-patterned surfaces via microcontact printing and adhesion-assisted, copper-free click reaction.[236]

7.3. Inkjet Printing

Drop-on-demand inkjet printing, one of the most promising 3D printing technologies, has emerged as a scalable, benign, and cost-effective approach to realizing arbitrary 3D patterning. Fine lines of PDA can be created by inkjet printing of aqueous PDA nanoparticles inks.[48,224] Recently, Liu et al. reported the fabrication of evenly-spaced and ultrafine PDA line arrays (Figure 12D).[48] Assisted by evaporation-driven convective particle self-assembly (Figure 12D, a–c), as well as control of the surface energy of substrate, patterns of defined single line width and line-to-line spacing could be attained (Figure 12D, d). After electroless metallization of silver, conductive patterns were readily generated to suit applications as fatigue-tolerant flexible transparent touch sensors (Figure 12D, e,f). This unique technique offers the advantages of fabricating conductive micropatterns at low-costs while provoking minimal environmental impact. It signifies the great potential for sustainable manufacturing of flexible electronics devices in the future.

7.4. Electropolymerization and Film Transfer

In addition to the discussed microfabrication techniques, electropolymerization offers a latent alternative for spatial control of DA polymerization in the fabrication of stable ultrathin PDA micropatterns. This method relies on the use of well-designed masking templates to allow for selective deposition of PDA. For example, PDA arrays could be fabricated via electropolymerization of DA onto a pre-patterned Au electrode.[225] Further, D'Alvise et al. recently prepared patterned PDA films by electropolymerization at the conductive areas of a PDMS selectively masked surface. Moreover, they demonstrated that these films could be delaminated and transferred to another substrate without disrupting their intactness (Figure 12E, a).[226] In addition, it offers the opportunity to embed nonconductive molecules or supramolecular structures into the PDA film. For instance, nonconductive phospholipid nanodiscs, with an integrated transmembrane domain of glycophorin A, were successfully embedded into the PDA films to form protein nanopores (Figure 12E, b). The incorporation of functional biological entities in the nanopores increased the permeability of PDA films. In this design, the embedded pores control material transport, closely mimicking the structure and functions of cellular membranes.

7.5. Others

Spatial control and patterning of PDA could also be accomplished by other modalities, including microfluidics, AFM-assisted lithography, and colloidal lithography.[105,227–229] Using a microfluidic technique, Shi et al. generated gradient of PDA which can be used to conjugate serum protein for instructing cell adhesion.[105] In another study, an AFM tip was adopted to directly deliver femtolitre volumes of DA solution onto specific locations of a substrate.[229] Defined patterns of PDA motifs would then be left on substrate after polymerization and solvent evaporation. Colloidal lithography, a benchtop and scalable method, has been presented by Ogaki et al. for cost-effective and precise positioning of biomolecules at the nanoscale.[228] Briefly, polystyrene particles were orderly self-assembled onto a PDA coating. After background filling, the polystyrene particles were lifted to leave uncoated zones that can be used for secondary functionalization.

8. Postpolymerization Control

Recall that PDA and derivative materials are consisted of various building blocks, including DA-, DHI-, and PCA-type oligomers. Such versatile surface compositions permit secondary reactions and thus post-tailoring of corresponding material properties. In this section, we shall deal with the following emergent topics: i) material recycling of PDA by deaggregation and reassembly, ii) altering physiochemical properties of PDA via degradation or deaggregation, and iii) secondary functionalization of PDA by ion chelation, inorganic deposition, molecular grafting, etc.

8.1. Deaggregation and Reassembly

A prime concern about the practical use of biopolymers is their stability under different physical, chemical, and biological conditions. Insufficient stability would adversely affect the performance and lifespan of PDA-based materials. PDA is inherently metastable owing to the existence of noncovalent bonds and environmentally sensitive moieties. Indeed, UV-induced structure changes of PDA have been observed. Under intensive UV exposure, a fraction of the six-membered benzyl ring can be broken and the indole can be potentially converted to furo[3,4-b]pyrrole.[237] In addition, PDA undergoes differing degrees of deaggregation/degradation in strong acidic/basic solutions and polar organic solvents.[50,238] Specially, particle detachment in basic milieus could be inhibited by an increased ionic strength, an occasion whereby the disassembly and further polymerization of PDA race with each other.[50] As we know, the PDA coating process is associated with unwanted particle formation in the solution. These particles can be disassembled by alkali. The resulting subunits, with abundant catechol groups, tend to complex with Fe^{3+} to develop coatings on various substrates, signifying the recyclability of PDA.[52] Recently, Lee group demonstrated the controlled disassembly and reassembly of PDA film by virtue of disrupting and restoring cation–π interactions. They suggested that NaOH would destroy the cation–π interaction through deprotonation of amines. However, under the same pH condition, the presence of additional cations, such as K^+, was able to effectively restore the noncovalent interaction.[20]

The deaggregation/degradation is expected to bring about totally different properties to PDA by simply altering its intramolecular and/or intermolecular interactions. A notable effect is the tunable fluorescence emission property. As already documented, PDA by classic synthesis is minimally fluorescent. This is primarily ascribed to its high degrees of chain entanglement and intra/intermolecular stacking (e.g., π–π stacking), which negatively affect fluorescence emission.[33] Whereas, after degradation of PDA, a process that destroys π–π stacking interactions and decreases the degree of conjugation, fluorescent PDA could be obtained.[195,239] In addition to that, chemical oxidation of PDA by certain oxidants (e.g., hydrogen peroxide) also favors fluorescence emission as it prompts structural rearrangement against the mentioned π–π effect.[191,240] Detailed mechanisms on these can be found in a recent review.[33]

In addition to its optical behaviors, the paramagnetism and redox properties of PDA were reported to be alterable by disassembly. Both suspensions and conformal coatings of PDA have manifested susceptibility to ionic liquids (ILs). Specifically, ILs can cause intact PDA to dissemble into nanoscale particles, which would then interact with the anion component in ILs. The resulting materials display altered paramagnetism and redox activity.[241,242] The differences originate from the ILs-mediated reorganization of free radical centers from C-centered radicals to O-centered semiquinone-type components. The redox-tuning properties of PDA can be utilized to install materials with exceptional photothermal effect, and pro-oxidant or radical-scavenging activities.[243]

8.2. Grafting Functionalization

Since its monumental discovery in 2007, mussel-inspired chemistry has served as a versatile platform for secondary functionalization to tailor the surface compositions and properties of different materials for widespread applications. To attain desirable efficacy for a specific material utility, the selection of a suitable functionalization route is of vital importance. On one side, the ability of PDA to coordinate with metals has been employed to immobilize inorganic species, including metal ions, metals, metal oxidants (M_xO_y), metal sulfides (M_xS_y), and MOF. On the other, the rich functional moieties in PDA allow for covalent grafting of organic species (e.g., biomolecules and polymers) by nucleophilic addition or supramolecular interactions or the combination thereof. Another feature deserving a particular remark is that the catechol chemistry can be easily coupled with other chemistries, such as surface-initiated ATRP (SI-ATRP) and click chemistry, to create robust multifunctional surfaces. Additionally, the synergistic use of surface patterning, PDA, and postfunctionalization gives rise to spatially defined chemical or biological functionalities. Furthermore, the carbonization of PDA and its functionalized derivatives has emerged as a beneficial approach to manufacture functional carbon materials. These shall be discussed below.

8.2.1. Immobilization of Inorganic Species

Precious and earth-abundant metals play an integral role in catalysis for production of modern chemicals, materials, fuels, and medicines.[244] A myriad of metals ions are beneficial for human health; for example, Mg^{2+}, Ca^{2+}, Sr^{2+}, and Cu^{2+} for bone development and function; Cu^{2+}, Co^{2+}, and Si^{4+} for blood vessel formation; Ag^+, Cu^{2+}, and Zn^{2+} for defense against microorganisms.[245] In addition, metal ions like Mn^{2+} have wide use as contrast enhancers for bioimaging.[246] In the structure of PDA, there exists multiple sites capable of recruiting metallic species, including catechol, amine, and imine.[49] Besides the intrinsic affinity to various metal ions, the mild reducing capability of PDA toward noble metal ions favors the in situ nucleation and growth of metallic nanomaterials, a process that is known otherwise as electroless metallization. We have currently developed four types of PDA–metal hybrid materials with varying compositions and properties, namely, PDA–M^{n+},[247] PDA–M,[248] and PDA–M_xO_y[88]/PDA–M_xS_y[249] and PDA–MOF.[250–251] These hybrids, with strong coordination between PDA and metals, can have greater stability and functionality for applications in energy, catalysis, and others.

Notwithstanding this, the binding of metal ions to PDA-decorated surfaces is hindered by the limited binding sites available, accounting for nonadjustable, low ion-loading capacity. Fortunately, this can be addressed by using a one-step coassembling strategy that enables simultaneous metal-assisted oxidation of DA to PDA, and the chelating of metal ions by PDA. For instance, adopting this strategy, Huang group has systematically demonstrated catechol/polyphenol–Cu^{2+} coatings with glutathione peroxidase-like catalytic activity for simultaneous generating therapeutic Cu^{2+} and nitric oxide (NO) to prevent stent thrombosis and restenosis.[252–254] Whereas, the basic

or oxidative conditions demanded by DA polymerization are detrimental to certain metal ions. The metal ion coordination can also affect the polymerization process, thus causing undesirable amorphous aggregates.[49] Recently, an ion exchange strategy has been put forward to remedy this,[255] which makes use of the variable affinities of PDA toward different metallic ions.[256] In this strategy, DA first copolymerizes with metal ion "M_1" to form a hybrid; and then, M_1 is preferentially substituted by another metal ion "M_2" to produce M_2–PDA hybrid. To sum, PDA can not only template classic assembling of metallic structures, but it might as well provide a useful platform for the immobilization of single-atom catalysts, alloy metal compounds, and biologically active metal ions.[257,258]

8.2.2. Immobilization of Organic Species

We have known that quinones moieties of PDA can react with amine/thiol-presenting molecules through Michael addition or Schiff-base reaction. Such reactivity enables easy-to-perform secondary surface functionalization, which has markedly lowered the barriers-to-entry for generating multifunctional materials. Noteworthily, both PDA per se and PDA-modified bulk surfaces and nanomaterials hold that reactivity. For example, Zhou et al. incorporated monodispersed PDA-functionalized bioactive glass nanoparticles into an amine-containing polymer network through Schiff-base reaction.[97] The resulting hybrid had self-healing capacity and was effective against multidrug-resistant infections and skin tumors, while promoting wound healing. In addition to quinones, the amino groups can react with acyl chloride compounds for the covalent immobilization of particular organic molecules.[219] Furthermore, the hydroxy groups were reported reactive to initiate ring-opening polymerization.[259,260] The hyperbranched polyglycerol (HPG) layer from glycerol polymerization allows for excellent dispersibility of PDA in salt-containing solution and strong resistance against aggregation in extremely acidic or basic solutions (**Figure 13**a). Apart from these, norepinephrine-derived coatings have been used to activate ring-opening polymerization, which can show greater efficacy due to the presence of alkyl hydroxyl.[8]

Another opportunity worthwhile pointing out is the coupling of catechol chemistry with SI-ATRP, which enables "grafting from" polymer brushes on various substrates.[261] Typically, a layer of ATRP initiator is anchored to a surface via catechol–substrate binding, followed by surface imitated polymerization.[261] For example, Liu et al. developed a rapid DA codeposition-mediated SI-ATRP strategy to grow branched PDMS brushes on commercial melamine-formaldehyde (MF) sponge for multitasking and highly efficient oil–water separation.[262] In particular, magnetic Fe_3O_4 nanoparticles were simultaneously incorporated into the system to result in a nonflammable, magnetic, and superhydrophobic sponge (Figure 13b).

Highly efficient and chemoselective secondary functionalization can be achieved when catechol chemistry is synergized with click chemistry, such as copper-catalyzed azide-alkyne cycloaddition (CuAAC), strain promoted azide-alkyne cycloaddition (SPAAC), temperature-dependent Diels–Alder reaction, and photoclick reaction (Figure 13c).[236,263–266] For example, CuAAC chemistry has been incorporated into mussel-inspired citrate-based antimicrobial bioadhesives to enhance their wet adhesion strength (Figure 13d).[267] Very recently, taking advantage of the efficient, orthogonal, and metal-free SPAAC reaction, Huang group grafted a NO-generating molecule, organoselenium, and an endothelial progenitor cell-targeting peptide onto a stent modified with mussel-inspired peptide (Figure 13e).[268] Thanks to the local release of therapeutic NO, the surface-engineered stents inhibited thrombosis and promoted the recruitment, adhesion, and proliferation of endothelial progenitor cells (Figure 13f–h), thus preventing in-stent restenosis (Figure 13i). In addition, catechol-based biomimetic anchors have been designed to allow temperature-dependent Diels–Alder reaction, by which titanium substrate can be functionalized with hydrophobic/hydrophilic molecules for tailored surface wettability.[264] Last but not least, certain molecules or nanomaterials could effectively interplay with PDA via supramolecular interactions, thus being attached. Recently, photosensitizer indocyanine green has been anchored onto PDA by π–π stacking to afford low-temperature photothermal therapy for biofilm elimination.[269] By means of electrostatic interaction, PDA was decorated with graphitic carbon nitride nanosheets, giving rise to a photocatalytic system with enhanced performance.[270]

8.3. Carbonization

The thermal annealing of PDA, which typically takes place in moderate temperature ranges (e.g., 100–300 °C), is known to convert catechol to quinone for enhanced intermolecular crosslinking and thus cohesion.[137,271] At sufficiently high temperatures, PDA undergoes carbonization to give carbon materials.[190] Compared to carbon materials obtained by traditional carbonization of phenol/formaldehyde resins, the content of sp^3 C is minimized by using PDA, thus favoring enhanced electroconductivity. There are additional merits about PDA. First, high-levels of electroactive nitrogen can be readily introduced into the carbon matrix as soon as carbonization is completed. Second, the carbonization of doped PDA is a facile approach to prepare heteroatoms (e.g., metal, N, S, B) codoped materials that are particularly valued for energy applications. Qiao group systematically investigated the effects of secondary heteroatoms of B, S, and P on the water-splitting performances of N-doped carbon nanosheets for hydrogen evolution. It was interesting to find that S, followed by P, had a promotional effect, while B decreased the activity of N-doped carbons.[272] One step further, they accomplished bifunctional catalytic activity for both hydrogen evolution reaction and oxygen evolution reaction, by codoping N and S into carbon nanotubes.[273]

8.4. Post-Tailoring of Polyphenol-Based Materials

Pertaining to the capability to be post-tailored, polyphenol (with gallol and quinone moieties) and PDA-based (with catechol and quinone moieties) materials should be equivalent, although current focus is more on the latter. It is envisioned that polyphenol-rendered functionalization would receive increasing interest in near future. Distinguished from catechols, polyphenols are

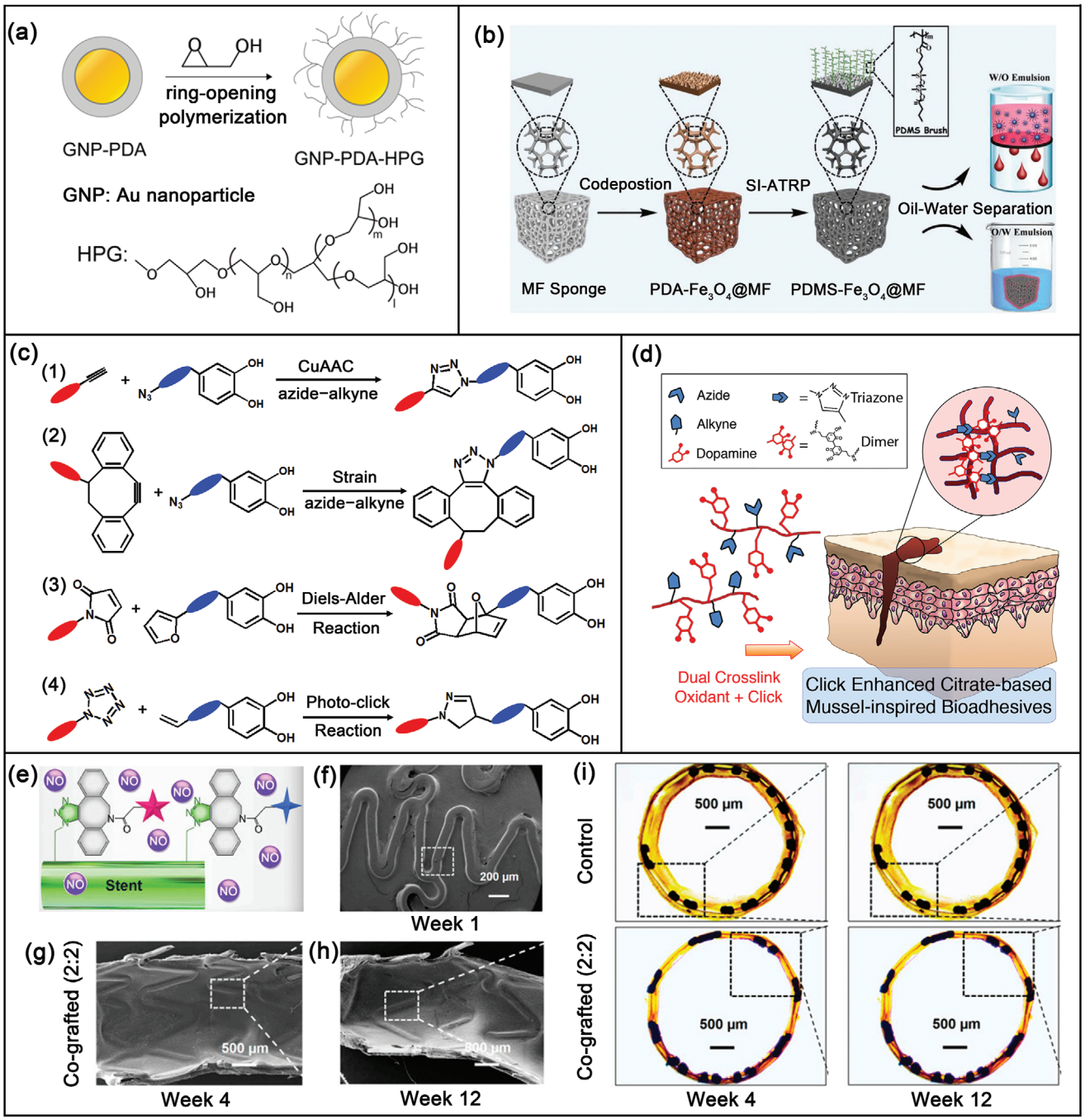

Figure 13. a) Hydroxy groups on PDA initiated the ring-opening polymerization of glycidol to form an HPG. Reproduced with permission.[259] Copyright 2019, American Chemical Society. b) Fabrication of PDMS–Fe_3O_4@MF for oil–water separation. Reproduced with permission.[262] Copyright 2019, Wiley. c) Surface anchoring for chemoselective grafting conjugation by click reaction. The red and blue ellipses refer to different chemical groups. d) CuAAC click reaction enhanced the crosslinking of citrate-based bioadhesive. Reproduced with permission.[267] Copyright 2017, Elsevier. e) Strain click reaction enabled the grafting of NO-generating organoselenium and an endothelial progenitor cell-targeting peptide, which led to f–h) inhibition of thrombosis and smooth muscle cell migration and i) prevention of in-stent restenosis. Reproduced with permission.[268] Copyright 2020, PNAS.

unique for eliciting reversible pH-sensitive hydrogen bonding/debonding and metal–polyphenol assembly/disassembly. Besides, the greater abundance of residual phenolic groups, as contrasted to catechols, signifies more robust, long-lasting adhesion. These properties could shift the current paradigm for producing dynamic functional materials/surfaces with stimuli-triggerable drug/ion delivery in biomedicine. Nevertheless, materials in other application sectors, such as bioadhesives and biocatalysts, are expected to be durable enough to long maintain their intended functionalities. In these cases, polyphenol–amine copolymerized networks would be a more suitable priming structure than pure polyphenols/MPNs for secondary

functionalization.[51,127,274] For example, Lee group has very recently developed a polymeric superglue by copolymerization of a polyphenol (PG) and an amine-containing polymer (PEI).[127] The observed superglue performances are majorly ascribed to the formation of phenol–amine crosslink networks, as well as adhesiveness from residual phenolic groups. Gaining inspiration from the coalification of phenolics, Lee group prepared conductive carbon sealant by carbonization of adhesive phenol–amine networks.[51]

9. Challenges and Future Prospects

In this review, we have summarized recent strategical innovations in spatiotemporal control of phenolic chemistries for the design, development, and applications of advanced functional phenolic materials. Specifically, we have introduced the chemical diversity and reactivity of catechols and polyphenols, while revisiting the mechanisms of polymerization/assembly, adhesion, and cohesion, as well as factors that have an impact on these. Meanwhile, the various modes of reversibility in catechol have been described for controlled production of dynamic materials. Measures for tuning the kinetics of PDA coatings have also been examined briefly. Then our focus has been turned onto how to synthesize PDA-based materials with tailored size and morphology, as well as how to impart spatial control to phenolic coatings via micropatterning and substrate engineering. Furthermore, an update on recent advances in postsynthesis modification of phenolic coatings and materials has been delivered, such as deaggregation and reassembly and post-polymerization grafting. Concomitantly, we have presented state-of-the-art examples in the applications of phenolic coatings, nanoparticles, adhesives, and other bulk or nanomaterials in many areas, ranging from biomedicine to energy, catalysis, and environmental science. Without any doubt, impressive achievements have been made in this fruitful field thus far, and the number and scope of investigations are likely to further expand. Nevertheless, what has been revealed thus far might be the tip of the iceberg. In order to fulfill the rising expectations, we consider it crucial to examine critical issues, which may serve both as an inspiration and stimulus to push forward this realm. Based on current limitations, in the below we suggest future goals and possibilities (**Figure 14**).

9.1. Mechanism

The first daunting challenge is to fully understand the underlying mechanisms. Specifically, we now have incomplete and sometimes controversial interpretations of PDA formation pathways, the structure of PDA, and effects of experimental variables on the former two. Another open question remains as to whether natural or synthetic analogs of DA/DOPA can undergo similar polymerization routes.[275] Additional uncertainties arise in several themes:[19] i) the role of the adjacency of catecholic and cationic moieties in cooperative adhesion; ii) the degradability and degradation mechanism of PDA and related materials; iii) the mechanism of copolymerization/codeposition. In order to elucidate these, further investigations should follow

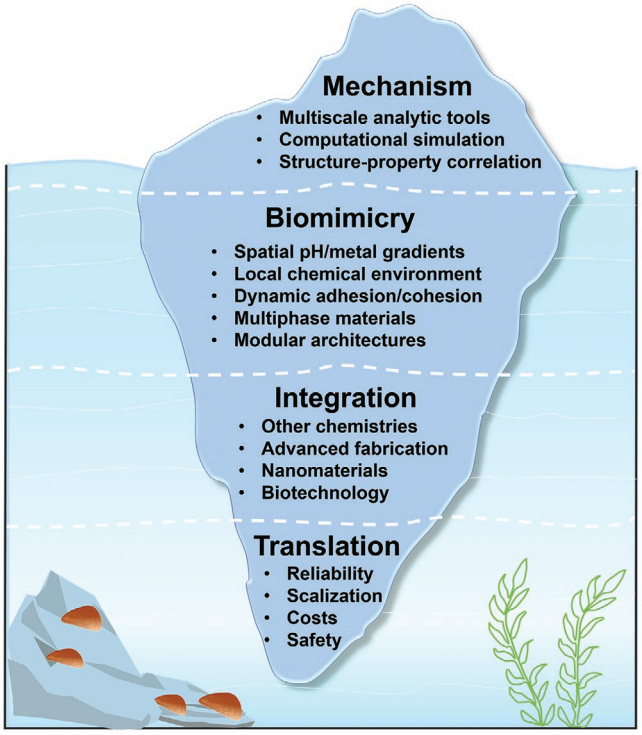

Figure 14. Challenges and opportunities for future research and applications.

to gather compelling evidence or full details based on comprehensive decoupling designs,[18,19] macro-to-atomic level analytic tools,[19] and rationale computational simulation,[276] among other tools and resources.

It is also essential to gain a causal understanding of the structure–property relationships for each type of phenolic materials in a given application. For example, rough PDA coatings have shown elevated bioactivity in orthopedics compared to a smooth one.[277] Compared to PDA and poly(DOPA), poly(norepinephrine) proves a more desirable blood-contacting material to coat cardiovascular stents and grafts owing to its uniform coverage and great anticoagulant activity.[278] Unlocking related knowledge will unquestionably provide clues for application-oriented spatiotemporal control of phenolic chemistries. Since the major challenge lies in the lack of inter-/intrastudy comparison power, the importance of consistent control for variables is worthy of attention in future research designs.

9.2. Biomimicry

Albeit for the tremendous excitement and vigor, to our mind, we are still far away from being capable of truly recreating Nature's masterpieces. For example, mussels' rapid, robust, durable, yet reversible wet adhesion is associated with, including but not limited to, catechol–substrate binding, catechol–thiol/amine crosslinking, and catechol–Fe coordination. Irrespective of insights into any of these, it remains a formidable challenge at the present state-of-the-art to synergize all these design elements into one material. The failure to do so might explain the inferior properties of artificial gules compared to that of

mussels. Additionally, in most researches, the roles of local environments, such as the gradient of pH and coexistence of multiphase materials and chemicals, have been significantly overlooked and often missing.

Spatiotemporally controlled phenolic chemistries, which are the key to replicating the dynamic behaviors of natural systems, are still in their infancy. We need to improve the level of spatial/temporal control in many aspects, e.g., the onset and termination, reaction kinetics, and reversibility of phenolic oxidization/assembly. Protecting chemistry, photochemistry, confined polymerization, stepwise enzymatic oxidization, etc. are effective strategies to achieve these, but they are less leveraged by the majority of material researchers, to whom polymerizing DA is a routine practice.[2] Another noticeable trend is to mimic PG-derived plant chemistries to develop dynamic materials/surfaces, targeting at stimuli-triggerable degradation and liberation behaviors.[279] Polyphenol–amine copolymerized networks are instrumental to the development of adhesives and catalysts with durable properties.[51,127] On the other hand, there is a paucity of work that mirrors Nature's strategy of synergizing phenolic chemistries with sophisticated multiscale architectures.[6] In other words, it is highly desirable to consider topology and microstructure engineering of phenolic materials to amplify the performances and add functionality.

9.3. Integration

To diversify this field, future efforts should be continuously dedicated to the judicious integration of phenolic chemistries with other lesser-explored or unvisited chemistries, such as SI-ATRP, click-like chemistry, lipid chemistry, and supramolecular interactions. Hopefully, synthetic derivatives of catechols and polyphenolics, carrying defined handle moieties or modular sequences, would provide a platform to orchestrate the diverse merits of universal substrate adhesiveness, on-demand chemical reactivity, and high fidelity and orthogonality. In addition, emerging opportunities lie in the marriage between phenolic chemistries and spatiotemporally precise fabrication tools, including micro/nanofabrication and additive manufacturing techniques and others. In particular, phenolic chemistries can readily fused with 3D and 4D printing in the form of phenolics-based inks to afford design freedom, spatial controllability, novel curing mechanism, and versatile functionality.[280–282] The hybridization of phenolic chemistries and nanomaterials is also conducive to attain enhanced or enriched properties for promising utilities in electronics, energy storage, and biomedicine. In such a composite material system, the latter can play multiple roles, including reinforcing fillers, templates for polymerization, anchors for crosslinking, and reservoirs of oxidants. Candidate nanomaterials include carbon nanomaterials, transition-metal dichalcogenide, black phosphorus, hexagonal boron nitride, layered double hydroxides, MOF, and covalent–organic frameworks. Last but not least, outstanding opportunities can lie ahead as a surprise in the integration of phenolic chemistries and living systems and biotechnology.[283–285] For example, phenolic polymerization/assembly can be adapted to engineer the interface or intracellular structures of living cells or protocells,[176,279,286,287] which can find emergent applications in cytoprotection, bioimaging, single cell manipulation, and origin-of-life modeling. Furthermore, we are keen to see the incorporation of phenolic chemistries into DNA origami and CRISPR-Cas technologies, which would give birth to programmable phenolic materials.[288] To bring these to fruition, hand-in-hand cooperation of researches from various disciplines is highly advocated.

9.4. Translation

Despite a near-ripe area, critically, many of the derivative materials fail to elicit real-world impact. Perhaps most restrictive is the inferior performances versus commercial products. For example, compared to glues on the market, catechol-containing adhesives have displayed slower curing kinetics and less stable or even unreliable bonding for different substrates and environments. The applications of phenolic materials in electrocatalysis and batteries are also frustrated by their low resilience in daily usages. Additionally, the translation is hindered by the limited capacity for scale-up production, which is associated with high-costs and low efficiency in material utilization. Indeed, catechol polymerization in solution leads to side products and waste of precursors, especially as the coating is priority. To address this, reagent-saving or site-specific coating methods and material-recycling approaches deserve serious consideration. On the other hand, the naturally abundant and cost-effective polyphenolics can be a future avenue of exploration. Methods for generating large-dimension and stable phenolic films can be invaluable in real application settings, thus desiderating development. Furthermore, PDA-based nanomaterials are restricted by their low dispersity and tendency to aggregate, which poses challenges in their storage, transportation, and thus commercialization.

In addition, the translation is impeded by field-specific requirements. There are instances where applying phenolic-based biomaterials and devices require higher levels of caution, especially in biomedicine. For example, PDA, the most studied phenolic material, has been regarded biocompatible from preliminary cell and animal studies, but its effects on human subjects are still unknown. The reactivity of catechols can be a double-edged sword, as it allows ease in functionalization but might also interference with biological activities of enzymes, proteins, and cells. Catechol-based adhesives can provoke safety issues with regard to special curing conditions (elevated pH, addition of oxidants, etc.) and the generation of detrimental radical species. Therefore, their effects on the biological systems should be monitored systematically yet in the long term as undesirable side effects can occur in many ways in vivo.[1,98] Any conclusion drawn needs case-specific justification with respect to factors such as particle sizes and geometries, surface properties, colloidal stability, degradation behaviors, etc. Only when these uncertainties are satisfactorily tackled, can PDA and its derivative materials/devices enter the phase of clinical translation.

To sum up, phenolic chemistries will continue to fuel materials science and the future is undoubtedly bright, especially as the outlined hurdles are gradually cleared. We expect that this tutorial review will not only provide a panoramic view of

strategies for spatiotemporal control of phenolic chemistries, but also inspire researchers to develop innovative phenolic materials with elegant and reliable properties in both research and translational settings.

Acknowledgements

Z.J. and M.W. contributed equally to this work. This work was financially supported by National Natural Science Foundation of China (Grant No. 51931001) and NMPA Key Laboratory for Dental Materials (PKUSS20200401).

Conflict of Interest

The authors declare no conflict of interest.

Keywords

catechols, functional materials, polydopamine, polyphenols, spatiotemporal control

Received: October 16, 2020
Revised: December 8, 2020
Published online:

[1] Y. L. Liu, K. L. Ai, L. H. Lu, *Chem. Rev.* **2014**, *114*, 5057.
[2] H. Lee, S. M. Dellatore, W. M. Miller, P. B. Messersmith, *Science* **2007**, *318*, 426.
[3] Q. Zhao, D. W. Lee, B. K. Ahn, S. Seo, Y. Kaufman, J. N. Israelachvili, J. H. Waite, *Nat. Mater.* **2016**, *15*, 407.
[4] H. Zhao, C. Sun, R. J. Stewart, J. H. Waite, *J. Biol. Chem.* **2005**, *280*, 42938.
[5] A. Miserez, T. Schneberk, C. Sun, F. W. Zok, J. H. Waite, *Science* **2008**, *319*, 1816.
[6] H. Lee, B. P. Lee, P. B. Messersmith, *Nature* **2007**, *448*, 338.
[7] J. H. Miaoer Yu, T. J. Deming, *J. Am. Chem. Soc.* **1999**, *121*, 5825.
[8] S. M. Kang, J. Rho, I. S. Choi, P. B. Messersmith, H. Lee, *J. Am. Chem. Soc.* **2009**, *131*, 13224.
[9] S. Quideau, D. Deffieux, C. Douat-Casassus, L. Pouysegu, *Angew. Chem., Int. Ed.* **2011**, *50*, 586.
[10] M. A. Rahim, S. L. Kristufek, S. J. Pan, J. J. Richardson, F. Caruso, *Angew. Chem., Int. Ed.* **2019**, *58*, 1904.
[11] T. S. Sileika, D. G. Barrett, R. Zhang, K. H. Lau, P. B. Messersmith, *Angew. Chem., Int. Ed.* **2013**, *52*, 10766.
[12] H. Ejima, J. J. Richardson, F. Caruso, *Nano Today* **2017**, *12*, 136.
[13] N. Patil, C. Jerome, C. Detrembleur, *Prog. Polym. Sci.* **2018**, *82*, 34.
[14] Z. Wang, H.-C. Yang, F. He, S. Peng, Y. Li, L. Shao, S. B. Darling, *Matter* **2019**, *1*, 115.
[15] H. A. Lee, E. Park, H. Lee, *Adv. Mater.* **2020**, 1907505.
[16] R. Batul, T. Tamanna, A. Khaliq, A. Yu, *Biomater. Sci.* **2017**, *5*, 1204.
[17] C. Zhang, B. Wu, Y. Zhou, F. Zhou, W. Liu, Z. Wang, *Chem. Soc. Rev.* **2020**, *49*, 3605.
[18] G. P. Maier, M. V. Rapp, J. H. Waite, J. N. Israelachvili, A. Butler, *Science* **2015**, *349*, 628.
[19] B. D. B. Tiu, P. Delparastan, M. R. Ney, M. Gerst, P. B. Messersmith, *Angew. Chem., Int. Ed.* **2020**, *59*, 16616.
[20] S. Hong, Y. Wang, S. Y. Park, H. Lee, *Sci. Adv.* **2018**, *4*, eaat7457.
[21] B. K. Ahn, *J. Am. Chem. Soc.* **2017**, *139*, 10166.
[22] M. A. North, C. A. Del Grosso, J. J. Wilker, *ACS Appl. Mater. Interfaces* **2017**, *9*, 7866.
[23] A. H. Hofman, I. A. van Hees, J. Yang, M. Kamperman, *Adv. Mater.* **2018**, *30*, 1704640.
[24] L. Han, X. Lu, K. Liu, K. Wang, L. Fang, L. T. Weng, H. Zhang, Y. Tang, F. Ren, C. Zhao, G. Sun, R. Liang, Z. Li, *ACS Nano* **2017**, *11*, 2561.
[25] F. Ponzio, J. Barthès, J. Bour, M. Michel, P. Bertani, J. Hemmerlé, M. d'Ischia, V. Ball, *Chem. Mater.* **2016**, *28*, 4697.
[26] X. Wang, Z. Chen, P. Yang, J. Hu, Z. Wang, Y. Li, *Polym. Chem.* **2019**, *10*, 4194.
[27] X. Du, L. Li, J. Li, C. Yang, N. Frenkel, A. Welle, S. Heissler, A. Nefedov, M. Grunze, P. A. Levkin, *Adv. Mater.* **2014**, *26*, 8029.
[28] M. Lee, S. H. Lee, I. K. Oh, H. Lee, *Small* **2017**, *13*, 1600443.
[29] M. K. Mun, Y. J. Jang, J. E. Kim, G. Y. Yeom, D. W. Kim, *RSC Adv.* **2019**, *9*, 12814.
[30] W. Zheng, H. Fan, L. Wang, Z. Jin, *Langmuir* **2015**, *31*, 11671.
[31] Q. Z. Zhong, S. Li, J. Chen, K. Xie, S. Pan, J. J. Richardson, F. Caruso, *Angew. Chem., Int. Ed.* **2019**, *58*, 12563.
[32] H. Lee, W. I. Kim, W. Youn, T. Park, S. Lee, T.-S. Kim, J. F. Mano, I. S. Choi, *Adv. Mater.* **2018**, *30*, 1805091.
[33] P. Yang, S. Zhang, X. Chen, X. Liu, Z. Wang, Y. Li, *Mater. Horiz.* **2020**, *7*, 746.
[34] S. Cho, T. S. Shim, J. H. Kim, D.-H. Kim, S.-H. Kim, *Adv. Mater.* **2017**, *29*, 1700256.
[35] S. Wang, S. Wannasarit, P. Figueiredo, J. Li, A. Correia, B. Xia, R. Wiwattanapatapee, J. Hirvonen, D. Liu, W. Li, H. A. Santos, *Mater. Horiz.* **2020**, *7*, 1573.
[36] X. Yu, H. Fan, L. Wang, Z. Jin, *Angew. Chem., Int. Ed.* **2014**, *53*, 12600.
[37] L. Sun, C. Wang, X. Wang, L. Wang, *Small* **2018**, *14*, 1800090.
[38] C. Li, J. Yao, Y. Huang, C. Xu, D. Lou, Z. Wu, W. Sun, S. Zhang, Y. Li, L. He, X. Zhang, *J. Mater. Chem. A* **2019**, *7*, 1404.
[39] J. Cui, Y. Wang, A. Postma, J. Hao, L. Hosta-Rigau, F. Caruso, *Adv. Funct. Mater.* **2010**, *20*, 1625.
[40] J. Xue, W. Zheng, L. Wang, Z. Jin, *ACS Biomater. Sci. Eng.* **2016**, *2*, 489.
[41] C. Wang, L. Sun, F. Zhang, X. Wang, Q. Sun, Y. Cheng, L. Wang, *Small* **2017**, *13*, 1701246.
[42] A. K. Awasthi, S. D. Bhagat, R. Ramakrishnan, A. Srivastava, *Chem. - Eur. J.* **2019**, *25*, 12905.
[43] W. Sheng, W. Li, B. Yu, B. Li, R. Jordan, X. Jia, F. Zhou, *Angew. Chem., Int. Ed.* **2019**, *58*, 12018.
[44] M. Zhang, L. Zhang, Y. Chen, L. Li, Z. Su, C. Wang, *Chem. Sci.* **2017**, *8*, 8067.
[45] Y. Tokura, S. Harvey, C. Chen, Y. Wu, D. Y. W. Ng, T. Weil, *Angew. Chem., Int. Ed.* **2018**, *57*, 1587.
[46] F. Behboodi-Sadabad, H. Zhang, V. Trouillet, A. Welle, N. Plumeré, P. A. Levkin, *Adv. Funct. Mater.* **2017**, *27*, 1700127.
[47] W. R. Chae, P. Q. H. Nguyen, J. W. Hong, N. Y. Lee, *Adv. Mater. Technol.* **2019**, *4*, 1800485.
[48] L. Liu, Y. Pei, S. Ma, X. Sun, T. J. Singler, *Adv. Eng. Mater.* **2020**, *22*, 1901351.
[49] Z. Wang, Y. Zou, Y. Li, Y. Cheng, *Small* **2020**, *16*, 1907042.
[50] W. Yang, C. Liu, Y. Chen, *Langmuir* **2018**, *34*, 3565.
[51] Y. Lee, K. Jun, K. Lee, Y. C. Seo, C. Jeong, M. Kim, I. K. Oh, H. Lee, *Angew. Chem., Int. Ed.* **2020**, *59*, 3864.
[52] P. Zhang, W. Hu, M. Wu, L. Gong, A. Tang, L. Xiang, B. Zhu, L. Zhu, H. Zeng, *Langmuir* **2019**, *35*, 4101.
[53] H. A. Lee, Y. F. Ma, F. Zhou, S. Hong, H. Lee, *Acc. Chem. Res.* **2019**, *52*, 704.
[54] T. G. Barclay, H. M. Hegab, S. R. Clarke, M. Ginic-Markovic, *Adv. Mater. Interfaces* **2017**, *4*, 1601192.
[55] Y. H. Ding, M. Floren, W. Tan, *Biosurf. Biotribol.* **2016**, *2*, 121.
[56] S. Hong, Y. S. Na, S. Choi, I. T. Song, W. Y. Kim, H. Lee, *Adv. Funct. Mater.* **2012**, *22*, 4711.

[57] Q. Lyu, N. Hsueh, C. L. L. Chai, *Langmuir* **2019**, *35*, 5191.
[58] N. F. Della Vecchia, R. Avolio, M. Alfe, M. E. Errico, A. Napolitano, M. d'Ischia, *Adv. Funct. Mater.* **2013**, *23*, 1331.
[59] Y. Ding, L. T. Weng, M. Yang, Z. Yang, X. Lu, N. Huang, Y. Leng, *Langmuir* **2014**, *30*, 12258.
[60] C.-T. Chen, F. Martin-Martinez, G. S. Jung, M. Buehler, *Chem. Sci.* **2016**, *8*, 1631.
[61] D. R. Dreyer, D. J. Miller, B. D. Freeman, D. R. Paul, C. W. Bielawski, *Langmuir* **2012**, *28*, 6428.
[62] J. Liebscher, R. Mrówczyński, H. A. Scheidt, C. Filip, N. D. Hădade, R. Turcu, A. Bende, S. Beck, *Langmuir* **2013**, *29*, 10539.
[63] M. L. Alfieri, R. Micillo, L. Panzella, O. Crescenzi, S. L. Oscurato, P. Maddalena, A. Napolitano, V. Ball, M. d'Ischia, *ACS Appl. Mater. Interfaces* **2018**, *10*, 7670.
[64] P. Delparastan, K. G. Malollari, H. Lee, P. B. Messersmith, *Angew. Chem., Int. Ed.* **2019**, *58*, 1077.
[65] A. Andersen, Y. Chen, H. Birkedal, *Biomimetics* **2019**, *4*, 30.
[66] J. Yu, W. Wei, E. Danner, J. N. Israelachvili, J. H. Waite, *Adv. Mater.* **2011**, *23*, 2362.
[67] H. Lee, N. F. Scherer, P. B. Messersmith, *Proc. Natl. Acad. Sci. USA* **2006**, *103*, 12999.
[68] J. Liebscher, *Eur. J. Org. Chem.* **2019**, *2019*, 4976.
[69] J. Saiz-Poseu, J. Mancebo-Aracil, F. Nador, F. Busque, D. Ruiz-Molina, *Angew. Chem., Int. Ed.* **2019**, *58*, 696.
[70] M. A. Gebbie, W. Wei, A. M. Schrader, T. R. Cristiani, H. A. Dobbs, M. Idso, B. F. Chmelka, J. H. Waite, J. N. Israelachvili, *Nat. Chem.* **2017**, *9*, 473.
[71] H. Birkedal, *Nat. Chem.* **2017**, *9*, 408.
[72] S.-C. Li, L.-N. Chu, X.-Q. Gong, U. Diebold, *Science* **2010**, *328*, 882.
[73] J. Yu, Y. Kan, M. Rapp, E. Danner, W. Wei, S. Das, D. R. Miller, Y. Chen, J. H. Waite, J. N. Israelachvili, *Proc. Natl. Acad. Sci. USA* **2013**, *110*, 15680.
[74] J. Yu, W. Wei, M. S. Menyo, A. Masic, J. H. Waite, J. N. Israelachvili, *Biomacromolecules* **2013**, *14*, 1072.
[75] M. Krogsgaard, M. R. Hansen, H. Birkedal, *J. Mater. Chem. B* **2014**, *2*, 8292.
[76] G. P. Maier, A. Butler, *J. Biol. Inorg. Chem.* **2017**, *22*, 739.
[77] N. Holten-Andersen, M. J. Harrington, H. Birkedal, B. P. Lee, P. B. Messersmith, K. Y. Lee, J. H. Waite, *Proc. Natl. Acad. Sci. USA* **2011**, *108*, 2651.
[78] M. J. Sever, J. T. Weisser, J. Monahan, S. Srinivasan, J. J. Wilker, *Angew. Chem., Int. Ed.* **2004**, *43*, 448.
[79] A. R. Narkar, B. Barker, M. Clisch, J. Jiang, B. P. Lee, *Chem. Mater.* **2016**, *28*, 5432.
[80] M. Shan, C. Gong, B. Li, G. Wu, *Polym. Chem.* **2017**, *8*, 2997.
[81] N. Budisa, T. Schneider, *ChemBioChem* **2019**, *20*, 2163.
[82] J. Zhou, B. Duan, Z. Fang, J. Song, C. Wang, P. B. Messersmith, H. Duan, *Adv. Mater.* **2014**, *26*, 701.
[83] J. Cai, J. Huang, S. Wang, J. Iocozzia, Z. Sun, J. Sun, Y. Yang, Y. Lai, Z. Lin, *Adv. Mater.* **2019**, *31*, 1806314.
[84] Z. Jia, P. Xiu, M. Li, X. Xu, Y. Shi, Y. Cheng, S. Wei, Y. Zheng, T. Xi, H. Cai, Z. Liu, *Biomaterials* **2016**, *75*, 203.
[85] J. Ryu, S. H. Ku, H. Lee, C. B. Park, *Adv. Funct. Mater.* **2010**, *20*, 2132.
[86] L. Guo, Q. Liu, G. Li, J. Shi, J. Liu, T. Wang, G. Jiang, *Nanoscale* **2012**, *4*, 5864.
[87] Q. Huang, J. Chen, M. Liu, H. Huang, X. Zhang, Y. Wei, *Chem. Eng. J.* **2020**, *387*, 124019.
[88] K. R. Yoon, K. A. Lee, S. Jo, S. H. Yook, K. Y. Lee, I.-D. Kim, J. Y. Kim, *Adv. Funct. Mater.* **2019**, *29*, 1806929.
[89] C. Lim, J. Huang, S. Kim, H. Lee, H. Zeng, D. S. Hwang, *Angew. Chem., Int. Ed.* **2016**, *55*, 3342.
[90] S. Hong, J. Yeom, I. T. Song, S. M. Kang, H. Lee, H. Lee, *Adv. Mater. Interfaces* **2014**, *1*, 1400113.
[91] D. G. Barrett, T. S. Sileika, P. B. Messersmith, *Chem. Commun.* **2014**, *50*, 7265.
[92] L. E. Aguilar, J. Y. Lee, C. H. Park, C. S. Kim, *Polymers* **2019**, *11*, 584.
[93] Y. He, Q. Chen, Y. Zhang, Y. Zhao, L. Chen, *ACS Appl. Mater. Interfaces* **2020**, *12*, 52104.
[94] M. Iacomino, J. I. Paez, R. Avolio, A. Carpentieri, L. Panzella, G. Falco, E. Pizzo, M. E. Errico, A. Napolitano, A. Del Campo, M. d'Ischia, *Langmuir* **2017**, *33*, 2096.
[95] S. Chen, X. Li, Z. Yang, S. Zhou, R. Luo, M. F. Maitz, Y. Zhao, J. Wang, K. Xiong, N. Huang, *Colloids Surf., B* **2014**, *113*, 125.
[96] J. Yang, M. A. C. Stuart, M. Kamperman, *Chem. Soc. Rev.* **2014**, *43*, 8271.
[97] L. Zhou, Y. Xi, Y. Xue, M. Wang, Y. Liu, Y. Guo, B. Lei, *Adv. Funct. Mater.* **2019**, *29*, 1806883.
[98] W. Cheng, X. W. Zeng, H. Z. Chen, Z. M. Li, W. F. Zeng, L. Mei, Y. L. Zhao, *ACS Nano* **2019**, *13*, 8537.
[99] H. W. Kim, B. D. McCloskey, T. H. Choi, C. Lee, M. J. Kim, B. D. Freeman, H. B. Park, *ACS Appl. Mater. Interfaces* **2013**, *5*, 233.
[100] W. Sheng, B. Li, X. Wang, B. Dai, B. Yu, X. Jia, F. Zhou, *Chem. Sci.* **2015**, *6*, 2068.
[101] Z. Wang, C. Xu, Y. Lu, G. Wei, G. Ye, T. Sun, J. Chen, *Polym. Chem.* **2017**, *8*, 4388.
[102] R. Ouyang, J. Lei, H. Ju, Y. Xue, *Adv. Funct. Mater.* **2007**, *17*, 3223.
[103] K. Kang, S. Lee, R. Kim, I. S. Choi, Y. Nam, *Angew. Chem., Int. Ed.* **2012**, *51*, 13101.
[104] S. H. Hong, S. Hong, M.-H. Ryou, J. W. Choi, S. M. Kang, H. Lee, *Adv. Mater. Interfaces* **2016**, *3*, 1500857.
[105] X. Shi, S. Ostrovidov, Y. Shu, X. Liang, K. Nakajima, H. Wu, A. Khademhosseini, *Langmuir* **2014**, *30*, 832.
[106] F. Bernsmann, V. Ball, F. Addiego, A. Ponche, M. Michel, J. J. Gracio, V. Toniazzo, D. Ruch, *Langmuir* **2011**, *27*, 2819.
[107] V. Ball, J. Gracio, M. Vila, M. K. Singh, M. H. Metz-Boutigue, M. Michel, J. Bour, V. Toniazzo, D. Ruch, M. J. Buehler, *Langmuir* **2013**, *29*, 12754.
[108] M. Salomaki, T. Ouvinen, L. Marttila, H. Kivela, J. Leiro, E. Makila, J. Lukkari, *J. Phys. Chem. B* **2019**, *123*, 2513.
[109] C. Zhang, Y. Ou, W.-X. Lei, L.-S. Wan, J. Ji, Z.-K. Xu, *Angew. Chem., Int. Ed.* **2016**, *55*, 3054.
[110] Q. Wei, F. Zhang, J. Li, B. Li, C. Zhao, *Polym. Chem.* **2010**, *1*, 1430.
[111] J. H. Ryu, P. B. Messersmith, H. Lee, *ACS Appl. Mater. Interfaces* **2018**, *10*, 7523.
[112] M. d'Ischia, A. Napolitano, A. Pezzella, E. Land, C. Ramsden, P. Riley, *Adv. Heterocycl. Chem.* **2005**, *89*, 1.
[113] J. P. Park, I. T. Song, J. Lee, J. H. Ryu, Y. Lee, H. Lee, *Chem. Mater.* **2014**, *27*, 105.
[114] Y. Tan, W. Deng, Y. Li, Z. Huang, Y. Meng, Q. Xie, M. Ma, S. Yao, *J. Phys. Chem. B* **2010**, *114*, 5016.
[115] J. Li, M. A. Baird, M. A. Davis, W. Tai, L. S. Zweifel, K. M. A. Waldorf, M. Gale Jr., L. Rajagopal, R. H. Pierce, X. Gao, *Nat. Biomed. Eng.* **2017**, *1*, 0082.
[116] S. Kim, S. Hong, *Adv. Healthcare Mater.* **2020**, *9*, 2000540.
[117] P. Yang, Z. Gu, F. Zhu, Y. Li, *CCS Chem.* **2020**, *2*, 128.
[118] I. You, H. Jeon, K. Lee, M. Do, Y. C. Seo, H. A. Lee, H. Lee, *J. Ind. Eng. Chem.* **2017**, *46*, 379.
[119] M. L. Alfieri, L. Panzella, S. L. Oscurato, M. Salvatore, R. Avolio, M. E. Errico, P. Maddalena, A. Napolitano, M. D'Ischia, *Biomimetics* **2018**, *3*, 26.
[120] J. Li, D. Zou, K. Zhang, X. Luo, P. Yang, Y. Jing, Y. Zhang, G. Cui, N. Huang, *J. Mater. Chem. B* **2017**, *5*, 8299.
[121] H.-C. Yang, R. Z. Waldman, M.-B. Wu, J. Hou, L. Chen, S. B. Darling, Z.-K. Xu, *Adv. Funct. Mater.* **2018**, *28*, 1705327.
[122] C. Luo, Q. Liu, *ACS Appl. Mater. Interfaces* **2017**, *9*, 8297.
[123] L. Yang, B. Gu, Z. Chen, Y. Yue, W. Wang, H. Zhang, X. Liu, S. Ren, W. Yang, Y. Li, *ACS Appl. Mater. Interfaces* **2019**, *11*, 30360.

[124] C. Zhang, L. Xiang, J. Zhang, L. Gong, L. Han, Z. K. Xu, H. Zeng, *Langmuir* **2019**, *35*, 5257.
[125] C. Zhang, B.-H. Wu, Y. Du, M.-Q. Ma, Z.-K. Xu, *J. Mater. Chem. C* **2017**, *5*, 3898.
[126] P. Yang, S. Zhang, N. Zhang, Y. Wang, J. Zhong, X. Sun, Y. Qi, X. Chen, Z. Li, Y. Li, *ACS Appl. Mater. Interfaces* **2019**, *11*, 42671.
[127] Y. Wang, E. J. Jeon, J. Lee, H. Hwang, S. W. Cho, H. Lee, *Adv. Mater.* **2020**, *32*, 2002118.
[128] S. Dubey, A. Roulin, *Pigm. Cell Melanoma Res.* **2014**, *27*, 327.
[129] M. d'Ischia, A. Napolitano, V. Ball, C.-T. Chen, M. J. Buehler, *Acc. Chem. Res.* **2014**, *47*, 3541.
[130] L. Panzella, G. Gentile, G. D'Errico, N. F. Della Vecchia, M. E. Errico, A. Napolitano, C. Carfagna, M. d'Ischia, *Angew. Chem., Int. Ed.* **2013**, *52*, 12684.
[131] J. Kuang, J. L. Guo, P. B. Messersmith, *Adv. Mater. Interfaces* **2014**, *1*, 1400145.
[132] C. Papuc, G. V. Goran, C. N. Predescu, V. Nicorescu, G. Stefan, *Compr. Rev. Food Sci. Food Saf.* **2017**, *16*, 1243.
[133] B. Kim, B. Kang, T. P. Vales, S. K. Yang, J. Lee, H.-J. Kim, *Macromol. Res.* **2017**, *26*, 35.
[134] J. Y. Kim, W. I. Kim, W. Youn, J. Seo, B. J. Kim, J. K. Lee, I. S. Choi, *Nanoscale* **2018**, *10*, 13351.
[135] T. Sun, Z.-j. Li, H.-g. Wang, D. Bao, F.-l. Meng, X.-b. Zhang, *Angew. Chem., Int. Ed.* **2016**, *55*, 10662.
[136] T. Nokami, T. Matsuo, Y. Inatomi, N. Hojo, T. Tsukagoshi, H. Yoshizawa, A. Shimizu, H. Kuramoto, K. Komae, H. Tsuyama, J.-i. Yoshida, *J. Am. Chem. Soc.* **2012**, *134*, 19694.
[137] K. G. Malollari, P. Delparastan, C. Sobek, S. J. Vachhani, T. D. Fink, R. H. Zha, P. B. Messersmith, *ACS Appl. Mater. Interfaces* **2019**, *11*, 43599.
[138] D. Gan, W. Xing, L. Jiang, J. Fang, C. Zhao, F. Ren, L. Fang, K. Wang, X. Lu, *Nat. Commun.* **2019**, *10*, 1487.
[139] D. Gan, Z. Huang, X. Wang, L. Jiang, C. Wang, M. Zhu, F. Ren, L. Fang, K. Wang, C. Xie, X. Lu, *Adv. Funct. Mater.* **2019**, *30*, 1907678.
[140] G. Tan, Y. Liu, Y. Wu, K. Ouyang, L. Zhou, P. Yu, J. Liao, C. Ning, *Electrochim. Acta* **2017**, *228*, 343.
[141] S. Daboss, J. Lin, M. Godejohann, C. Kranz, *Anal. Chem.* **2020**, *92*, 8404.
[142] M. S. Akram Bhuiyan, J. D. Roland, B. Liu, M. Reaume, Z. Zhang, J. D. Kelley, B. P. Lee, *J. Am. Chem. Soc.* **2020**, *142*, 4631.
[143] J. Horsch, P. Wilke, M. Pretzler, M. Seuss, I. Melnyk, D. Remmler, A. Fery, A. Rompel, H. G. Borner, *Angew. Chem., Int. Ed.* **2018**, *57*, 15728.
[144] S. Arias, S. Amini, J. Horsch, M. Pretzler, A. Rompel, I. Melnyk, D. Sychev, A. Fery, H. G. Borner, *Angew. Chem., Int. Ed.* **2020**, *59*, 18495.
[145] H. M. Siebert, J. J. Wilker, *ACS Sustainable Chem. Eng.* **2019**, *7*, 13315.
[146] B. K. Ahn, D. W. Lee, J. N. Israelachvili, J. H. Waite, *Nat. Mater.* **2014**, *13*, 867.
[147] P. Argust, *Biol. Trace Elem. Res.* **1998**, *66*, 131.
[148] R. Pizer, L. Babcock, *Inorg. Chem.* **1977**, *16*, 1677.
[149] L. He, D. E. Fullenkamp, J. G. Rivera, P. B. Messersmith, *Chem. Commun.* **2011**, *47*, 7497.
[150] J. Guo, H. Sun, K. Alt, B. L. Tardy, J. J. Richardson, T. Suma, H. Ejima, J. Cui, C. E. Hagemeyer, F. Caruso, *Adv. Healthcare Mater.* **2015**, *4*, 1796.
[151] Y. Ma, P. He, X. Tian, G. Liu, X. Zeng, G. Pan, *ACS Appl. Mater. Interfaces* **2019**, *11*, 23948.
[152] S. Sieste, T. Mack, C. V. Synatschke, C. Schilling, C. Meyer Zu Reckendorf, L. Pendi, S. Harvey, F. S. Ruggeri, T. P. J. Knowles, C. Meier, D. Y. W. Ng, T. Weil, B. Knoll, *Adv. Healthcare Mater.* **2018**, *7*, 1701485.
[153] C. Kim, H. Ejima, N. Yoshie, *J. Mater. Chem. A* **2018**, *6*, 19643.
[154] C. Kim, H. Ejima, N. Yoshie, *RSC Adv.* **2017**, *7*, 19288.
[155] A. O. Hirotaka Ejima, N. Yoshie, *J. Photopolym. Sci. Technol.* **2018**, *31*, 75.
[156] L. Liu, X. Tian, Y. Ma, Y. Duan, X. Zhao, G. Pan, *Angew. Chem., Int. Ed.* **2018**, *57*, 7878.
[157] P. Klan, T. Solomek, C. G. Bochet, A. Blanc, R. Givens, M. Rubina, V. Popik, A. Kostikov, J. Wirz, *Chem. Rev.* **2013**, *113*, 119.
[158] M. Hauf, F. Richter, T. Schneider, T. Faidt, B. M. Martins, T. Baumann, P. Durkin, H. Dobbek, K. Jacobs, A. Möglich, N. Budisa, *ChemBioChem* **2017**, *18*, 1819.
[159] J. Heo, T. Kang, S. G. Jang, D. S. Hwang, J. M. Spruell, K. L. Killops, J. H. Waite, C. J. Hawker, *J. Am. Chem. Soc.* **2012**, *134*, 20139.
[160] Y. Li, Y. Xie, Z. Wang, N. Zang, F. Carniato, Y. Huang, C. M. Andolina, L. R. Parent, T. B. Ditri, E. D. Walter, M. Botta, J. D. Rinehart, N. C. Gianneschi, *ACS Nano* **2016**, *10*, 10186.
[161] E. Filippidi, T. R. Cristiani, C. D. Eisenbach, J. H. Waite, J. N. Israelachvili, B. K. Ahn, M. T. Valentine, *Science* **2017**, *358*, 502.
[162] Y. K. Jeong, J. W. Choi, *ACS Nano* **2019**, *13*, 8364.
[163] Q. Li, D. G. Barrett, P. B. Messersmith, N. Holten-Andersen, *ACS Nano* **2016**, *10*, 1317.
[164] B. P. Lee, S. Konst, *Adv. Mater.* **2014**, *26*, 3415.
[165] B. P. Lee, A. Narkar, R. Wilharm, *Sens. Actuators, B* **2016**, *227*, 248.
[166] H. Zeng, D. S. Hwang, J. N. Israelachvili, J. H. Waite, *Proc. Natl. Acad. Sci. USA* **2010**, *107*, 12850.
[167] Z. Xu, *Sci. Rep.* **2013**, *3*, 2914.
[168] Q. Xu, M. Xu, C. Y. Lin, Q. Zhao, R. Zhang, X. Dong, Y. Zhang, S. Tian, Y. Tian, Z. Xia, *Adv. Sci.* **2019**, *6*, 1902043.
[169] H. Ejima, J. J. Richardson, K. Liang, J. P. Best, M. P. van Koeverden, G. K. Such, J. Cui, F. Caruso, *Science* **2013**, *341*, 154.
[170] G. Yun, J. J. Richardson, M. Capelli, Y. Hu, Q. A. Besford, A. C. G. Weiss, H. Lee, I. S. Choi, B. C. Gibson, P. Reineck, F. Caruso, *Adv. Funct. Mater.* **2019**, *30*, 1905805.
[171] N. Bertleff-Zieschang, M. A. Rahim, Y. Ju, J. A. Braunger, T. Suma, Y. Dai, S. Pan, F. Cavalieri, F. Caruso, *Chem. Commun.* **2017**, *53*, 1068.
[172] M. A. Rahim, K. Kempe, M. Müllner, H. Ejima, Y. Ju, M. P. van Koeverden, T. Suma, J. A. Braunger, M. G. Leeming, B. F. Abrahams, F. Caruso, *Chem. Mater.* **2015**, *27*, 5825.
[173] J. Guo, Y. Ping, H. Ejima, K. Alt, M. Meissner, J. J. Richardson, Y. Yan, K. Peter, D. von Elverfeldt, C. E. Hagemeyer, F. Caruso, *Angew. Chem., Int. Ed.* **2014**, *53*, 5546.
[174] Y. Ping, J. Guo, H. Ejima, X. Chen, J. J. Richardson, H. Sun, F. Caruso, *Small* **2015**, *11*, 2032.
[175] W. Li, W. Bing, S. Huang, J. Ren, X. Qu, *Adv. Funct. Mater.* **2015**, *25*, 3775.
[176] B. J. Kim, S. Han, K.-B. Lee, I. S. Choi, *Adv. Mater.* **2017**, *29*, 1700784.
[177] B. J. Kim, H. Cho, J. H. Park, J. F. Mano, I. S. Choi, *Adv. Mater.* **2018**, *30*, 1706063.
[178] W. Youn, J. Y. Kim, J. Park, N. Kim, H. Choi, H. Cho, I. S. Choi, *Adv. Mater.* **2020**, *32*, 1907001.
[179] M. A. Rahim, M. Björnmalm, N. Bertleff-Zieschang, Q. Besford, S. Mettu, T. Suma, M. Faria, F. Caruso, *Adv. Mater.* **2017**, *29*, 1606717.
[180] J. Kang, G. Bai, S. Ma, X. Liu, Z. Ma, X. Guo, X. Wang, B. Dai, F. Zhou, X. Jia, *Adv. Mater. Interfaces* **2019**, *6*, 1801789.
[181] Q.-Z. Zhong, J. J. Richardson, S. Li, W. Zhang, Y. Ju, J. Li, S. Pan, J. Chen, F. Caruso, *Angew. Chem., Int. Ed.* **2020**, *59*, 1711.
[182] T. Park, W. I. Kim, B. J. Kim, H. Lee, I. S. Choi, J. H. Park, W. K. Cho, *Langmuir* **2018**, *34*, 12318.
[183] G. Yun, W. Youn, H. Lee, S. Y. Han, M. B. Oliveira, H. Cho, F. Caruso, J. F. Mano, I. S. Choi, *Chem. Mater.* **2020**, *32*, 7746.
[184] M. Salomaki, L. Marttila, H. Kivela, T. Ouvinen, J. Lukkari, *J. Phys. Chem. B* **2018**, *122*, 6314.

[185] M. Kohri, Y. Nannichi, T. Taniguchi, K. Kishikawa, *J. Mater. Chem. C* **2015**, *3*, 720.
[186] Q. Zhang, Q. Yang, P. Phanlavong, Y. Li, Z. Wang, T. Jiao, Q. Peng, *ACS Sustainable Chem. Eng.* **2017**, *5*, 4161.
[187] K.-Y. Ju, Y. Lee, S. Lee, S. B. Park, J.-K. Lee, *Biomacromolecules* **2011**, *12*, 625.
[188] D. R. Amin, C. Sugnaux, K. H. A. Lau, P. B. Messersmith, *Biomimetics* **2017**, *2*, 17.
[189] Y. Xie, J. Wang, Z. Wang, K. A. Krug, J. D. Rinehart, *Nanoscale* **2018**, *10*, 12813.
[190] K. Ai, Y. Liu, C. Ruan, L. Lu, G. M. Lu, *Adv. Mater.* **2013**, *25*, 998.
[191] B. Ma, F. Liu, S. Zhang, J. Duan, Y. Kong, Z. Li, D. Tang, W. Wang, S. Ge, W. Tang, H. Liu, *J. Mater. Chem. B* **2018**, *6*, 6459.
[192] Q. Yue, M. Wang, Z. Sun, C. Wang, C. Wang, Y. Deng, D. Zhao, *J. Mater. Chem. B* **2013**, *1*, 6085.
[193] J. B. Nofsinger, T. Ye, J. D. Simon, *J. Phys. Chem. B* **2001**, *105*, 2864.
[194] B. Xiong, Y. Chen, Y. Shu, B. Shen, H. N. Chan, Y. Chen, J. Zhou, H. Wu, *Chem. Commun.* **2014**, *50*, 13578.
[195] J. H. Lin, C. J. Yu, Y. C. Yang, W. L. Tseng, *Phys. Chem. Chem. Phys.* **2015**, *17*, 15124.
[196] Y. Liu, M. Yang, J. Li, W. Zhang, X. Jiang, *Anal. Chem.* **2019**, *91*, 6754.
[197] P. Ding, H. Wang, B. Song, X. Ji, Y. Su, Y. He, *Anal. Chem.* **2017**, *89*, 7861.
[198] Q. Ci, J. Liu, X. Qin, L. Han, H. Li, H. Yu, K. L. Lim, C. W. Zhang, L. Li, W. Huang, *ACS Appl. Mater. Interfaces* **2018**, *10*, 35760.
[199] R. O. Prum, R. H. Torres, S. Williamson, J. Dyck, *Nature* **1998**, *396*, 28.
[200] M. Xiao, Y. Li, M. C. Allen, D. D. Deheyn, X. Yue, J. Zhao, N. C. Gianneschi, M. D. Shawkey, A. Dhinojwala, *ACS Nano* **2015**, *9*, 5454.
[201] W. Jiang, X. Zhang, Y. Luan, R. Wang, H. Liu, D. Li, L. Hu, *Polymers* **2019**, *11*, 1754.
[202] D. Fan, X. Zhu, Q. Zhai, E. Wang, S. Dong, *Anal. Chem.* **2016**, *88*, 9158.
[203] H. Zhao, C.-C. Weng, Z.-P. Hu, L. Ge, Z.-Y. Yuan, *ACS Sustainable Chem. Eng.* **2017**, *5*, 9914.
[204] Z. Ye, S. Wu, C. Zheng, L. Yang, P. Zhang, Z. Zhang, *Langmuir* **2017**, *33*, 12952.
[205] Y. Wang, L. Yu, X. W. Lou, *Angew. Chem., Int. Ed.* **2016**, *55*, 14668.
[206] H. Li, Y. Jia, A. Wang, W. Cui, H. Ma, X. Feng, J. Li, *Chem. - Eur. J.* **2014**, *20*, 499.
[207] Z. Dong, L. Feng, Y. Hao, M. Chen, M. Gao, Y. Chao, H. Zhao, W. Zhu, J. Liu, C. Liang, Q. Zhang, Z. Liu, *J. Am. Chem. Soc.* **2018**, *140*, 2165.
[208] H. Fan, X. Yu, Y. Liu, Z. Shi, H. Liu, Z. Nie, D. Wu, Z. Jin, *Soft Matter* **2015**, *11*, 4621.
[209] Z. X. Jin, H. L. Fan, *Polym. Int.* **2016**, *65*, 1258.
[210] L. Sun, C. Wang, L. Wang, *ACS Nano* **2018**, *12*, 4002.
[211] F. Chen, Y. Xing, Z. Wang, X. Zheng, J. Zhang, K. Cai, *Langmuir* **2016**, *32*, 12119.
[212] P. Qi, D. Zhang, Y. Wan, *Talanta* **2017**, *170*, 173.
[213] H. Su, C. A. Hurd Price, L. Jing, Q. Tian, J. Liu, K. Qian, *Mater. Today Bio.* **2019**, *4*, 100033.
[214] P. Winterwerber, S. Harvey, D. Y. W. Ng, T. Weil, *Angew. Chem., Int. Ed.* **2020**, *59*, 6144.
[215] Y. Liu, J. Li, W. Zhang, *Chem. Commun.* **2020**, *56*, 6229.
[216] C. Yun, J. W. Han, M. H. Kang, Y. H. Kim, B. Kim, S. Yoo, *ACS Appl. Mater. Interfaces* **2019**, *11*, 47143.
[217] S. Zatti, A. Zoso, E. Serena, C. Luni, E. Cimetta, N. Elvassore, *Langmuir* **2012**, *28*, 2718.
[218] J. Hou, T. Liu, R. Chen, J. Liu, J. Chen, C. Zhao, L. Yin, C. Li, X. Xu, Q. Shi, J. Yin, *Chem. Commun.* **2017**, *53*, 6708.
[219] C. Rodriguez-Emmenegger, C. M. Preuss, B. Yameen, O. Pop-Georgievski, M. Bachmann, J. O. Mueller, M. Bruns, A. S. Goldmann, M. Bastmeyer, C. Barner-Kowollik, *Adv. Mater.* **2013**, *25*, 6123.
[220] D. Hafner, L. Ziegler, M. Ichwan, T. Zhang, M. Schneider, M. Schiffmann, C. Thomas, K. Hinrichs, R. Jordan, I. Amin, *Adv. Mater.* **2016**, *28*, 1489.
[221] H. W. Chien, W. H. Kuo, M. J. Wang, S. W. Tsai, W. B. Tsai, *Langmuir* **2012**, *28*, 5775.
[222] H. Wu, L. Wu, X. Zhou, B. Liu, B. Zheng, *Small* **2018**, *14*, 1802128.
[223] L. Zhao, W. Wang, W. Hu, *Anal. Chem.* **2016**, *88*, 10357.
[224] S. Ma, L. Liu, V. Bromberg, T. J. Singler, *J. Mater. Chem. C* **2014**, *2*, 3885.
[225] G. Loget, J. B. Wood, K. Cho, A. R. Halpern, R. M. Corn, *Anal. Chem.* **2013**, *85*, 9991.
[226] T. Marchesi D'Alvise, S. Harvey, L. Hueske, J. Szelwicka, L. Veith, T. P. J. Knowles, D. Kubiczek, C. Flaig, F. Port, K. E. Gottschalk, F. Rosenau, B. Graczykowski, G. Fytas, F. S. Ruggeri, K. Wunderlich, T. Weil, *Adv. Funct. Mater.* **2020**, *30*, 2000378.
[227] S. H. Ku, J. S. Lee, C. B. Park, *Langmuir* **2010**, *26*, 15104.
[228] R. Ogaki, D. T. Bennetsen, I. Bald, M. Foss, *Langmuir* **2012**, *28*, 8594.
[229] M. Guardingo, M. J. Esplandiu, D. Ruiz-Molina, *Chem. Commun.* **2014**, *50*, 12548.
[230] F. Behboodi-Sadabad, V. Trouillet, A. Welle, P. B. Messersmith, P. A. Levkin, *ACS Appl. Mater. Interfaces* **2018**, *10*, 39268.
[231] M. Krishnamoorthy, S. Hakobyan, M. Ramstedt, J. E. Gautrot, *Chem. Rev.* **2014**, *114*, 10976.
[232] Y. Zeng, X. Du, W. Hou, X. Liu, C. Zhu, B. Gao, L. Sun, Q. Li, J. Liao, P. A. Levkin, Z. Gu, *Adv. Funct. Mater.* **2019**, *29*, 1901875.
[233] Q. Wei, B. Yu, X. Wang, F. Zhou, *Macromol. Rapid Commun.* **2014**, *35*, 1046.
[234] C. Y. Liu, C. J. Huang, *Langmuir* **2016**, *32*, 5019.
[235] K. Sun, L. Song, Y. Xie, D. Liu, D. Wang, Z. Wang, W. Ma, J. Zhu, X. Jiang, *Langmuir* **2011**, *27*, 5709.
[236] J. Zheng, Y. Chen, A. Karim, M. L. Becker, *ACS Macro Lett.*. **2014**, *3*, 1084.
[237] W. Li, Z. Wang, M. Xiao, T. Miyoshi, X. Yang, Z. Hu, C. Liu, S. S. C. Chuang, M. D. Shawkey, N. C. Gianneschi, A. Dhinojwala, *Biomacromolecules* **2019**, *20*, 4593.
[238] H. Wei, J. Ren, B. Han, L. Xu, L. Han, L. Jia, *Colloids Surf., B* **2013**, *110*, 22.
[239] G. E. Gu, C. S. Park, H. J. Cho, T. H. Ha, J. Bae, O. S. Kwon, J. S. Lee, C. S. Lee, *Sci. Rep.* **2018**, *8*, 4393.
[240] X. Chen, Y. Yan, M. Mullner, M. P. van Koeverden, K. F. Noi, W. Zhu, F. Caruso, *Langmuir* **2014**, *30*, 2921.
[241] P. Manini, P. Margari, C. Pomelli, P. Franchi, G. Gentile, A. Napolitano, L. Valgimigli, C. Chiappe, V. Ball, M. d'Ischia, *J. Phys. Chem. B* **2016**, *120*, 11942.
[242] M. Ambrico, P. Manini, P. F. Ambrico, T. Ligonzo, G. Casamassima, P. Franchi, L. Valgimigli, A. Mezzetta, C. Chiappe, M. d'Ischia, *Phys. Chem. Chem. Phys.* **2019**, *21*, 12380.
[243] H. Liu, X. Qu, H. Tan, J. Song, M. Lei, E. Kim, G. F. Payne, C. Liu, *Acta Biomater.*. **2019**, *88*, 181.
[244] R. M. Bullock, J. G. Chen, L. Gagliardi, P. J. Chirik, O. K. Farha, C. H. Hendon, C. W. Jones, J. A. Keith, J. Klosin, S. D. Minteer, R. H. Morris, A. T. Radosevich, T. B. Rauchfuss, N. A. Strotman, A. Vojvodic, T. R. Ward, J. Y. Yang, Y. Surendranath, *Science* **2020**, *369*, eabc3183.
[245] S. Bose, G. Fielding, S. Tarafder, A. Bandyopadhyay, *Trends Biotechnol.*. **2013**, *31*, 594.
[246] D. Pan, A. H. Schmieder, S. A. Wickline, G. M. Lanza, *Tetrahedron* **2011**, *67*, 8431.
[247] Q. Meng, H. Zhang, Y. Liu, S. Huang, T. Zhou, X. Yang, B. Wang, W. Zhang, H. Ming, Y. Xiang, M. Li, G. Cao, Y. Huang, L.-z. Fan, H. Zhang, Y. Guan, *Nano Res.*. **2019**, *12*, 2919.
[248] Y. Yang, Y. Liu, Y. Shen, *Adv. Funct. Mater.* **2020**, *30*, 1910172.

[249] Y. Zou, Z. Wang, Z. Chen, Q.-P. Zhang, Q. Zhang, Y. Tian, S. Ren, Y. Li, *J. Phys. Chem. C* **2019**, *123*, 5345.
[250] J. Zhou, P. Wang, C. Wang, Y. T. Goh, Z. Fang, P. B. Messersmith, H. Duan, *ACS Nano* **2015**, *9*, 6951.
[251] A. Yao, X. Jiao, D. Chen, C. Li, *ACS Appl. Mater. Interfaces* **2019**, *11*, 7927.
[252] F. Zhang, Q. Zhang, X. Li, N. Huang, X. Zhao, Z. Yang, *Biomaterials* **2019**, *194*, 117.
[253] Z. Yang, Y. Yang, K. Xiong, J. Wang, H. Lee, N. Huang, *Chem. Mater.* **2018**, *30*, 5220.
[254] X. Li, H. Qiu, P. Gao, Y. Yang, Z. Yang, N. Huang, *NPG Asia Mater.* **2018**, *10*, 482.
[255] Z. Wang, F. Carniato, Y. Xie, Y. Huang, Y. Li, S. He, N. Zang, J. D. Rinehart, M. Botta, N. C. Gianneschi, *Small* **2017**, *13*, 1701830.
[256] B. Larsson, H. Tjälve, *Acta Physiol. Scand.* **1978**, *104*, 479.
[257] Y. P. Qiu, Q. Shi, L. L. Zhou, M. H. Chen, C. Chen, P. P. Tang, G. S. Walker, P. Wang, *ACS Appl. Mater. Interfaces* **2020**, *12*, 18617.
[258] C. Cui, Y. Liu, S. Mehdi, H. Wen, B. Zhou, J. Li, B. Li, *Appl. Catal., B* **2020**, *265*, 118612.
[259] S. Sotoma, Y. Harada, *Langmuir* **2019**, *35*, 8357.
[260] J. Y. Kim, S. Kim, S. Han, S. Y. Han, C. P. Passos, J. Seo, H. Lee, E. K. Kang, J. F. Mano, M. A. Coimbra, J. H. Park, I. S. Choi, *ChemNanoMat* **2020**, *6*, 379.
[261] J. Kuang, P. B. Messersmith, *Langmuir* **2012**, *28*, 7258.
[262] Y. Liu, X. Wang, S. Feng, *Adv. Funct. Mater.* **2019**, *29*, 1902488.
[263] G. Xu, P. Liu, D. Pranantyo, K.-G. Neoh, E.-T. Kang, S. Lay-Ming Teo, *ACS Sustainable Chem. Eng.* **2018**, *7*, 1786.
[264] W. Laure, P. Woisel, J. Lyskawa, *Chem. Mater.* **2014**, *26*, 3771.
[265] C. Chen, D. Y. W. Ng, T. Weil, *Prog. Polym. Sci.* **2020**, *105*, 101241.
[266] I. Kaminska, M. R. Das, Y. Coffinier, J. Niedziolka-Jonsson, J. Sobczak, P. Woisel, J. Lyskawa, M. Opallo, R. Boukherroub, S. Szunerits, *ACS Appl. Mater. Interfaces* **2012**, *4*, 1016.
[267] J. S. Guo, G. B. Kim, D. Y. Shan, J. P. Kim, J. Q. Hu, W. Wang, F. G. Hamad, G. Qian, E. B. Rizk, J. Yang, *Biomaterials* **2017**, *112*, 275.
[268] Z. Yang, X. Zhao, R. Hao, Q. Tu, X. Tian, Y. Xiao, K. Xiong, M. Wang, Y. Feng, N. Huang, G. Pan, *Proc. Natl. Acad. Sci. USA* **2020**, *117*, 16127.
[269] Z. Yuan, C. Lin, Y. He, B. Tao, M. Chen, J. Zhang, P. Liu, K. Cai, *ACS Nano* **2020**, *14*, 3546.
[270] H. Wang, Q. Lin, L. Yin, Y. Yang, Y. Qiu, C. Lu, H. Yang, *Small* **2019**, *15*, 1900011.
[271] X. Dong, B. Ding, H. Guo, H. Dou, X. Zhang, *ACS Appl. Mater. Interfaces* **2018**, *10*, 38101.
[272] K. Qu, Y. Zheng, X. Zhang, K. Davey, S. Dai, S. Z. Qiao, *ACS Nano* **2017**, *11*, 7293.
[273] K. Qu, Y. Zheng, Y. Jiao, X. Zhang, S. Dai, S.-Z. Qiao, *Adv. Energy Mater.* **2017**, *7*, 1602068.
[274] H. Park, D. Lee, H. Lee, S. Hong, *Mater. Horiz.* **2020**, *7*, 1387.
[275] R. Mrowczynski, R. Markiewicz, J. Liebscher, *Polym. Int.* **2016**, *65*, 1288.
[276] S. Mondal, A. Thampi, M. Puranik, *J. Phys. Chem. B* **2018**, *122*, 2047.
[277] A. J. Steeves, F. Variola, *J. Mater. Chem. B* **2020**, *8*, 199.
[278] X. Tan, P. Gao, Y. Li, P. Qi, J. Liu, R. Shen, L. Wang, N. Huang, K. Xiong, W. Tian, Q. Tu, *Bioact. Mater.* **2021**, *6*, 285.
[279] H. Lee, J. Park, S. Y. Han, S. Han, W. Youn, H. Choi, G. Yun, I. S. Choi, *Chem. Commun.* **2020**, *56*, 13748.
[280] M. Shin, J. H. Galarraga, M. Y. Kwon, H. Lee, J. A. Burdick, *Acta Biomater.* **2019**, *95*, 165.
[281] M. K. Wlodarczyk-Biegun, J. I. Paez, M. Villiou, J. Feng, A. Del Campo, *Biofabrication* **2020**, *12*, 035009.
[282] H. Cui, W. Zhu, M. Nowicki, X. Zhou, A. Khademhosseini, L. G. Zhang, *Adv. Healthcare Mater.* **2016**, *5*, 2174.
[283] B. An, Y. Wang, X. Jiang, C. Ma, M. Mimee, F. Moser, K. Li, X. Wang, T.-C. Tang, Y. Huang, Y. Liu, T. K. Lu, C. Zhong, *Matter* **2020**, *3*, 2080.
[284] X. Wang, J. Pu, Y. Liu, F. Ba, M. Cui, K. Li, Y. Xie, Y. Nie, Q. Mi, T. Li, L. Liu, M. Zhu, C. Zhong, *Nat. Sci. Rev.* **2019**, *6*, 929.
[285] C. Zhang, J. Huang, J. Zhang, S. Liu, M. Cui, B. An, X. Wang, J. Pu, T. Zhao, C. Fan, T. K. Lu, C. Zhong, *Mater. Today* **2019**, *28*, 40.
[286] S. H. Yang, S. M. Kang, K.-B. Lee, T. D. Chung, H. Lee, I. S. Choi, *J. Am. Chem. Soc.* **2011**, *133*, 2795.
[287] J. Geng, W. Li, Y. Zhang, N. Thottappillil, J. Clavadetscher, A. Lilienkampf, M. Bradley, *Nat. Chem.* **2019**, *11*, 578.
[288] M. A. English, L. R. Soenksen, R. V. Gayet, H. de Puig, N. M. Angenent-Mari, A. S. Mao, P. Q. Nguyen, J. J. Collins, *Science* **2019**, *365*, 780.

Zhaojun Jia is a postdoc researcher in the Department of Chemistry and Chemical Biology, Rutgers University, New Brunswick. He received his Ph.D. degree in Biomechanics and Medical Engineering from Peking University in 2017. His research interests include multifunctional biomaterials, catechol surface chemistry, and biohybrid materials.

Min Wen is a postdoc researcher in Shenzhen Institutes of Advanced Technology, Chinese Academy of Sciences. She received her Ph.D. degree in Chemistry from the Technical Institute of Physics and Chemistry, Chinese Academy of Sciences in 2017. Her research interests focus on the design of functional nanomaterials and their application in energy conversion by photocatalysis.

Yufeng Zheng is a professor in the Department of Materials Science and Engineering, College of Engineering, Peking University. He is a fellow of Biomaterials Science and Engineering (FBSE) and the American Institute for Biological and Medical Engineering (AIMBE). He obtained his Ph.D. degree from Harbin Institute of Technology in 1998. His interests and past activities are mainly focused on the design and development of novel biomaterials and biomedical devices.